UNIONE EUROPEA

Ministero dell'Istruzione, dell'Università e della Ricerca

DELIVERABLE OF RESEARCH PROJECT

DiGriFlex

Real-time Distribution Grid Control and Flexibility Provision under Uncertainties

Report

Deliverable D2.2

Forecasting systems and corresponding solution algorithms for real-time control of distribution networks in presence of uncertainties

Technical report including the validation of the forecasting systems using appropriate test bench and scenarios in a numerical environment

Project title: **DiGriFlex**

MIUR project ID: ENSGPLUSREGSYS18_00016

Partners: Università di Napoli Federico II, Università di Napoli Parthenope, Haute Ecole d'Ingénierie et de Gestion du Can-ton de Vaud (HEIG-VD) - Institut d'Énergie et Systèmes Électriques (IESE)

Report on the activities developed in the period September 1st 2019 - February 2nd 2021.

Date: 1st November 2021

CONTENTS

Ministero dell'Istruzione, dell'Università e della Ricerca

1. LIST OF FIGURES

UNIONE EUROPEA

Ministero dell'Istruzione, dell'Università e della Ricerca

2. LIST OF TABLES

3. INTRODUCTION

The DiGriFlex project is aimed at proposing and validating effective forecasting and optimal control algorithms to ensure efficient and secure operation of low voltage distribution grids, as well as to provide flexibility (from distribution grids toward upstream grids) under uncertainties. A two-level rolling optimization framework is developed and experimentally validated. The first level deals with prescheduling of controllable resources in a time ahead basis, whereas the second level deals with real-time online scheduling of all the controllable resources. An appropriate forecasting system is developed to provide day-ahead and near real-time forecast of uncertain parameters, in accordance with the optimization framework. The proposed methodology will be validated, and its effectiveness demonstrated under realistic uncertainty sources, this activity being object of the final part of the project.

This report refers to the activities of the project referring to the first two years of activities of the project. The activities within this period which involved the University of Naples Federico II are included in the WP2 (*Development of appropriate day-ahead and real-time forecasting systems for renewable generation and loads*) and are related to Tasks 2.1 and 2.3:

Task 2.1 refers to “Data collection, data pre-processing and exploratory data analysis”.

Task 2.3 refers to “Development of real-time forecasting systems for renewable generation and loads”.

The activities of Task 2.1 include the i) collection of time series data, ii) data pre-processing and iii) exploratory data analysis.

The activities of Task 2.3 include the i) development of methods for real-time forecasting of renewable generation power and loads, ii) identification of possible combination of models in ensemble approaches, iii) comparison with relevant state-of-the-art benchmarks.

More specifically, in Task 2.1 the activities include all the data collection and data pre-processing tasks that were necessary to create a large robust database of variables which could be exploited to develop forecasting systems for renewable generation and loads. Since the forecasting methodology will be integrated into the grid optimization models that are the object of the WP3, data and pre-processing were made with reference to the site of the installation of the test distribution grid of the ReIne laboratory. Other variables that were not available at the site of installation of the test distribution grid of the ReIne laboratory were taken from the literature and/or collected at different sites, in order to develop the forecasting systems.

Exploratory data analysis was aimed at discarding uninformative predictors which are the input datasets for the forecasting systems developed in the Task 2.3, particularly with reference to those methods which require large historical datasets.

With reference to Task 2.3, the development of methods and models able to obtain accurate real-time forecasting of PV generation and load (electric vehicle load) focused on both deterministic and probabilistic approaches. As deterministic approach, two persistence-based methods were proposed. Probabilistic methods referred to hybrid physical-statistical models based on multiple linear regression and random forests. The identification of the best combination type for these underlying models in ensemble approach is also explored. Finally, a comparison with the relevant state-of-the-art benchmarks is carried out. More_specifically, the models proposed in the research activity are the:

- derivative-persistence method for real-time photovoltaic power forecasting;
- Caputo-derivative method for real-time photovoltaic power forecasting;
- Bayesian bootstrapping in real-time probabilistic photovoltaic power forecasting;
- hierarchical probabilistic electric vehicle load forecasting.

In what follows, after a brief illustration of the objectives of the tasks (Section 5), a description of the state of the art on real-time forecasting methods is proposed with reference to both renewable generation and load (Section 6). The specific activities of Tasks 2.1 and 2.3 are detailed in Sections 7 and 8. Finally, a comparison with expected results, the human resources involved in the project and the publications produced during the first year are reported in Sections 10-12.

4. OBJECTIVES

Objectives of the Tasks involved in this Milestone focus on forecast of loads and renewable generation in active distribution networks. More specifically, objective of the activities of the research unit was the development of online forecasting systems and algorithms for renewable generation and loads with reference to both deterministic and probabilistic frameworks.

5. STATE OF THE ART

Real-time operation of smart grids is based on intra-hour strategies which require to handle real-time forecast of input data such as photovoltaic (PV) or wind source power production. Due to the requirements in terms of real-time computing, these data need to be available in very short time (i.e., very-short-term or ultra-short-term forecasting) [1]-[3].

5.1. RENEWABLE GENERATION PREDICTION

Focusing on renewable generation prediction, the persistence model, which is based on the assumption that the quantity to be forecasted will remain constant over time, has been always considered performant *in real-time forecasts* [4]. Statistical approaches, which are based on historical time series and use mathematical equations to extract the pattern and correlation from past input data, show accurate performance in very-short-term horizons. These methods can be divided into two groups, that are machine learning and time series-based models [5] which are both used for real-time forecasting. Physical forecasting models, such as numerical weather prediction models, which are based on physical parameters for future predictions, are typically used for longer lead times (i.e., from short-term to long-term forecasting), but they cannot be considered performant for very-short-term scenarios since they would increment the computational time with negligible improvement.

With reference to the persistence method, it is often adopted to forecast renewable power generation due to its ease of implementation, since it does not need weather forecast data or on in-built toolboxes for implementation. In case of real-time operation, the persistence forecasting method allows obtaining an almost instantaneous estimate of the forecasting power based on the most recent measurements. This is crucial to catch the fast variations of power generated by renewable based systems which are highly variable by nature. Focusing on forecasting horizons up to few hours, the persistence method has been recognized in the literature as accurate enough and its predictions are usually adopted as a benchmark in deterministic [6] and also probabilistic [7] frameworks. It is also worth to note that persistence is often used as a fallback model to provide forecasts in case more sophisticated models fail.

Focusing on PV generation, in literature, the persistence method is used for both PV power production and solar radiation forecasts. The persistence method is adopted in [8] for short-term forecast of PV power production based on historical power data without using numerical weather predictions. Still with reference to solar generation prediction, a comparison between auto-regressive moving average (ARMA) and persistence models is performed in [9], showing that persistence model performs better at very-short-term forecasting intervals. The proposal shows great accuracy improvement of short-term forecasts. Smart persistence methods are also proposed in the literature. They consist in decomposing solar power production in a stationary and in a stochastic component [10]. Usually, the stationary term is associated to the clear sky production and the stochastic term to the cloud-induced change [11]. In [12] a modification is presented that keeps unvaried the stochastic part of the time series. A method which applies the persistence approach to the cloudiness is used in [13]. The method presented in [14] adopts the ramp persistence approach. In [15], a smart persistence method is used as input of a machine learning technique. In [4] a physical smart persistence model is proposed to forecast solar irradiance that is capable to better capture cloud conditions than typical persistence models. More specifically, the persistence model is improved by adding a clear-sky index correction factor (that is, the ratio of radiation measurements divided by clear-sky radiation) which is then multiplied by future clear-sky radiation to obtain a forecast. The clear-sky radiation is forecasted through the computation of three variables by using different models.

Also, in [16] a physics-based smart persistence model is adopted, for intra-hour forecasting of solar radiation. It decomposes global horizontal irradiance into cloud albedo and cloud fraction using simulated extra-terrestrial solar radiation and solar zenith angle. In [17] an improved persistence-based real-time forecasting method is proposed by implementing the incremental and decremental patterns on solar generation at sunrise and sunset hours.

With reference to probabilistic approaches, they produce forecasts in the form of quantiles, intervals or density functions, which provide more comprehensive information compared to point forecasts. Nevertheless, the technical literature scarcely deals with probabilistic approaches. The methods typically used in probabilistic framework are statistical models or hybrid physical-statistical models. By focusing on forecast methods of solar irradiance and PV power production, quantile regression (QR) models are proposed in [18], [19]. [18] uses QR approach to predict distribution of outcomes. [19] carries out probabilistic models for intra-day solar forecasting in the case of highly variable sky conditions based on linear QR method. Other approaches are based on machine learning techniques [20], [21]. Particularly, [20] compares the performance of k-nearest-neighbours and gradient boosting for intra-hour forecasting of solar irradiance. [21] is a hybrid physical-statistical model which uses QR Forests to forecast power output employing as inputs predicted meteorological variables from a numerical weather forecast model, and actual power measurements of PV plants. It is worth to note that it is crucial to improve predictions of some weather variables though proper model selection which allows selecting the most informative predictors and discarding uninformative inputs. To do that the exploitation of available input data must be maximized. In probabilistic energy forecasting this has been successfully done through ensemble approaches [22]. Among these, widely applicable and powerful tools are those based on the bootstrap methodology. The bootstrap is a statistical tool which can be tailored to quantify the uncertainty related to a specific estimator or statistical learning method. In the bootstrap method, small range of samples are repeatedly taken along with their statistic and relevant average features. For each of these set of samples, models are derived, and their performance is assessed through the samples which are not included in the set used to build the model itself. Regarding the suitability of this technique for real-time applications, it must be noted that, despite bootstrap can appear characterized by a heavy computational burden, it is a flexible technique which can be applied on some selected suitable parameters, thus reducing the computational time. Focusing on real-time application, bootstrap technique has been used to monitor PV power plant output in [23]. A two-stage method is proposed in [24] to estimate uncertainty of PV forecasting. The forecasting is based on the bootstrap method applied to short-term deterministic predictions obtained from a hybrid intelligent model that combines wavelet transform technique for data pre-processing, and radial basis function neural network method. Within the Bayesian framework – which is successfully applied to short-term photovoltaic forecasting, e.g. [25] and [26] – bootstrapping techniques have also been used to improve the probabilistic forecasts. Bayesian bootstrap techniques for short term forecasting methods have been rarely adopted. [27] proposes this approach in the transportation sector.

5.2. LOAD PREDICTION

With reference to load prediction, particularly important is the forecast of EV load due to the characteristics of the EV demand (i.e., non-constant patterns, seasonal effects, weather and social correlation, high volatility and jumps) which make the forecasting problem a critical issue.

Various models have been developed to determine the impact of the EVs on electricity distribution networks, distinguishing between deterministic and probabilistic approaches. At the very early point of research on EV load forecasting, the lack of consistent actual EV load data determined the development of Monte Carlo approaches to build experimental scenarios [28]-[32]. The availability of actual EV load data changed the approach to EV load forecasting, allowing for the exploitation of consolidated load forecasting techniques based on stochastic and data-driven approaches [33], [34]. Time series approaches based on AutoRegressive Integrated Moving Average (ARIMA) models [35], [36] and their seasonal extensions [37], [38] were applied to forecast EV load. Supervised data-driven models, such as Support Vector Regression (SVR), Artificial Neural Network (ANN), and Random Forest (RFs) have been used in [39]-[41]. Although the existing review of the literature shows that deterministic EV load forecasting has undergone a relevant development process, Probabilistic EV Load Forecasting (PEVLF) has not received the same attention. Recent studies (e.g., [42]) have applied probabilistic forecasting models to EV charging time and to the required energy approximated by the upcoming trip distance, but the temporal probabilistic prediction of the EV load is not yet established.

Adapting conventional probabilistic load forecasting models to develop PEVLF systems is however complex. The periodicity and fluctuation related to the large distribution of EVs make conventional probabilistic techniques less effective [43], [44]. In order to overcome the problem, relevant research efforts have been developed in the last years, turning a light on PEVLF [45]-[48]. A relevant outcome of the literature review determines the importance of the spatial-temporal analysis in the development of a probabilistic method to forecast EV from different areas, due to their capillarity over the distribution networks [44]. This problem is prone to be tackled from a hierarchical perspective, proceeding by a series of successive merges of prediction made at a different level of aggregation [49], [50]. In hierarchical load forecasting, the information contained in the load at low-level aggregation (for example, the load at the HV/MV nodes in a HV network, or the load of small regions) is used to predict the load at high-level aggregation (for example, the overall load of the entire HV network, or the overall load of a geographic region). Hierarchical methodologies to merge probabilistic forecasts have been recently applied for probabilistic load forecast purposes [51], [52]. They are however challenging, mostly because the problem is usually formulated as a nonlinear and non-convex optimization problem, so that global optimality cannot be guaranteed, and the combined results may be worse than individual forecasts [52].

6. RESULTS OF ACTIVITIES OF TASK 2.1

The activities included:

- the collection of time series that include both target variables (photovoltaic power and loads) and predictor variables;
- the development of methods to pre-process the data to eliminate outliers and missing/bad values;
- the exploratory data analysis aimed at discarding uninformative predictors to reduce the dimensionality of the forecasting problems.

Activities included all the data collection and data pre-processing tasks that were necessary to create a large robust database of variables which could be exploited to develop forecasting systems for renewable generation and loads.

6.1. GENERATION DATA COLLECTION, PRE-PROCESSING AND EXPLORATORY ANALYSIS

With reference to renewable generation, the research activities completed in Task 2.1 resulted in:

- the collection of large, robust datasets of photovoltaic (PV) power generation and weather variables at the site of installation of the test distribution grid of the ReIne laboratory;
- the collection of large, robust datasets of weather variables available from the relevant literature and from public databases;
- the pre-processing of the collected data, aiming at individuating and correcting missing data, bad data and outliers;

- the exploratory data analysis to reduce the dimensionality of the input datasets, favouring the development of adequate forecasting systems for renewable generation and load.

6.1.1 DATA COLLECTION

Two PV systems have been continuously monitored. The first PV installation (PVI1) is a 30-kWp system equipped with 4 8.5-kWp inverters. PVI1 is part of the test distribution grid of the ReIne laboratory. Since it has been installed only recently, the data collection is ongoing since August 24, 2019 at a 1-minute time resolution. This PV system has a relatively short operation life of utilization so these data could be not sufficient for validating and testing some PV power forecasting models. For this reason, a second PV installation (PVI2), located close to the test distribution grid of the ReIne laboratory, has been monitored since January 1, 2016 until December 31, 2018 at a 1-minute time resolution. Also, datasets including solar irradiance measurements (**SI1**) have been used which are taken by a dedicated weather station installed at the same location of the test distribution grid of the ReIne laboratory. The data collection started on August 24, 2019, with a 1-minute time resolution. The solar irradiance data taken from this dataset were used as target data for the verification of the maximum PV power forecasting system; since the utilization of these data for validating and testing forecasting models was unfeasible at the progress stage of the first year of project activities, this dataset was included only in the most recent experimental frameworks.

A dedicated weather station is installed at the location of the test distribution grid of the ReIne laboratory. This station allows collecting weather data at the same time resolution and for the same time periods of the PV power data, allowing their usage as exogenous variables for PV power forecasting models. Twenty-six variables are monitored in this way.

Eventually, weather forecast data have been gathered from the European Centre for Medium-range Weather Forecasts (ECMWF) for the corresponding time periods. Requests have been prepared in Python3.7 and sent via the ECMWF Application Programming Interface (API). Forecasts for nine variables are obtained in this way. These data are related to the noon run (i.e., forecasts are issued at 12:00 A.M. of day D-1 for the entire day D) and to the midnight run (i.e., forecasts are issued at 12:00 P.M. of day D-1 for the entire day D). This differentiation in the weather forecast lead time allows developing models diversified for day-ahead control and real-time control of the distributed energy resources.

UNIONE EUROPEA

Ministero dell'Istruzione, dell'Università e della Ricerca

6.1.2 DATA PRE-PROCESSING: CLEANSING

The initial analysis upon the PVI1 and PVI2 data and on weather data collected by the weather station revealed some potential outliers, missing and bad data. If not corrected, these data may significantly deteriorate the performance of the PV power forecasting models.

One of the principal objectives of the pre-processing activity is therefore to correct and remove this harmful effect by cleansing the data. Bad and missing data are easy to be individuated by visual inspection. Potential outliers instead are more subtle, since they cannot be immediately individuated by visual inspection. A slight modification of the Tukey's test has been applied in order to individuate potential outliers. Tukey's test acts by examining and individuating data which lie beyond a specific band of tolerance, in which the null hypothesis can be rejected. For the generic variable y, the band of tolerance is individuated through its lower bound $y_{T,low}$ ($y_{T,low} = y^{\langle 0.25 \rangle} - 3 \cdot (y^{\langle 0.75 \rangle} - y^{\langle 0.25 \rangle})$ and upper bound $y_{T,up}$ ($y_{T,up} = y^{\langle 0.75 \rangle} + 3 \cdot (y^{\langle 0.75 \rangle} - y^{\langle 0.25 \rangle})$), where $y^{\langle 0.25 \rangle}$ and $y^{\langle 0.75 \rangle}$ are respectively the 0.25-quantile (25-percentile) and the 0.75-quantile (75-percentile) of the samples collected in the entire dataset. Due to the strong seasonality of the PV power data pattern (which suggests heteroskedasticity), the Tukey's test has been differentiated for each hour of the day, accounting for different sample quantiles during the 24 hours of the day.

Potential outliers, bad data and missing data are treated in the same manner, i.e., they are entirely discarded. It is important to note that ECMWF weather forecasts are already pre-processed by the original source, therefore data cleansing activity has not been developed on them.

6.1.3 DATA PRE-PROCESSING: AVERAGING

Another important objective of the data pre-processing activity is to average values collected at a one-minute time resolution in order to obtain hourly data. This has been performed in R environment using the lubridate package. In presence of too many removed data (i.e., beyond 30% of the total observations in the considered hour), the entire hourly value is set at the mean value from the two nearest hourly values. In presence of fewer removed data (i.e., less than 30% of the total observations in the considered hour), the entire hourly value is set at the mean value of the one-minute observations within the considered hour.

It is important to note that ECMWF weather forecasts are already provided at hourly time resolution by the original source, therefore data averaging activity has not been developed on them.

6.1.4 DATA PRE-PROCESSING: NORMALIZATION

The last objective of the data pre-processing activity is to normalize hourly values in the range 0-1. This accommodation is usually necessary when the ranges in which the considered variables are included are very different. Although some forecasting models are insensitive to data normalization, other models may be significantly affected by the lack of normalization. At this progress stage, data are normalized in order to be used in any case. The normalized value $\tilde{y}_h$ of the generic variable y occurred at hour h is $\tilde{y}_h = \frac{y_h - y_{\min}}{y_{\max} - y_{\min}}$, where y_h is the value observed at hour h, and $y_{\min}$ and $y_{\max}$ are respectively the minimum and maximum values observed in the entire dataset.

6.1.5 EXPLORATORY DATA ANALYSIS

The database resulting from the data pre-processing activities consists of hourly observations of several exogenous weather variables and hourly observations of PV power. In order to reduce the dimensionality of the problem, an exploratory data analysis has been carried out to individuate exogenous variables which are informative for the PV power, and to discard uninformative exogenous variables.

At this progress stage, the exploratory data analysis has been performed only to individuate potential relationship between the PV power of PVI2 and ECMWF weather forecasts. This was performed via graphical inspection of relative scatter plots.

As an example, scatter plots of the normalized PV power versus the normalized clear-sky irradiance forecasts Fig. 1.a) and versus the normalized solar irradiance forecasts Fig. 1.b) evidence clear relationship among these variables. Nevertheless, this relationship is not steady across the hour of the day, as patterns clearly differ considering, for example, 12 A.M., 9 A.M., and 6. P.M in the figures.

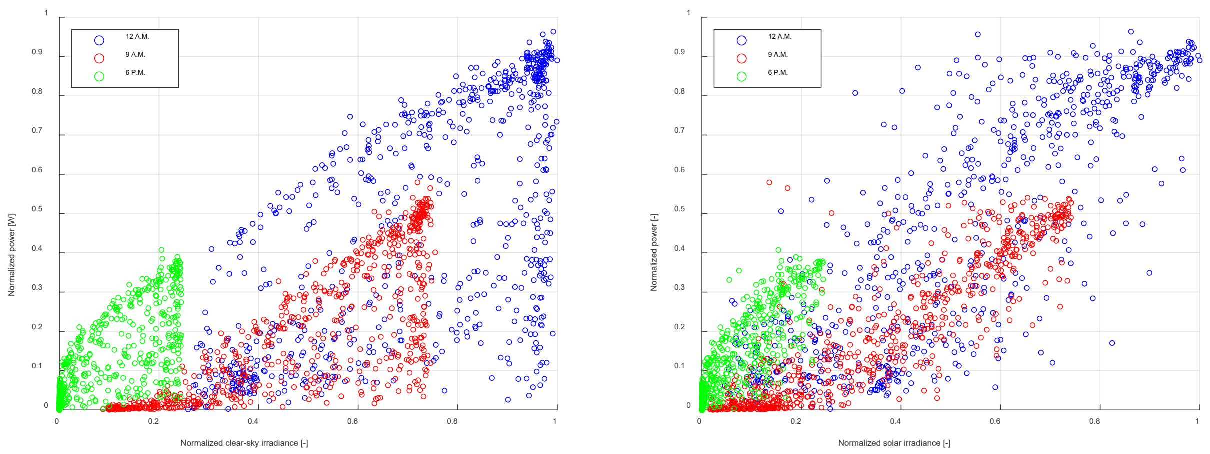

(a) (b)

Fig. 1 - Scatter plots of the normalized PV power versus the normalized clear-sky irradiance forecasts (a) and versus the normalized solar irradiance forecasts (b) for three different hours of the day.

From the graphical inspection of Fig. 1, it is suggested to add normalized clear-sky irradiance forecasts and normalized solar irradiance forecasts as candidate predictors of PV power forecasting models and to add a dummy variable to differentiate among the hours of the day.

The exploratory data analysis also allows discarding some variables which cannot be considered informative for predicting PV power. As significant example, Fig. 2 shows the scatter plots of the normalized PV power versus the normalized forecasts of wind speed at 10 m. No clear relationship can be evidenced from this plot, as the cloud of points is very irregular. Also, there are no clear patterns differentiated among the hours of the day. For this reason, it can be considered safe to discard normalized forecasts of wind speed at 10 m to reduce the dimensionality of the problem.

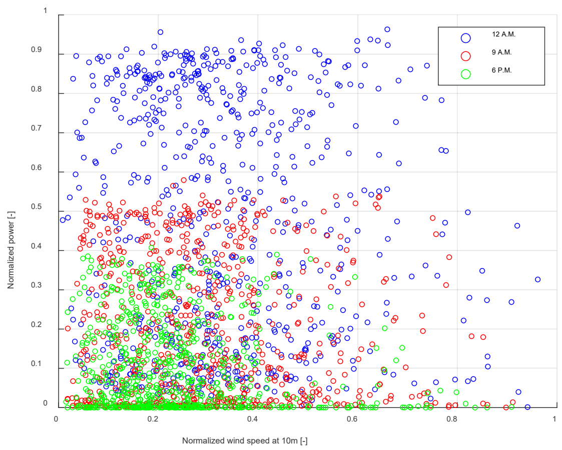

Fig. 2 - Scatter plots of the normalized PV power versus the normalized forecasts of wind speed at 10 m, for three different hours of the day.

6.2. EV LOAD DATA COLLECTION, PRE-PROCESSING AND EXPLORATORY ANALYSIS

The data pre-processing unit described in this Section refers to a large-scale charging dataset and a weather dataset and aims to get the time series of EV load and the arranged predictors for the probabilistic models described in Section 8.3.

6.2.1 DATA SOURCES

The EVnetNL dataset has been provided for research purposes by the ElaadNL, the Dutch knowledge and innovation centre in the field of smart charging infrastructure [53]. The dataset is organized in two database tables, “Transactions” and “Meter readings”. Table “Transactions” contains 1 822 884 rows, each corresponding to a unique charging transaction event, which is characterized by the charging station and the charging point identifiers, latitude and longitude, the initial and the final state of the meter, maximum power charged during the transaction, the RFID (hashed) card starting and finishing the charging transaction and the Coordinated Universal Time (UTC) timestamp of the start and the end of the charging transaction. Table "Meter readings" has 52 294 851 rows, each corresponding to one reading of a meter status. The readings are done regularly every 15 minutes from the time when a charging transaction is initiated until it is terminated (i.e. when the EV is unplugged). A unique identifier of the charging transaction, UTC timestamp of the reading, transferred energy and the value of the meter characterizes each meter reading. The EVnetNL dataset includes transaction data from January 1, 2012 to June 30, 2018.

To use only the most recent data, all the transactions that ended before June 30, 2015 and the meter readings corresponding to such transactions were discarded.

The potential impact of weather conditions on charging behaviour has been considered by employing both the real and forecasted meteorological data for the area of the Netherlands [54]. The meteorological data (precipitation [m], snowfall [m (of water equivalent)], temperature [°C], wind speed [m/s]) are associated with geographical locations characterized by the latitude and the longitude forming regular grids that fully contain the studied geographical areas. The considered period coincides with the charging data and predictions of weather are issued at midnight of day D-1 for day D, with an hourly time resolution.

From the collected data, a time series of energy consumption and a set of potentially relevant predictors were compiled.

6.2.2 ENERGY CONSUMPTION TIME SERIES: DATA CLEANING

The EVnetNL dataset has been already partially cleaned and, to ensure validity and consistency of analysed data, missing and unexpected values (e.g. unusually high values or negative values of consumed energy) in the data were checked for. However, no such cases were found. Further, inconsistencies between the "Transactions" and "Meter readings" tables we checked for. 565 transactions with no information were found in the "Meter readings" table. Such cases were removed also from the Transactions tables.

6.2.3 ENERGY CONSUMPTION TIME SERIES: SELECTION OF THE PERIOD

The EVnetNL dataset covers a relatively long-time interval. In the early years, the number of charging stations was gradually growing as the charging network was built, and it stabilized only around the year 2015 [55]. In the first half of 2017, ElaadNL gave over the responsibility for the operation of more than 50% of charging stations to municipalities [56]. Consequently, data recordings for some charging stations were discontinued. To minimize the impact of these developments on the analysed data, years 2016 and 2017 were selected and only stations active in the whole selected period were considered (i.e. stations where, according to the EVnetNL dataset, at least one charging transaction was initiated before the year 2016 and at least one charging transaction was accomplished after the year 2017). After these steps, 1 137 120 and 35 936 734 observations respectively remained in the "Transactions" and the "Meter readings" datasets.

6.2.4 ENERGY CONSUMPTION TIME SERIES: SELECTION OF GEOGRAPHIC AREAS

Predictions of energy consumption for an individual station are very challenging and hardly generalizable [57] as the temporal pattern of energy consumption is driven by the stochasticity of EV drivers charging behaviour, by the available smart charging technologies and by the EV characteristics (charging power, battery capacity, etc.). Since the energy predictions that could be useful in the power grid management applications, where a single charging station plays only a minor role, are of interest for this research project, the energy consumption has been spatially aggregated. To maintain the geographical closeness of charging stations, the COROP regions were used which divide the area of the Netherlands into 40 continuous spatial units that are typically used for statistical purposes [58]. Each charging station was assigned to the COROP region and for further analyses, four COROP regions were selected with the largest aggregated energy consumption in the considered period. Selected COROP regions are Zuidoost-Noord-Brabant, Rijnmond, Noordoost-Noord-Brabant and Utrecht, with 104, 91, 71 and 40 active charging stations, respectively. In Figure 3, the positions of the EVnetNL charging stations located in the selected COROP regions are shown.

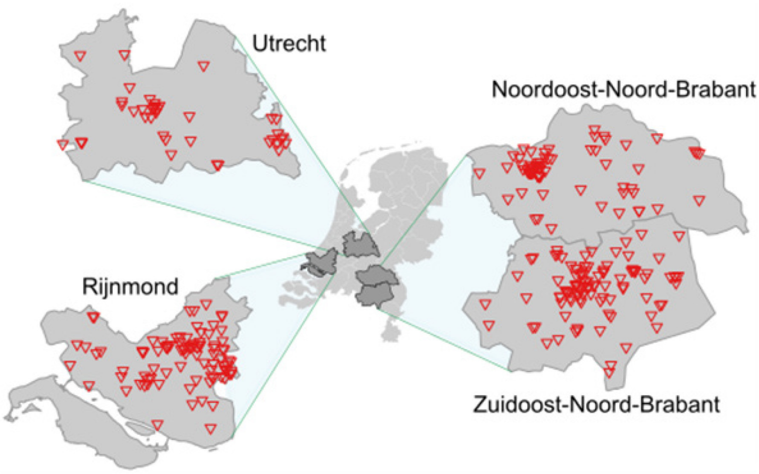

Fig. 3 - Locations of the EVnetNL charging stations in the selected COROP regions, together with the map of the Netherlands showing where the COROP regions are situated.

6.2.5 ENERGY CONSUMPTION TIME SERIES: COMPILATION OF TIME SERIES

A time series is a set of observations, each one defined at a specific time, with time difference between two consecutive observations that is equal for all the observations [59]. From the EVnetNL dataset, time series of energy consumption were extracted, with an observation every hour, for the period from July 1, 2015 to June 30, 2018 and for the four COROP regions. A meter reading of consumed energy within the last 15 minutes that fully overlapped with the hourly time interval, was added to the corresponding value of the time series. If the 15 minutes period of a meter reading overlapped with two hourly intervals, the energy was divided between the intervals proportionally to the length of the time overlap.

Panel A of Figure 4 displays 3 years of data selected for the analysis, together with the aggregated energy consumption in all four COROP regions.

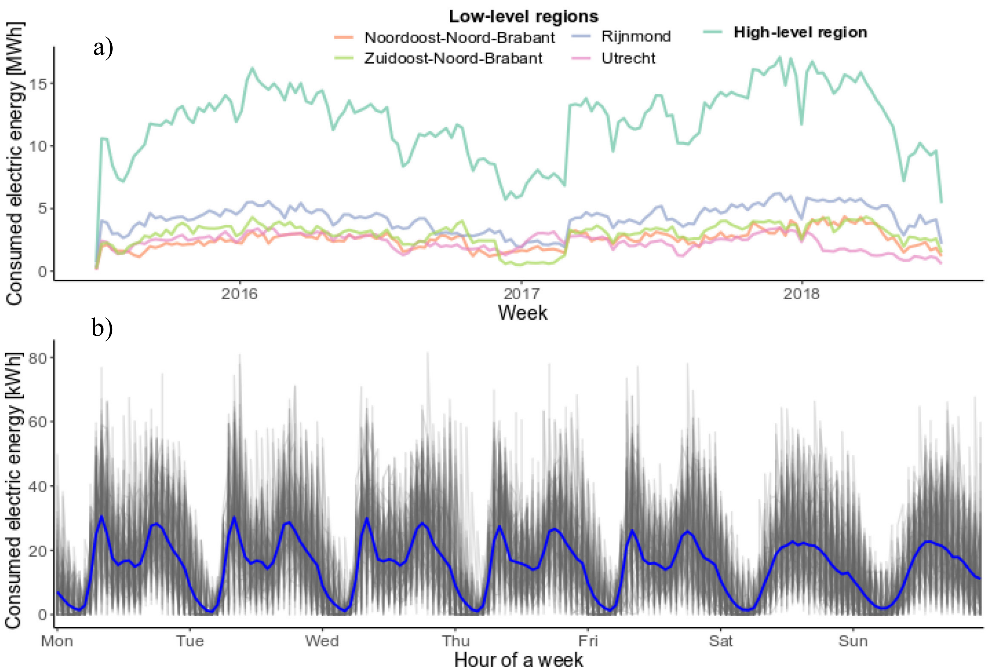

Fig. 4 - (a) Time series of weekly consumption for the considered period for all four used low-level regions and the high-level region (sum of the four regions). (b) Time series of aggregated energy consumption with hourly resolution obtained for the EVnetNL charging stations located in the Noordoost-Noord-Brabant region recorded in the period from February 6 2017 until October 16 2017.

In Fig. 4.a), to illustrate intra-day and weekly seasonality, the time series are overlaid, and the average value is visualized with the thick blue line. The dropdown in energy consumption at the end of 2016 and at the beginning of 2017, most visible for the Zun Brabant and the Rijnmond regions, was caused by the refurbishment of some charging stations to smart charging ready stations and thus they were out of service during this period. The time series of energy consumption of the Noordoost-Noord-Brabant COROP region is displayed in panel B of Figure 4. Similarly, as in the other selected COROP regions, the data display approximately regular patterns with the daily and weekly seasonality. The largest difference in daily patterns is between weekdays and weekend days.

6.2.6 PREPARATION OF PREDICTORS

The exogenous predictors included in the forecasting models are of three types: weather predictors, super-user predictors, and calendar predictors.

Weather forecast data for the area [54] were included to address possible interaction among weather and EV charging patterns. The weather data are associated with geographical locations of the Netherlands having the latitude and the longitude forming regular grids that fully contain the studied low-level geographical regions. As data are typically provided in 0.1°×0.1° partitions, there are multiple weather predictors for a given low-level region, and some weather predictors are shared for two or more low-level regions (this occurs when the 0.1°×0.1° square overlaps two or more low-level regions in proximity to the region borders). It is also worth noting that the EV charging stations are not evenly distributed in the low-level regions, as typically the station distribution is more dense near cities. Therefore, the impact of weather forecasts that are spatially distributed is not theoretically even across the regions. All of the weather forecasts related to the 0.1°×0.1° squares that cover the entire low-level regions are however used as predictors of the forecasting models, but since many of them could be only little informative for the EV load, they are manipulated in a Principal Component Analysis (PCA) module to reduce their dimensionality.

Super-user predictors have been recognized in previous publications as influential for energy consumption [60]. Super users form a relatively small group of EV users that has the above-average energy consumption. Charging patterns of these users are less random and therefore can constitute useful predictors. The number of charging users and the aggregated energy consumption of 100, 300 and 500 users with the highest energy consumption for each region were used as predictors. From these data, the following four predictors were extracted: 1-hour-lagged, 24-hour-lagged, 48-hour-lagged, and 168-hour-lagged energy consumption. Super-user data are manipulated in the PCA module, too.

Eventually, calendar predictors are typical inputs in load forecasting. They capture the social behavior of the EV users that, for example, may change during holidays or weekdays or during the different hours of the day. In this paper, two calendar predictors were considered: a working/nonworking dummy variable *hol* (0 if the observation corresponds to a working day, and 1 otherwise), and an hour-of-the-day integer variable *hod* that assumes a value equal to the hour of the day in which the observation occurs [61]. Calendar predictors are not manipulated in the PCA module but are instead directly included in the vectors of predictors for the baseline models.

For sake of completeness, other types of predictors, such as the total number of circulating EVs in a given region or the total number of charging stations, could be used to forecast the EV load. These predictors are time-varying, but they reasonably do not vary significantly in short-term horizons; therefore, their impact on short-term predictability is limited, whereas it might be of major importance at medium-term horizons. Since this research specifically targets short-term EV load forecasting, these types of predictors are not included in the research.

6.2.7 Principal Component Analysis

PCA is a popular dimension reduction method [62]. The set of predictors is replaced by a smaller set of orthogonal principal component directions along which the data vary the most. This way, the remaining principal components capture most of the variability in data and the number of predictors is reduced.

The number of used predictors is 219. To reduce the dimensionality of inputs, the PCA was applied because the training process of probabilistic forecast approaches is very time consuming and sensitive to the number of predictors. The PCA was applied to all predictors with the exception of calendar predictors, and four principal components were picked as predictors for the baseline models.

7. Results of activities of Task 2.3

Methods for real-time forecast of PV generation and electric vehicle (EV) load have been proposed. More specifically the following models have been carried out:

- two derivative-persistence methods for real-time photovoltaic power forecasting;
- a Bayesian bootstrapping in real-time probabilistic photovoltaic power forecasting;
- a hierarchical probabilistic electric vehicle load forecasting.

With reference to the derivative-persistence method for real-time photovoltaic power forecasting, we focused to forecasting time horizons ranging from few minutes up to few hours, that are those typically categorized as very short-term and short-term forecasting, and that are included in the intra-day scenarios. A derivative-persistence method has been proposed based on information on measured data of the PV power production in the intervals preceding the forecast horizon. Also, a further derivative-persistence method, the Caputo-derivative, has been proposed which uses fractional derivatives in order to take into account the memory effect of the power production.

With regard to the Bayesian bootstrapping in real-time, the research has focused on the application of Bayesian bootstrap in short-term probabilistic PV forecasting. The Bayesian bootstrap was specifically suited up to be applied to three different underlying probabilistic models in order to evaluate potential improvements due to its application. The major aim of this research was indeed to evaluate if the Bayesian bootstrap enabled for better performance and increased skill of the forecasts, compared to the stand-alone usage of the underlying probabilistic models and compared to the application of the traditional bootstrap. Another contribution of the research was the development of the three probabilistic forecasting systems under a new framework that makes the Bayesian bootstrap operate directly on the PV power forecasts, rather than on the parameters of the models. This approach allows reducing the overall computational effort, which is particularly important in short-term forecasting, thanks to the fact that there is no need to pass through the sample bootstrap distributions of the parameters since the sample Bayesian bootstrap distribution of the predictive quantile of PV power is directly provided.

The hierarchical probabilistic EV load forecasting is performed by proposing a methodology dedicated to probabilistic EV load forecasting for low-level geographic regions, which implements a hierarchical perspective to forecast the aggregate load of a high-level geographic region. This methodology can provide comprehensive information on electricity consumption at different levels. The hierarchical approach is applied to decompose the problem into lower-level sub-problems which are resolved through standard probabilistic models.

The proposal was validated using Dataset_PVI2 and Dataset_PVI3, together with the corresponding NWPs contained in Dataset_weath_ECMWF and Dataset_weath_PV [63]. Also, a dataset of measured PV power produced by the GECAD N system installed in Portugal at the Instituto Superior de Engenharia do Porto/Politécnico do Porto was used to test the Caputo-derivative approach [64].

Regarding the PV forecast, the developed methods have been applied to both the actual PV power of the MPPT-controlled PV system and the maximum PV power that can be produced by a controlled PV system. In this latter case, the total solar irradiance is forecasted instead of the PV power output, being the maximum PV power obtained from the solar irradiance through a linear relationship.

7.1. DERIVATIVE-PERSISTENCE METHOD FOR REAL-TIME PHOTOVOLTAIC POWER FORECASTING

The derivative-persistence method deals with a real-time forecasting technique which aims at predicting, on a very-short-term basis, PV power production, based on information on measured data of the PV power production

UNIONE EUROPEA

Ministero dell'Istruzione, dell'Università e della Ricerca

in the intervals preceding the forecast horizon. The same procedure is applied to the forecast of solar irradiance to derive the maximum PV power based on information on measured data of the solar irradiance in the intervals preceding the forecast horizon.

The method is based on the idea to conveniently weight information on past data by imposing continuity of the function, of the first derivative and of the second derivative so obtaining three estimates of the function in the forecast interval. The three estimates are then opportunely weighted to provide the forecast.

The continuity of the function relies to the classical persistence method [4] where the estimate of the power value at the time interval k, $y_{1s}(k)$, is given by

$$y_{1s}(k) = y(k-1) \tag{1}$$

where $y(k-1)$ is the available measured data of PV power at the preceding time interval.

The continuity of the first derivative, $y'(k)$, is imposed at the time instants $(k-1)$ and $(k-2)$, i.e.:

$$y'(k-1) = y'(k-2) \tag{2}$$

where:

$$y'(k-1) = \frac{y(k) - y(k-2)}{2\Delta t} \tag{3}$$

$$y'(k-2) = \frac{y(k-1) - y(k-3)}{2\Delta t} \tag{4}$$

with Δt the duration of the time intervals.

By substituting (3) and (4) in (2) a further estimate of $y(k)$, $y_{2s}(k)$, is found which is given by:

$$y_{2s}(k) = y(k-1) + y(k-2) - y(k-3) \tag{5}$$

The third information is given by imposing the continuity of the second derivative, $y''(k)$, at the time instants $(k-1)$ and $(k-2)$, i.e.:

$$y''(k-1) = y''(k-2) \tag{6}$$

where:

$$y''(k-1) = \frac{y(k) - 2y(k-1) + y(k-2)}{\Delta t^2} \tag{7}$$

$$y''(k-2) = \frac{y(k-1) - 2y(k-2) + y(k-3)}{\Delta t^2} \tag{8}$$

By substituting (7) and (8) in (6) a further estimate of $y(k)$, $y_{3s}(k)$, is found which results:

$$y_{3s}(k) = 3y(k-1) - 3y(k-2) + y(k-3) \tag{9}$$

The forecasted value, $\hat{y}(k)$, is conceived as a proper weighted combination of the three estimates:

$$\hat{y}(k) = \alpha_1(k)\, y_{1s}(k) + \alpha_2(k)\, y_{2s}(k) + \alpha_3(k)\, y_{3s}(k) \tag{10}$$

The weights $\alpha_1(k)$, $\alpha_2(k)$ and $\alpha_3(k)$ are evaluated as detailed in the following equations (11), (12): the weighting procedure is performed in a manner that, in high variability conditions, more weight is given to the first estimate. More specifically, the weights are normalized as follows:

$$\alpha_1(k) = \sqrt{\frac{y_{2s}^2(k) + y_{3s}^2(k)}{y_{1s}^2(k) + y_{2s}^2(k) + y_{3s}^2(k)}} \tag{11}$$

$$\alpha_2(k) = \alpha_3(k) = \frac{1 - \alpha_1(k)}{2} \tag{12}$$

By using equations (11) and (12) to evaluate the weights, the proposed method shapes up to be a non-linear regression being the coefficients $\alpha_1(k)$, $\alpha_2(k)$ and $\alpha_3(k)$ not constant.

7.2. CAPUTO-DERIVATIVE-PERSISTENCE METHOD FOR REAL-TIME PHOTOVOLTAIC POWER FORECASTING

The proposed method deals with a real-time forecasting technique which aims at predicting, on a very-short-term basis, PV power production, based on information on measured data of the PV power production in the intervals preceding the forecast horizon. The same procedure is applied to the forecast of solar irradiance to derive the maximum PV power based on information on measured data of the solar irradiance in the intervals preceding the forecast horizon.

This method carries out estimates of the variable to be forecasted by imposing the continuity of the Caputo derivative of the function at two consecutive time steps.

The Caputo derivative of order α of $y(t)$ is defined as [65]:

$$y^{(\alpha)}(t) = \frac{1}{\Gamma(1-\alpha)} \int_0^t \frac{y'(\xi)}{(t-\xi)^\alpha} d\xi \tag{13}$$

where $\Gamma(\cdot)$ is the Euler Gamma function and $0 < \alpha < 1$.

Let Δt be the time resolution of the forecasting and $y_n = y(n\Delta t)$ be the value of the function y at the point $t_n = n\Delta t$. The approximation of the Caputo derivative proposed in [66] can be constructed by dividing the interval [0, t] into subintervals of equal length Δt and approximating the first derivative on each subinterval using a second-order central difference approximation:

$$y_n^{(\alpha)} = \frac{1}{\Gamma(2-\alpha)\Delta t^{\alpha}} \sum_{k=0}^{n} \sigma_k^{(\alpha)} \, y_{n-k} + \mathcal{O}(\Delta t^{2-\alpha}) \tag{14}$$

where $\mathcal{O}(\Delta t^{2-\alpha})$ is the accuracy of the approximation and the following cases apply for α:

$\sigma_0^{(\alpha)} = 1,$

$\sigma_n^{(\alpha)} = (n-1)^{1-\alpha} - n^{1-\alpha}$

$\sigma_k^{(\alpha)} = (k+1)^{1-\alpha} - 2k^{1-\alpha} + (k-1)^{1-\alpha}, \quad (k = 2, \dots, n-1).$

Eq. (14) can be approximated by neglecting the accuracy $\mathcal{O}(\Delta t)$ so obtaining:

$$y_n^{(\alpha)} = \frac{1}{\Gamma(2-\alpha)\Delta t^{\alpha}} \sum_{k=0}^{n} \sigma_k^{(\alpha)} \, y_{n-k} \tag{15}$$

Starting from this approximation, the continuity of the α-th derivative at the time intervals n and $n-1$ can be imposed (i.e., $y_n^{(\alpha)} = y_{n-1}^{(\alpha)}$):

$$y_n^{(\alpha)} = \frac{1}{\Gamma(2-\alpha)\Delta t^{\alpha}} \sum_{k=0}^{n} \sigma_k^{(\alpha)} \, y_{n-k} = y_{n-1}^{(\alpha)} = \frac{1}{\Gamma(2-\alpha)\Delta t^{\alpha}} \sum_{k=0}^{n-1} \sigma_k^{(\alpha)} \, y_{n-1-k} \tag{16}$$

that is:

$$\sum_{k=0}^{n} \sigma_k^{(\alpha)} \, y_{n-k} = \sum_{k=0}^{n-1} \sigma_k^{(\alpha)} \, y_{n-1-k} \tag{17}$$

and, by isolating the term $k = 0$ by the rest of the sum in the left side of (17), an estimate of y at the nth interval is obtained, given the value of the function in the preceding n intervals:

$$\hat{y}_n = -\sum_{k=1}^{n} \sigma_k^{(\alpha)} \, y_{n-k} + \sum_{k=0}^{n-1} \sigma_k^{(\alpha)} \, y_{n-1-k}. \tag{18}$$

The choice of the number of intervals to include in the sums, indeed, depends on the available historical data and based on the features of their time variation. Its value strictly affects the accuracy of the prediction and then, must be determined according to sensitivity analyses.

The value of α, which is in the range [0,1], can be evaluated at each interval by minimizing the error on the estimates of the predicted variable over a known set of previous measures. Thus, the following formulation based on the root mean squared error is proposed:

$$\alpha = \operatorname{argmin} \sqrt{\frac{1}{n_k} \sum_{k \in \Omega_k} (\hat{y}_k - y_k)^2} \tag{19}$$

subject to

$$0 < \alpha < 1$$

where Ω_k is the set of previous, measured values of the variable and is composed of n_k elements (i.e., $\Omega_k = \{y_{k-n_k}, \dots, y_{k-1}\}$); $\hat{y}_k$ is evaluated according to (18). The number of previous intervals n_k can be determined offline and empirically evaluated on the basis of several issues such as, available data, sensitivity analysis of the forecasted values, computational effort, etc.

7.3. BAYESIAN BOOTSTRAPPING IN REAL-TIME PROBABILISTIC PHOTOVOLTAIC POWER FORECASTING

The use of Bayesian bootstrap has been also proposed for short-time forecast of photovoltaic generation. The same procedure is applied to the forecast of solar irradiance to derive the maximum PV power. The inputs of the PV power forecasting system are NWPs NW and historical PV power data, whereas the inputs of the maximum PV power forecasting system are total irradiance data. Note that NWPs are not added as predictors of the maximum PV power forecasting system due to the limitations encountered in the actual implementation of the forecasting system, but they could be theoretically included as well.

Let's assume to be interested into characterizing a target statistic $\varphi(\boldsymbol{x}) \in \mathbb{R}^s$ that is a function of a (row) vector $\boldsymbol{x} = \{x_1, \dots, x_N\}$ of N_b variables, and let's assume that an estimation $\hat{\varphi}(\boldsymbol{x})$ of the target statistic can be characterized using an available dataset $\boldsymbol{X} = \{\boldsymbol{x}_1, \dots, \boldsymbol{x}_M\}$ that contains M known occurrences of $\boldsymbol{x}$. Bootstrapping is a resampling approach that allows estimating the probabilistic properties of the target statistic by randomly sampling with replacement from data $\boldsymbol{X}$ [67], [68]. Under the previous assumptions, $\boldsymbol{X}$ is a $M \times N_b$ matrix and its generic m^{th} row is $\boldsymbol{x}_m = \{x_{m,1}, \dots, x_{m,N_b}\}$. The M rows of $\boldsymbol{X}$ can theoretically be assumed as M elements extracted from an unknown N_b-variate distribution $F(\boldsymbol{x}) \in \mathcal{F}$, and within a probability distribution framework the estimated target statistic $\hat{\varphi}(\boldsymbol{x})$ retains the statistical properties of a function $G[\cdot]$ applied to $F(\boldsymbol{x})$, i.e., $G[F(\boldsymbol{x})]$, that maps from $\mathcal{F}$ to $\mathbb{R}^s$.

Bootstrapping estimates the target statistic in terms of an empirical R-sample bootstrap distribution $G[F^{\langle 1 \rangle}(\boldsymbol{x})], \dots, G[F^{\langle R \rangle}(\boldsymbol{x})]$, obtained by applying the function $G[\cdot]$ to R replicates $F^{\langle 1 \rangle}(\boldsymbol{x}), \dots, F^{\langle R \rangle}(\boldsymbol{x})$. Specifically, bootstrapping assumes the type of the unknown distribution $F(\boldsymbol{x})$ to be:

$$F(\boldsymbol{x}) = \sum_{m=1}^{M} w_m \cdot \delta_{x_m}, \qquad \sum_{m=1}^{M} w_m = 1 \text{ and } w_m \geq 0, \tag{20}$$

where w_m is a weight assigned to the m^{th} occurrence, and δ_{x_m} is a degenerate probability measure for the m^{th} vector $\boldsymbol{x}_m$. The generic r^{th} replicate is:

$$F^{\langle r\rangle}(\boldsymbol{x}) = \sum_{m=1}^{M} w_m^{\langle r\rangle} \cdot \delta_{x_m}, \qquad \sum_{m=1}^{M} w_m^{\langle r\rangle} = 1 \text{ and } w_m^{\langle r\rangle} \geq 0, \tag{21}$$

where the weights $\boldsymbol{w}^{\langle r\rangle} = \{w_1^{\langle r\rangle}, \dots, w_M^{\langle r\rangle}\}$ are extracted randomly from an assigned M-variate distribution $f_{\boldsymbol{w}}$.

In traditional bootstrap, the distribution $f_{\boldsymbol{w}}$ from which the weights $\boldsymbol{w}^{\langle r\rangle}$ are extracted is the multinomial distribution in M dimensions with equal probabilities $1/M$, i.e.:

$$f_{\boldsymbol{w}} = \mathrm{Mul}(w_1, \dots, w_M | M; 1/M, 1/M, \dots, 1/M) = \frac{M!}{w_1! \dots w_M!} \prod_{m=1}^{M} \left(\frac{1}{M}\right)^{w_m}; \tag{22}$$

the M-variate sample extracted from (22) is then normalized by M, to meet the constraint $\sum_{m=1}^{M} w_m^{\langle r\rangle} = 1$.

In Bayesian bootstrap, instead, the weights $\boldsymbol{w} = \{w_1, \dots, w_M\}$ are estimated through the Bayesian inference upon the observed probabilities $\widehat{\boldsymbol{w}} = \{\widehat{w}_1, \dots, \widehat{w}_M\}$ of data $\boldsymbol{x}_1, \dots, \boldsymbol{x}_M$ in $\boldsymbol{X}$. The posterior distribution $p(\boldsymbol{w}|\widehat{\boldsymbol{w}}, \boldsymbol{\alpha})$ of the weights is obtainable by assigning a prior distribution $p(\boldsymbol{w}|\boldsymbol{\alpha})$ to the objective weights $\boldsymbol{w}$, which has parameters $\boldsymbol{\alpha}$. To allow the calculation of the posterior distribution in closed form, the prior distribution is selected as a conjugate prior of the likelihood. Since the likelihood is multinomial [69], [70], the prior distribution is a symmetric Dirichlet:

$$p(\boldsymbol{w}|\boldsymbol{\alpha}) = \mathrm{Dir}(w_1, \dots, w_M | \alpha, \dots, \alpha) = \frac{1}{\mathrm{B}(\boldsymbol{\alpha})} \cdot \prod_{m=1}^{M} w_m^{(\alpha-1)}, \tag{23}$$

where $\mathrm{B}(\boldsymbol{\alpha})$ is the Beta function calculated on the M-dimensional vector $\boldsymbol{\alpha} = \{\alpha, \dots, \alpha\}$. With this position, the corresponding posterior distribution is a Dirichlet too:

$$p(\boldsymbol{w}|\widehat{\boldsymbol{w}}, \boldsymbol{\alpha}) = \mathrm{Dir}(w_1, \dots, w_M | \alpha + M\widehat{w}_1, \dots, \alpha + M\widehat{w}_M) = \frac{1}{\mathrm{B}(\alpha + M\widehat{w}_1, \dots, \alpha + M\widehat{w}_M)} \cdot \prod_{m=1}^{M} w_m^{(\alpha + M\widehat{w}_m - 1)}. \tag{24}$$

If the prior is uninformative, as in [69], [70], $\alpha = 0$ and:

$$p(\boldsymbol{w}|\widehat{\boldsymbol{w}}, \boldsymbol{0}) = \mathrm{Dir}(w_1, \dots, w_M | M\widehat{w}_1, \dots, M\widehat{w}_M) = \frac{1}{\mathrm{B}(M\widehat{w}_1, \dots, M\widehat{w}_M)} \cdot \prod_{m=1}^{M} w_m^{(M\widehat{w}_m - 1)}, \tag{25}$$

which, for continuous variables, can be further and reasonably written as $\mathrm{Dir}(w_1, \dots, w_M | 1, \dots, 1)$ since the observed rows $\boldsymbol{x}_1, \dots, \boldsymbol{x}_M$ likely have the probability $1/M$ to occur (i.e., only once in the entire dataset $\boldsymbol{X}$) [69].

In Bayesian bootstrap, in summary, the distribution $f_{\boldsymbol{w}}$ from which the weights $\boldsymbol{w}^{\langle r\rangle}$ are directly extracted is the M-variate flat Dirichlet distribution, i.e.:

$$f_{\boldsymbol{w}} = \mathrm{Dir}(w_1, \dots, w_M | 1, \dots, 1). \tag{26}$$

Once the weights are extracted, the function $G[\cdot]$ is applied to $F^{\langle 1\rangle}(\boldsymbol{x}), \dots, F^{\langle R\rangle}(\boldsymbol{x})$ given by (3), and the R-sample Bayesian bootstrap distribution $G\left[F^{\langle 1\rangle}(\boldsymbol{x})\right], \dots, G[F^{\langle 1\rangle}(\boldsymbol{x})]$ is the output of the Bayesian bootstrap that gives an estimation $\hat{\varphi}(\boldsymbol{x})$ of the target statistic.

7.3.1 Applications of the Bayesian bootstrap to probabilistic models for PV power forecasting

Traditional bootstrap is commonly applied in forecasting problems to generate probabilistic predictions or to characterize the uncertainty of predictive parameters [67]. In this research, the Bayesian bootstrap is applied to three probabilistic forecasting models – Linear Quantile Regression (LQR), Gradient Boosting Regression Tree (GBRT) and Quantile Regression Neural Network (QRNN) - to provide sample bootstrap distributions of the predictive quantiles of PV power. The models, selected from the literature, are purposely very heterogeneous by nature in order to evaluate the performance of the Bayesian bootstrap within different forecasting frameworks.

The three probabilistic forecasting model are briefly recalled in Appendix; then the role of Bayesian bootstrap in the forecasting system and a procedure to optimize the Bayesian-bootstrap-based predictions are detailed in the second part of this Section.

As discussed above, in either the LQR, the GBRT or the QRNN the α_q-quantile $P_h^{\langle\alpha_q\rangle}$ of PV power for the target horizon h can be viewed as a function of the predictors $\boldsymbol{z}$ and of the PV power $\boldsymbol{P}$. In this sense, the predictive α_q-quantile $\hat{P}_h^{\langle\alpha_q\rangle}$ of PV power for the target horizon h can be viewed as a function of the training data $\boldsymbol{Y}^{\langle tr\rangle} = [\boldsymbol{P}^{\langle tr\rangle}\ \boldsymbol{Z}^{\langle tr\rangle}]$, and thus it can be viewed as a target statistic calculated on M_{tr} variables, with occurrences contained in $\boldsymbol{Y}^{\langle tr\rangle}$. Therefore, the Bayesian bootstrap can be directly applied to evaluate the sample Bayesian bootstrap distribution of the predictive α_q-quantile $\hat{P}_h^{\langle\alpha_q\rangle}$ of PV power, with the following correspondences:

$$
\begin{aligned}
&\boldsymbol{x} = \boldsymbol{y} = [\boldsymbol{P}\ \boldsymbol{z}], \qquad && \boldsymbol{X} = \boldsymbol{Y}^{\langle tr\rangle} = [\boldsymbol{P}^{\langle tr\rangle}\ \boldsymbol{Z}^{\langle tr\rangle}],\\
&\varphi(\boldsymbol{x}) = P_h^{\langle\alpha_q\rangle}(\boldsymbol{y}), && \hat{\varphi}(\boldsymbol{x}) = \hat{P}_h^{\langle\alpha_q\rangle}\left(\boldsymbol{Y}^{\langle tr\rangle}\right),\\
&M = M_{tr}, \qquad N_b = N + 1. &&
\end{aligned} \tag{27}
$$

The sample Bayesian bootstrap distribution is constituted by R replicates of the predictive α_q-quantile $P_h^{\langle\alpha_q\rangle}$ of PV power, i.e., $\hat{\boldsymbol{P}}_h^{\langle\alpha_q\rangle} = \{\hat{P}_h^{\langle\alpha_q,1\rangle}, \dots, \hat{P}_h^{\langle\alpha_q,R\rangle}\}$. The necessary steps to calculate them are hereby summarized:

1) R weight samples $\boldsymbol{w}^{\langle 1\rangle}, \dots, \boldsymbol{w}^{\langle R\rangle}$ are independently drawn from distribution (48) (reported in Appendix);

2) $F^{\langle 1\rangle}(\boldsymbol{x}), \dots, F^{\langle R\rangle}(\boldsymbol{x})$ are calculated by applying (21);

3) $G\left[F^{\langle 1\rangle}(\boldsymbol{x})\right], \dots, G\left[F^{\langle R\rangle}(\boldsymbol{x})\right]$ are calculated by applying either (51)-(53) (reported in Appendix) for the LQR, (60)-(64) (reported in Appendix) for the GBRT, or (66)-(67) (reported in Appendix) for the QRNN;

4) $\hat{P}_h^{\langle\alpha_q,r\rangle} = G\left[F^{\langle r\rangle}(\boldsymbol{x})\right]$ for $r = 1, \dots, R$.

7.3.2 OPTIMIZING THE BAYESIAN-BOOTSTRAP-BASED PREDICTIONS

Dealing with a sample bootstrap distribution of predictive quantiles may be not friendly for power system operators, who are the end-users of the PV power forecasts but are usually unaware of the statistical background behind the predictions. Also, most of the probabilistic decision-making tools in power systems accept input probabilistic forecasts of PV power given either in terms of predictive distribution or in terms of a set of predictive quantiles [71]. For this reason, two procedures to extract an optimal predictive quantile from the sample Bayesian bootstrap distribution are developed in this research, in order to put the forecasting system in line with the needs of operators and practitioners.

The first procedure (SM-BB) is naïve and it simply consists of picking the sample mean from the sample Bayesian bootstrap distribution $\widehat{\boldsymbol{P}}_h^{\langle\alpha_q\rangle}$ as the optimal predictive α_q-quantile of PV power $\hat{P}_h'^{\langle\alpha_q\rangle}$ for the target horizon h, i.e.:

$$\hat{P}_h'^{\langle\alpha_q\rangle} = \frac{1}{R}\sum_{r=1}^{R} \hat{P}_h^{\langle\alpha_q,r\rangle}. \tag{28}$$

The sample mean performs well in most scenarios, plus it does not exactly require a rigorous "optimization", allowing for its usage per se.

The second procedure Optimal Quantile Bayesian Bootstrap (OQ-BB) consists of picking a sample quantile from the sample Bayesian bootstrap distribution $\widehat{\boldsymbol{P}}_h^{\langle\alpha_q\rangle}$ as the optimal predictive α_q-quantile of PV power $\hat{P}_h'^{\langle\alpha_q\rangle}$ for the target horizon h, i.e.:

$$\hat{P}_h'^{\langle\alpha_q\rangle} = \hat{P}_h^{\langle\alpha_q,r^*\rangle}, \tag{29}$$

where $\hat{P}_h^{\langle\alpha_q,r^*\rangle}$ is the value that is smaller than a σ^* fraction of the samples in $\widehat{\boldsymbol{P}}_h^{\langle\alpha_q\rangle}$ or, equivalently, $100 \cdot (1-\sigma^*)\%$ of the samples in $\widehat{\boldsymbol{P}}_h^{\langle\alpha_q\rangle}$ are greater than $\hat{P}_h^{\langle\alpha_q,r^*\rangle}$. The fraction σ^* is a result of an optimization problem that minimizes the Pinball Score (PS) over a validation dataset with indices $\Omega^{\langle va\rangle}$ (this validation dataset may or may not have overlap with the training dataset; the latter option is preferable). It is:

$$\sigma^* = \underset{\sigma}{\operatorname{argmin}} \sum_{t\in\Omega^{\langle va\rangle}} \left\{\alpha_q - \mathrm{I}\left[P_t \le \hat{P}_t^{\langle\alpha_q,r^*\rangle}\right]\right\} \cdot \left(P_t - \hat{P}_t^{\langle\alpha_q,r^*\rangle}\right), \tag{30}$$

with $\hat{P}_t^{\langle\alpha_q,r^*\rangle} = \inf\{\hat{P}_t^{\langle\alpha_q,r\rangle} \in \widehat{\boldsymbol{P}}_t^{\langle\alpha_q\rangle} : \hat{F}_{BB,t}^{\langle\alpha_q\rangle}\left(P_t \le \hat{P}_t^{\langle\alpha_q,r\rangle}\right) \ge \sigma\}$, and $\hat{F}_{BB,t}^{\langle\alpha_q\rangle}$ is the cumulative distribution obtained from the sample Bayesian bootstrap distribution of the predictive α_q-quantile of PV power at time t.

UNIONE EUROPEA

Ministero dell'Istruzione, dell'Università e della Ricerca

7.3.3 Hints on the selection of the size of the sample Bayesian bootstrap distribution

The size R of the sample bootstrap distribution certainly has an impact on the overall performance of the forecasting system. This topic has been discussed extensively in the literature in the traditional bootstrap framework, but there is no general agreement about how the sample size should be arranged with respect to the number of available data M. Optimizing R through a random search upon a validation set is in general a good practice and this should also be valid for the Bayesian bootstrap; theoretically, there are no boundaries in which the optimal R should be searched. However, there are some practical limitations:

1) the Bayesian bootstrap is originally applied in this research to a particular statistic, i.e., the predictive quantile of PV power, and therefore the function $G[\cdot]$ intrinsically contains the formulation of the training procedure of the probabilistic forecasting model. For models that require a non-trivial solution of the training procedure (as in the case of the GBRT and QRNN), increasing R determines an increased computational complexity that is not in line with some short-term forecasting lead times using standard workstations;

2) increasing R does not necessarily increase the performance of the forecasts. We found in our numerical experiments that optimal values for R are across a 1:100 ratio between R and M, as performance deteriorates with greater R.

For these reasons, the search for the optimal R is performed within this range.

7.3.4 Background of the performance assessment

The performance of Bayesian bootstrap in probabilistic PV power forecasting is assessed in a wide comparative framework. Several benchmarks and error indices and scores are exploited for this assessment.

Benchmarks

Several benchmarks are considered to compare the outcomes of the Bayesian-bootstrap-based forecasts and to highlight pros and cons with respect to existing literature.

The first group of benchmarks aims at evaluating how the Bayesian bootstrap performs with reference to the traditional bootstrap. This group therefore includes three forecasting systems (LQR-TB, GBRT-TB, and QRNN-TB) that apply the traditional bootstrap to build the sample traditional bootstrap distribution of the predictive quantiles of PV power, respectively applying an LQR, a GBRT and a QRNN model. The extraction of the optimal prediction from the traditional bootstrap distribution is performed applying the SM and the OQ procedures. Therefore, the only difference with the presented Bayesian-bootstrap forecasts consists of the different bootstrap procedure applied in first place.

The second group of benchmarks aims at evaluating if, in general, the bootstrap increases the performance or not. This group therefore includes three forecasting systems (LQR-NB, GBRT-NB, and QRNN-NB) that directly predict the quantiles of PV power, respectively applying an LQR, a GBRT and a QRNN model, without any bootstrap.

The third group of benchmarks is instead based on persistence models, and they are provided as an unbiased reference for the performance evaluation. This group includes two benchmarks: the PM1 that assumes the predictive quantiles for the target horizon equal to the last observed PV power, i.e.:

$$\hat{P}_h^{\langle\alpha_q\rangle} = P_{h-k}, \qquad \forall q = 1, \dots, Q, \tag{31}$$

and the PM2 that assumes the predictive quantiles for the target horizon equal to the PV power observed in the same time slot of the day before. For an hourly time resolution, e.g., the PM2 returns:

$$\hat{P}_h^{\langle\alpha_q\rangle} = P_{h-24}, \qquad \forall q = 1, \dots, Q. \tag{32}$$

Probabilistic error indices and scores

Three error indices are used to compare the accuracy of the proposed forecasting method with the other methods which have been used as benchmark. In what follows, the definition of the PS metric is first recalled. Beyond comparisons, this metric is also used into the application of the linear LQR method. Then, the average absolute coverage error (AACE) and the prediction intervals normalized width (PINAW) are briefly introduced.

Pinball score

PS allows addressing the accuracy of the prediction by evaluating, at the same time, the reliability and the sharpness of the forecasted values [72], [73]. It is used in all the three considered models as the loss function to be minimized to train the corresponding parameters as it is a negatively oriented error measure (i.e., a smaller PS indicates a better forecast performance). It is here recalled that PS is defined as:

$$PS\left[P_h, \hat{P}_h^{\langle\alpha_q\rangle}\right] = \left\{\alpha_q - \mathrm{I}\left[P_h \le \hat{P}_h^{\langle\alpha_q\rangle}\right]\right\} \cdot \left(P_h - \hat{P}_h^{\langle\alpha_q\rangle}\right). \tag{33}$$

In order to obtain a measure of the forecast performance in a comprehensive manner, the value of PS can be evaluated by averaging the values it assumes across multiple forecast issues and summing over the Q quantiles. In the numerical experiments, a normalized version of the PS is used for evaluating performance in the test period. The Normalized Pinball Score (NPS) is defined as:

$$NPS\left[P_h, \hat{P}_h^{\langle\alpha_q\rangle}\right] = \frac{PS\left[P_h, \hat{P}_h^{\langle\alpha_q\rangle}\right]}{\bar{P}_{\mathrm{rated}}}, \tag{34}$$

where $\bar{P}_{\mathrm{rated}}$ is the rated power of the PV system.

Average Absolute Coverage Error

The AACE is used to assess the reliability of the forecasting method, by quantifying the difference of the predicted values and the nominal coverages of the predictive quantiles [74]. AACE can only be formulated for multiple forecast issues. For a test set with indices $\Omega^{\langle te\rangle}$, the estimated α_q-coverage $\hat{\alpha}_q$ is provided by:

$$\hat{\alpha}_q = \frac{1}{M_{te}} \sum_{t\in\Omega^{\langle te\rangle}} \mathrm{I}\left[P_t, \hat{P}_t^{\langle\alpha_q\rangle}\right], \tag{35}$$

with M_{te} the size of the considered test set. The absolute coverage error on the nominal α_q-quantile, $ACE^{\langle\alpha_q\rangle}$, is defined as:

$$ACE^{\langle\alpha_q\rangle} = \left|\alpha_q - \hat{\alpha}_q\right|. \tag{36}$$

and the percentage value of AACE, $AACE_{\%}$, across the Q coverages can be easily derived as a percentage value of $ACE^{\langle\alpha_q\rangle}$, as:

$$AACE_{\%} = \frac{100}{Q} \cdot \sum_{q=1}^{Q} ACE^{\langle\alpha_q\rangle}. \tag{37}$$

AACE is a negatively oriented metric, i.e., smaller is the value it assumes, more reliable is the forecast method.

Prediction intervals normalized width

The PINAW is used to assess the sharpness of the forecasting method, by quantifying the width of the prediction intervals [74]. It is a property of the forecast by itself, so this index is not calculated considering the actual PV power outcomes. For a test set of size M_{te} with indices $\Omega^{\langle te\rangle}$, the PINAW at the nominal prediction interval rate λ is:

$$PINAW^{\lambda} = \frac{1}{M_{te}} \sum_{t\in\Omega^{\langle te\rangle}} \frac{\hat{P}_t^{\langle 0.5+\lambda/2\rangle} - \hat{P}_t^{\langle 0.5-\lambda/2\rangle}}{\bar{P}_{\text{rated}}}, \tag{38}$$

PINAW is a negatively oriented metric, i.e., smaller is the value it assumes, sharper are the forecasts

7.4. HIERARCHICAL PROBABILISTIC ELECTRIC VEHICLE LOAD FORECASTING

A hierarchical approach for PEVLF is proposed, focusing on several probabilistic forecasting models that have been used with success [75]-[77] in PLF (i.e., LQR [78], GBRT [79], Quantile Regression Forests (QRFs) [80], and QRNN [81]). The hierarchical approach is applied to decompose the problem into lower-level sub-problems, i.e., forecasting the EV load of smaller lower-level geographic regions, which are resolved through standard probabilistic models (either GBRT, QRF and QRNN). Differently from other works, the PEVLF problem is finalized at higher-level through an ensemble methodology based on an l1-Penalized LQR (PLQR) model, in which the penalization adds robustness to the hierarchical model with respect to outliers and abnormal inputs.

Compared to a single-model approach for each series within a higher-level hierarchy, forecasts are improved thanks to the exploitation of information related to lower-level regions.

The proposed hierarchical PEVLF system consists of three main units: i) an input data pre-processing unit, including the PCA reported in Section 7.2 to reduce the data dimensionality; ii) the baseline probabilistic forecasting unit for the low-level regions; iii) the hierarchical probabilistic forecasting unit for the high-level region. Figure 5 illustrates the workflow of the proposed hierarchical PEVLF system.

For consistency of symbols, the forecast horizon is indicated with h, the forecast lead time is indicated with k, and thus the forecast origin is $h-k$. To differentiate vectors from scalars, the former are indicated with bold symbols. We will also refer to data (and forecasts) having hourly time resolution, for sake of clarity; nevertheless the proposal can be easily adapted to other time resolution frameworks.

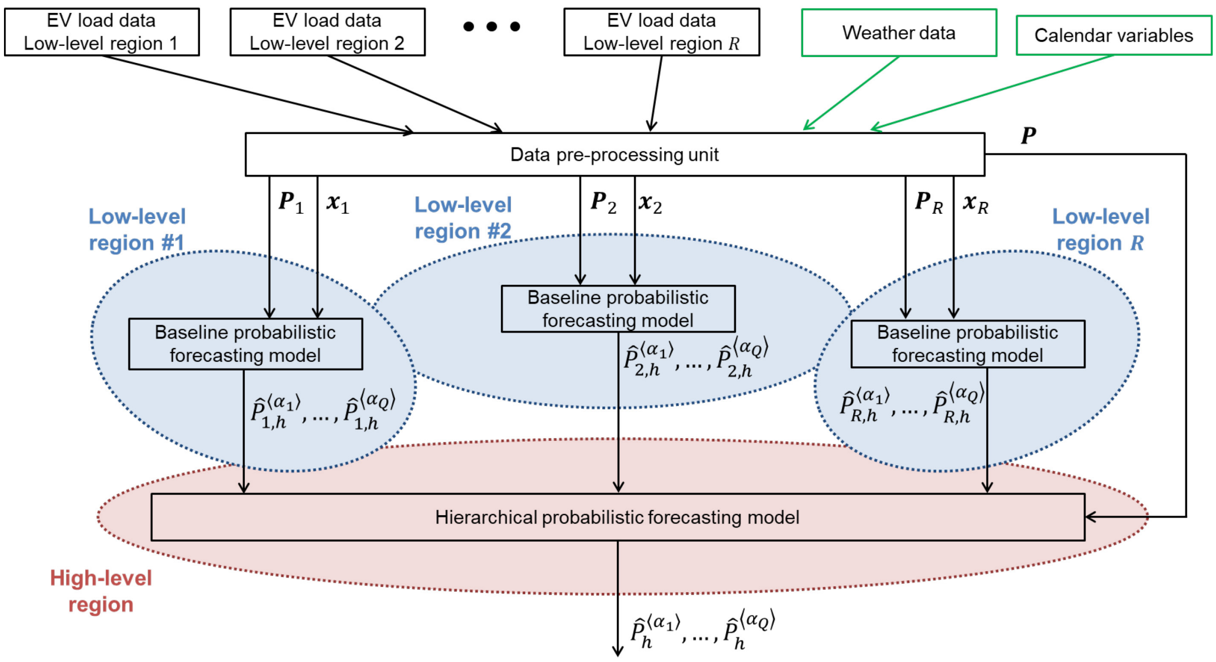

Fig. 5 - Workflow of the hierarchical PEVLF system.

7.4.1 DATA PRE-PROCESSING UNIT

The data pre-processing unit reported in Section 7.2 is aimed at: i) extracting the time series of EV load at the desired time resolution for the low-level regions ($\boldsymbol{P}_i = \{P_{i,1}, P_{i,2}, \ldots, P_{i,n}, \ldots, P_{i,h-k}\}$, $i = 1, \ldots, R$) and for the high-level region ($\boldsymbol{P} = \{P_1, P_2, \ldots, P_n, \ldots, P_{h-k}\}$) from the available readings at the charging stations; ii) preparing the predictors of the forecasting models that include also external data, such as numeric weather predictions (e.g., precipitation forecasts) and calendar predictors (e.g., a dummy variable to discern working days from holidays); iii) arranging the predictor data in a Principal Component Analysis (PCA) module that allows reducing the dimensionality of the problem, which is particularly challenging in probabilistic forecasting as model training is computationally intensive. This allows getting the arranged predictors for the low-level regions ($\boldsymbol{x}_i = \{\boldsymbol{x}_{i,1}, \boldsymbol{x}_{i,2}, \dots, \boldsymbol{x}_{i,n}, \dots, \boldsymbol{x}_{i.h-k}\}$, $i = 1, \dots, R$), that are inputs of the baseline probabilistic models.

7.4.2 BASELINE PROBABILISTIC FORECASTING UNIT

The baseline probabilistic forecasting unit is responsible for the generation of the probabilistic predictions of EV load at the i^{th} low-level region, exploiting the input data (historical EV load data $\boldsymbol{P}_i = \{P_{i,1}, P_{i,2}, \dots, P_{i,n}, \dots, P_{i,h-k}\}$ and predictors $\boldsymbol{x}_i = \{\boldsymbol{x}_{i,1}, \boldsymbol{x}_{i,2}, \dots, \boldsymbol{x}_{i,n}, \dots, \boldsymbol{x}_{i,h-k}\}$, $i = 1, \dots, R$) pre-processed in the previous unit. In order to evaluate the performance of the hierarchical system under different conditions and to demonstrate that, no matter which is the baseline model used at low-level regions, the hierarchical system is able to improve the skill of the forecasts at the high-level region when compared to a direct non-hierarchical approach, three different models are used in this unit: GBRT, QRF and QRNN. The outputs of the baseline probabilistic forecasting unit consist of Q predictive EV load quantiles $\hat{P}_{i,h}^{\langle\alpha_1\rangle}, \dots, \hat{P}_{i,h}^{\langle\alpha_Q\rangle}$ at coverages $\alpha_1, \dots, \alpha_Q$ of the i^{th} low-level region for the target forecast horizon h. This is obviously accomplished for $i = 1, \dots, R$, where R is the total number of considered low-level regions.

7.4.3 HIERARCHICAL PROBABILISTIC FORECASTING UNIT

The hierarchical probabilistic forecasting unit is dedicated to combine the predictions coming from the previous unit in order to generate the probabilistic forecasts $\hat{P}_h^{\langle\alpha_1\rangle}, \dots, \hat{P}_h^{\langle\alpha_Q\rangle}$ of EV load at the high-level region for the target horizon h. This combination is performed through a PLQR model, which is applied to an input dataset that includes the baseline forecasts and historical high-level EV load data $\boldsymbol{P} = \{P_1, P_2, \dots, P_n, \dots, P_{h-k}\}$. The penalization is applied to make the model more robust towards outliers. The hierarchical system is expected to increase the skill of the forecasts at the high-level region by exploiting the information contained at the lower level. Also, the PLQR model parameters can be estimated iteratively as new observations become available, thus allowing for exploiting the information brought by recent loads without re-training the baseline models (this would be more challenging in terms of computational time, because multiple models - one for each low-level region - should be trained iteratively).

In this research the EV load forecasts at the low-level regions are obtained through a baseline probabilistic model. Probabilistic forecasts of the i^{th} region for the forecast horizon h are provided in each case through Q

predictive EV load quantiles $\hat{P}_{i,h}^{\langle\alpha_1\rangle},\dots,\hat{P}_{i,h}^{\langle\alpha_Q\rangle}$, at coverages $\alpha_1,\dots,\alpha_Q$ respectively. Three different baseline models were explored (i.e., GBRT, QRF and QRNN) in our proposal, in order to evaluate performance under different circumstances. Brief analytic details on these models are reported in Appendix. Analytic formulations are generically referred to the EV load in the i^{th} low-level region, reminding that this is iterated for $i=1,\dots,R$. Eventually, $\Omega_{tra}^{\langle B\rangle}$ denotes the index set that individuates the data used to train the baseline models. For example, the dataset $\boldsymbol{P}_{i,tra}^{\langle B\rangle}=\{P_{i,n},n\in\Omega_{tra}^{\langle B\rangle}\}$ contains the historical EV loads in the i^{th} low-level region that are the dependent variables to train the baseline models for the i^{th} low-level region.

7.4.4 HIGHER LEVEL OF THE HIERARCHICAL PROBABILISTIC FORECASTING UNIT

A hierarchical PLQR model is applied to combine the baseline forecasts of EV load at the low-level regions, generating the forecasts at the high-level region. The hierarchical PLQR model is trained upon the data individuated by an index set $\Omega_{tra}^{\langle H\rangle}$ (for example, $\boldsymbol{P}_{tra}^{\langle H\rangle}=\{P_n,n\in\Omega_{tra}^{\langle H\rangle}\}$ is the dataset that contains the EV loads in the high-level region that are the dependent variables of the PLQR model). The B predictors $\boldsymbol{x}_h^{\langle H\rangle}$ of the PLQR model for the target horizon h are the baseline forecasts of the R considered low-level regions $\hat{P}_{i,h}^{\langle\alpha_1\rangle},\dots,\hat{P}_{i,h}^{\langle\alpha_Q\rangle}$, $\forall i=1,\dots,R$, and lagged high-level EV loads (up to the 24-hours lagged EV load, i.e., $P_{h-k},P_{h-k-1},\dots,P_{h-24}$, 2-days lagged EV load P_{h-48}, and 1-week lagged EV load P_{h-168}).

The predictive α_q-quantile of the high-level EV load at the target horizon h returned by the PLQR model is analytically formulated as:

$$\hat{P}_h^{\langle\alpha_q\rangle}=\boldsymbol{x}_h^{\langle H\rangle}\cdot\hat{\boldsymbol{\beta}}^{\langle\alpha_q\rangle}\ , \tag{39}$$

where $\hat{\boldsymbol{\beta}}^{\langle\alpha_q\rangle}$ is the vector (having the same cardinality B of $\boldsymbol{x}_h^{\langle H\rangle}$) of coefficients for the α_q-quantile, and they are estimated by solving the following l1-penalized minimization problem over the high-level EV load training dataset $\boldsymbol{P}_{tra}^{\langle H\rangle}=\{P_n,n\in\Omega_{tra}^{\langle H\rangle}\}$:

$$\hat{\boldsymbol{\beta}}^{\langle\alpha_q\rangle}=\underset{\boldsymbol{\beta}^{\langle\alpha_q\rangle}}{\operatorname{argmin}}\frac{1}{\dim\left(\Omega_{tra}^{\langle H\rangle}\right)}\sum_{n\in\Omega_{tra}^{\langle H\rangle}}\left[\Psi\left(P_n,\hat{P}_n^{\langle\alpha_q\rangle}\right)\right]+\lambda\sum_{b=1}^{B}\left|\beta_b^{\langle\alpha_q\rangle}\right|\ , \tag{40}$$

where $\dim(\Omega_{tra}^{\langle H\rangle})$ is the number of training points in the set $\Omega_{tra}^{\langle H\rangle}$, λ is the parameter that controls the regularization effectiveness, and $\Psi\left(P_n,\hat{P}_n^{\langle\alpha_q\rangle}\right)$ is the PS as defined above. The minimized function in (40) is indeed easily interpretable, since it is the PS penalized by the l1-norm of the coefficient vector.

The selection of the predictors $\boldsymbol{x}_h^{\langle H\rangle}$ is performed by exploiting the intrinsic properties of the l1-regularized model. In practice, the penalization effect (driven by the value of λ) sets some estimated parameters in the vector $\hat{\boldsymbol{\beta}}^{\langle\alpha_q\rangle}$ as zero. This is equivalent to performing model selection, since predictors that are multiplied by zero coefficients have no impact on the dependent variable. Obviously, λ becomes an important hyper-parameter of the PLQR, as greater λ values determine more parameters that are set as zero (or, equivalently, more predictors that are discarded). Therefore, it is optimized in 10-fold cross-validation across the training dataset $\boldsymbol{P}_{tra}^{\langle H \rangle} = \{P_n, n \in \Omega_{tra}^{\langle H \rangle}\}$.

7.4.5 FORECAST ASSESSMENT: BENCHMARKS AND ERROR INDICES

The proposed hierarchical probabilistic EV load forecasting model is validated considering its performance against several benchmarks. Since the proposal performs forecasts for the low-level regions and forecasts for the high-level regions, different benchmarks are developed for the baseline forecasts and for the hierarchical forecasts, in order to highlight the improvements brought by the proposal in each stage. The comparative assessment framework is based in both cases on the usage of relevant probabilistic error indices [82].

Benchmarks for baseline forecasts

To evaluate the skill of the forecasts provided by the baseline models for the low-level regions (these will be indicated as "GBRT baseline", "QRF baseline" and "QRNN baseline" hereinafter), four benchmarks are introduced.

The first three benchmarks consist of the application of GBRT, QRF and QRNN models using input predictors that are not processed through PCA. These benchmarks are respectively labeled as "GBRT no PCA", "QRF no PCA" and "QRNN no PCA". They are introduced in the comparative framework in order to evaluate whether the PCA yields additive skill to the baseline forecasts, with respect to the case in which raw predictors are directly sent to the probabilistic underlying models. To fairly compare the outcomes, the same predictors and the same model selection procedure are considered for the GBRT, QRF and QRNN models in the "baseline" and in "no PCA" benchmarks.

The fourth benchmark (BPersB) is a persistence model that is introduced in order to provide a simple, unbiased reference. BPersB returns the last observed value in one-step-ahead forecasting:

$$\hat{P}_{i,h}^{\langle \alpha_q \rangle} = P_{i,h-1} \qquad \text{for } q = 1, \dots, Q, \tag{41}$$

or the homologous value observed the day before in day-ahead forecasting:

$$\hat{P}_{i,h}^{\langle \alpha_q \rangle} = P_{i,h-24} \qquad \text{for } q = 1, \dots, Q. \tag{42}$$

Thus, the predicted value is the same, whatever the quantile nominal coverage is. Although based on a naïve approach, this benchmark is often presented in the energy forecasting literature [77] to allow for a straightforward evaluation of different models against the same reference.

Benchmarks for hierarchical forecasts

Seven benchmarks are introduced with the scope to evaluate the skill of the forecasts provided by the hierarchical forecasting system for the high-level region.

The first three benchmarks consist of the application of GBRT, QRF and QRNN models to directly forecasts the EV load at the high-level region. These benchmarks, respectively labeled as "GBRT direct", "QRF direct", and "QRNN direct", are introduced in order to check if a direct approach for forecasting the EV load at the high-level region performs better than passing through the baseline forecasts of the component regions.

The fourth benchmark consists of applying a simple sum-and-sort (SaS) of the homologous baseline predictive quantiles returned by the baseline forecasting models [52]. This benchmark performs the simplest combination of individual forecasts because it simply sums up the sorted homologous quantiles. It is therefore useful to evaluate it against the proposal that considers instead a PLQR-based combination of baseline forecasts, to check whether a simplest combination approach would surpass the proposal.

The fifth benchmark consists of a non-penalized quantile regression model (NPLQR, i.e., with $\lambda = 0$) using the same inputs considered for the PLQR model discussed above. This benchmark is introduced to evaluate whether the l_1-penalization is useful in order to reduce the importance of uninformative predictors at the high-level forecasting.

The sixth benchmark consists of a PLQR model using only the baseline forecasts, without exploiting the lagged high-level EV loads as additional predictors. This benchmark denoted as "PLQR no recency" is added to validate the importance of recency effects in hierarchical forecasting.

The seventh benchmark (HPersB) consists of a persistence model that is again introduced in order to provide a simple, unbiased reference.

Probabilistic error indices

The skill of probabilistic forecasts is comprehensively evaluated through strictly proper scores [82]. However, the reliability of probabilistic forecasts should be separately investigated in order to evaluate if the predictive coverages are close to the nominal coverages [83].

In this paper, the PS is the strictly proper score used to comprehensively evaluate the accuracy of forecasts. The PS of forecasts, belonging to a generic index set Ω, is calculated as:

$$PS = \sum_{q=1}^{Q}\left[\frac{1}{\dim(\Omega)}\sum_{n\in\Omega}\Psi\left(P_n, \hat{P}_n^{\langle\alpha_q\rangle}\right)\right] = \sum_{q=1}^{Q}\left[\frac{1}{\dim(\Omega)}\sum_{n\in\Omega}\left(P_n - \hat{P}_n^{\langle\alpha_q\rangle}\right)\cdot\left(\alpha_q - \mathrm{I}\left\{P_n \le \hat{P}_n^{\langle\alpha_q\rangle}\right\}\right)\right], \tag{43}$$

with $\dim(\Omega)$ the number of points in the set Ω. The PS is therefore a negatively oriented score, since smaller values denote more accurate probabilistic forecasts.

The reliability of forecasts is instead evaluated qualitatively through the reliability diagrams [84], which plot the predictive coverages $\hat{\alpha}_q$ against the nominal coverages α_q, $q = 1, \dots, Q$. The predictive coverages of forecasts belonging to a set Ω are evaluated as:

$$\hat{\alpha}_q = \frac{1}{\dim(\Omega)} \sum_{n\in\Omega} \mathrm{I}\left\{P_n \leq \hat{P}_n^{(\alpha_q)}\right\}. \tag{44}$$

The closer the diagrams are to the bisector of the positive quadrant, the more reliable are the forecasts.

Reliability is also evaluated quantitatively through the Percentage Average Absolute Coverage Error ($AACE_{\%}$) index, that is:

$$AACE_{\%} = \frac{100}{Q} \sum_{q=1}^{Q} \left|\alpha_q - \hat{\alpha}_q\right|. \tag{45}$$

The $AACE_{\%}$ is therefore a negatively oriented index, since smaller values denote more reliable probabilistic forecasts.

7.5. NUMERICAL APPLICATIONS ON REAL-TIME GENERATION AND LOAD FORECASTING

The methods detailed above have been tested by means of numerical simulations performed with respect to an actual dataset of measured power produced by a PV system installed at a reconfigurable low voltage distribution grid (ReIne laboratory [85]) located in Switzerland and the actual EVnetNL dataset on EV load collected in the Netherlands which has been provided for research purposes by the ElaadNL [53].

7.5.1 APPLICATION OF THE DERIVATIVE PERSISTENCE FORECASTING METHOD

The derivative persistence forecasting method has been applied to a data set of measured power produced by a PV system installed at a reconfigurable low voltage distribution grid (ReIne laboratory [85]) located in Switzerland. The generation system has a total capacity of 30 kW and includes four AC/DC power inverters. The data considered in this application refer to the measured power at the AC side of one inverter having a capacity of 8.5 kW. Particularly, the data refer to a measurement set recorded in the period August 24, to December 19, 2019. This set of data is useful for testing purposes since it refers to different seasons and represents daily power profiles with different degree of variability. Some examples of daily power production are reported in Fig. 6.

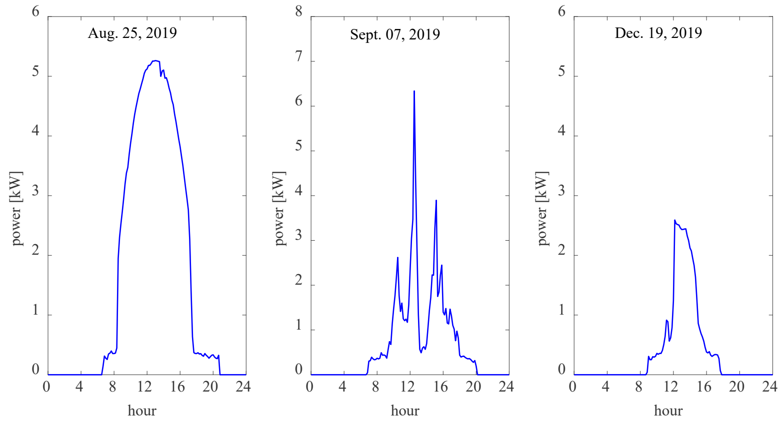

Fig. 6 - Four days selected among the available measurement data

The data refer to measurements sampled at intervals of ten minutes (original measurements are sampled at 1 minute intervals, then the average values over 10 minutes intervals are computed). Based on the historical measured data, the real-time forecasting is requested to generate the forecasts of the PV power produced during the following 10 minutes (i.e., this is one-step-ahead forecasting with 10 minutes lead time).

To validate the proposed approach and highlight its peculiarities in terms of real-time estimation, the forecasted values of power are compared with those of the persistence method of which the proposal is an improvement and ARMA method which is recognized as popular statistical tool for time series analysis forecast.

ARMA model considers the lagged past values and errors as [6]:

$$\hat{y}(k) = \sum_{i=1}^{p} \phi_i \, y(k-i) + \sum_{i=1}^{q} \theta_i \, e(k-i) \tag{46}$$

where $y(k-i)$ and $e(k-i)$ are the lagged past values and errors, with p and q parameters and ϕ_i and θ_i coefficients of the model. In this application, to derive these coefficients the system identification toolbox of Matlab® has been used [86]. The values $p = 1$ and $q = 2$ have been used since in this application they generally gave the best results. Approaches for the ARMA model development based on Akaike Information Criterion or Bayesian Information Criterion, or based on the *auto-ARIMA* function in R environment, may show slightly different results, but are not presented in these experiments for brevity.

To check the accuracy of the proposed approach, the performance metrics summarized in Tab. 1 are used [10], [87].

TAB.1 PERFORMANCE METRICS

Symbol	Metric
• *MAE*	$\frac{1}{N}\sum_{k=1}^{N}\lvert y(k)-\hat{y}(k)\rvert$
• *NMAPE*	$100\,\frac{1}{N}\sum_{k=1}^{N}\frac{\lvert y(k)-\hat{y}(k)\rvert}{P_n}$
• *MdAPE*	$100\,\underset{i=1,..,N}{median}\left(\frac{\lvert y(k)-\hat{y}(k)\rvert}{y(k)}\right)$
• *RMSE*	$\sqrt{\frac{1}{N}\sum_{k=1}^{N}(y(k)-\hat{y}(k))^2}$

The mean absolute error (MAE) assesses the average distance between the measured values, $y(k)$ and the model predictions, $\hat{y}(k)$, of the N forecasted values; normalized mean absolute percentage error (NMAPE) evaluates the magnitude of the prediction error normalized with respect to the system capacity (P_n); compared to the MAPE, median absolute percentage error (MdAPE) is used since it is less sensitive to outliers; root mean square error (RMSE) is useful since it penalizes large errors.

The proposed forecasting method has been iteratively applied to all the available days. With reference to days of Fig. 6 (i.e., Aug. 25, Sept. 7 and Dec. 19, 2019), the results of the proposed forecasting method are reported in Fig. 7, Fig. 8, and Fig. 9, respectively. For comparison purposes, the forecasted values of persistence and ARMA model are also reported.

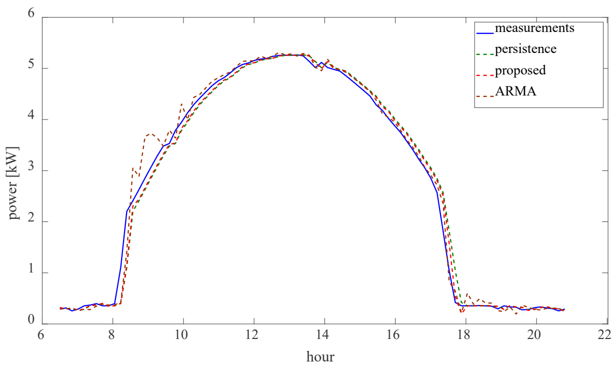

Fig. 7 - Comparison among measurements and different forecasting models (day August 25, 2019)

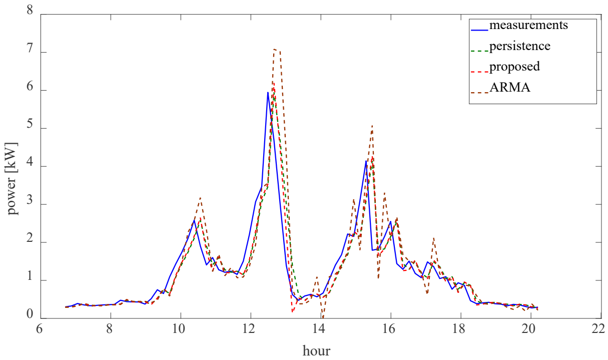

Fig. 8 - Comparison among measurements and different forecasting models (day September 7, 2019)

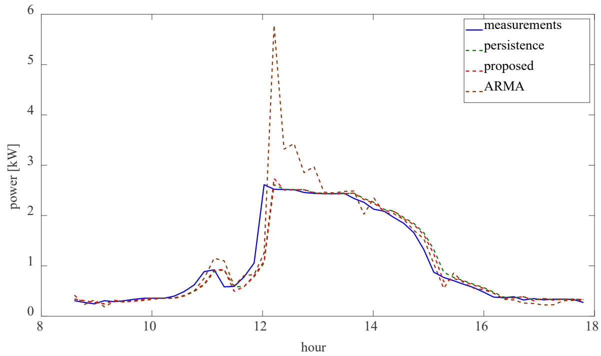

Fig. 9 - Comparison among measurements and different forecasting models (day December 19, 2019)

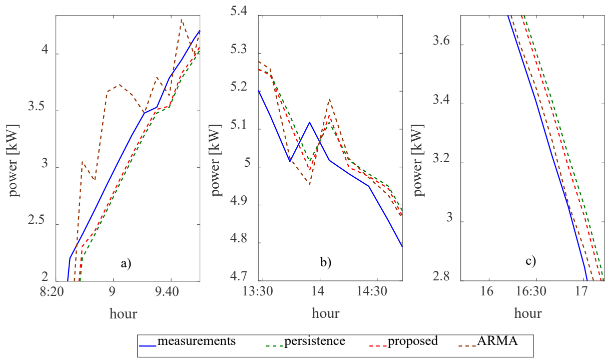

Fig. 10 - Zooms of the comparison among measurements and different forecasting models (August 25, 2019)

In the case of Fig. 7, the daily profile of the power production shows small variations, thus obtaining the typical profile of the PV power. Based on a rough analysis, the three models provide quite similar results. However, by analyzing the zooms of the figure reported in Fig. 10, the proposed approach always provides a slightly better prediction compared to the persistence model. In the zooms, it also appears that these improvements slightly decrease when the variability of the power increases. In these circumstances, the prediction of the proposed approach is also batter than the ARMA approach, as shown in Fig. 10.a) and Fig. 10.b). During the periods when the power profile shows smaller variations (Fig. 10.c), the ARMA model allows predicting with a significant better accuracy. The case of Fig. 8 refers to a power daily profile with large variability. In this case a rough analysis shows how the prediction errors of all forecasting models increase and, particularly, the differences between the persistence and the proposed approaches seem smaller than the case of Fig. 7 – even though the curve of the proposed approach is closest to the curve of the real measured values. Fig. 9 refers to the case of a low production scenario. Compared to the persistence model, the proposed approach still provides a slightly more accurate forecast. The ARMA approach shows a significant error in the period when fast variations appear. In order to better investigate on the accuracy of the proposed method, the performance metrics shown in Tab. 1 are evaluated for the three methods with reference to daily forecasting horizons. The results related to the days of Fig. 6 are reported in Tab. 2.

The results of Tab. 2 confirm the qualitative analyses of Figs. 7 - 10. Indeed, with reference to the day August 25, 2019, the values that all metrics assume in the case of the proposed approach are lower than those assumed by the persistence method. Compared to the persistence model, the NMAPE and MdAPE of the proposed model are 16% and 22% lower, respectively. The values of RMSE and MAE also show better performance of the proposed approach. It is interesting to note that in case of the day August 25, 2019 the ARMA model allows obtaining an accuracy better than the persistence model and worse than the proposed approach. With reference to the other days of the measured data, this generally happens in the days characterized by small variability.

In the case of the day September 7, 2019, the prediction errors of all the three forecasting methods are larger, compared to the previous considered day. In this case also, the metrics of the proposed approach are better than those of the persistence model, even if the differences among methods decrease. Regarding the NMAPE, both the proposed and the persistence allow containing the error within 4%, whereas the ARMA approach implies errors larger than 39%. In this case, the large error of ARMA is due to the high variability of the power during the day. This error slightly reduces on the day December 19 for which similar considerations can be drawn regarding the comparison of the three methods. The unique exception is for the MdAPE, since the value it assumes in the case of the proposed approach is slightly larger than that assumed in the case the persistence approach is applied.

TAB.2 PERFORMANCE COMPARISON

Model	MAE [W]	NMAPE [%]	MdAPE [%]	RMSE [W]
day August 25, 2019				
Persistence	127.36	1.50	3.79	224.94
Proposed	105.92	1.25	2.96	191.54
ARMA	120.26	1.41	3.02	212.55
day September 7, 2019				
Persistence	334.58	3.94	15.13	593.57
Proposed	318.99	3.75	14.94	569.12
ARMA	467.43	5.50	20.40	891.78
day December 19, 2019				
Persistence	108.95	1.28	7.43	249.43
Proposed	104.35	1.23	8.53	240.81
ARMA	221.50	2.61	13.99	540.07

The same analysis has been repeated for all the days of the available measured data. The results, which are not reported here for the sake of conciseness are coherent with those of Tab. 2. Particularly, the skill score, ss, has been evaluated which is defined as [9]:

$$ss = 1 - \frac{RMSE}{RMSE_p} \tag{47}$$

being $RMSE_p$ referred to the persistence and $RMSE$ referred to the test approach. The skill score is typically used to compare a test forecasting approach to the persistence model. In the case analysed in this application, the mean value assumed by the skill score is 0.0026 and its maximum value is 0.14, thus demonstrating a generalized improvement of the proposed approach compared to the persistence model. As expected, the skill score of the ARMA is negative, showing the inaccuracy of this model compared to the persistence in the regard of the real-time forecasting. This is aligned to the literature, such as in [9]. Moreover, still referring to the peculiarities relevant to the real-time forecasting, it has to be noted that ARMA approach implies computational time hugely larger than the one implied by the proposed or persistent model.

7.5.2 APPLICATION OF THE CAPUTO-DERIVATIVE FORECASTING METHOD

The proposed forecasting method has been applied to a data set of measured PV power produced by the GECAD N system installed in Portugal at the Instituto Superior de Engenharia do Porto/Politécnico do Porto [88]. The installation power is 10 kW. The data refer to the period July 27, 2016-November 16, 2016, with a sampling time of one minute. Regarding the validation metrics, in addition to those reported in Tab. 1, the following metrics were used to validate the method:

- the relative Root Mean Squared Error (rRMSE) which evaluates the RMSE normalized with respect to the mean value of the measured values:

$$\textbf{rRMSE} \qquad \frac{1}{\bar{y}}\sqrt{\frac{1}{N}\sum_{k=1}^{N}(\hat{y}_k - y_k)^2} \tag{48}$$

- the Pearson correlation coefficient (R) which is based on the method of covariance and gives a measure of the correlation between the forecasted and measured values has been also included for the sake of completeness even if it is less suited for evaluating forecasting methods:

$$\textbf{R} \qquad \frac{\frac{1}{\bar{y}}\sum_{k=1}^{N}(\hat{y}_k-\bar{\hat{y}})(y_k-\bar{y})}{\sqrt{\sum_{k=1}^{N}(\hat{y}_k-\bar{\hat{y}})^2\sum_{k=1}^{N}(y_k-\bar{y})^2}} \tag{49}$$

where $\bar{y}$ and $\bar{\hat{y}}$ are the average value of the measured dataset and of the forecasted dataset, respectively.

Some examples of daily power production are reported in Fig. 11 with reference to two days characterized by regular and irregular weather conditions (i.e., September 24 and September 12, respectively).

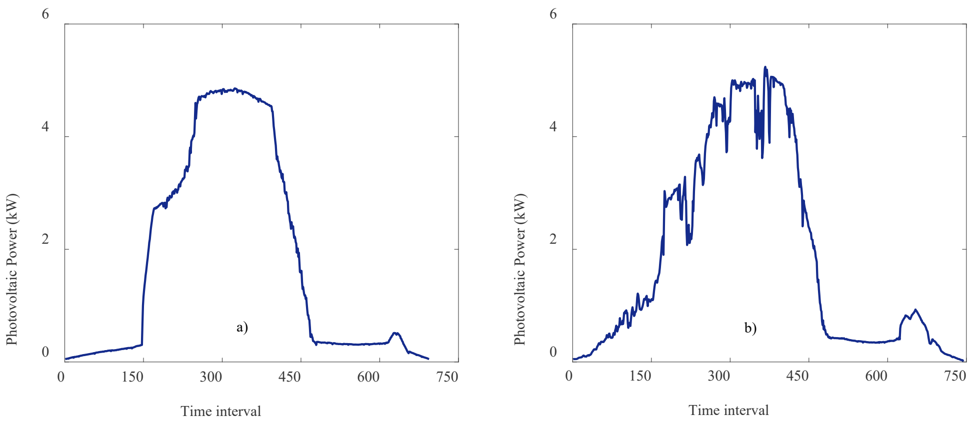

Fig. 11 - Measured PV power profile of the 59th day, September 24 (a) and of the 47th day, September 12 (b)

UNIONE EUROPEA

Ministero dell'Istruzione, dell'Università e della Ricerca

The following experiments refer to different time intervals which are relevant to real-time applications for distribution networks operation, that are one minute, five minutes and ten minutes. Since the original measurements are sampled at one-minute intervals, with the aim to handle also the other considered time scales, the average values of the measurements over five-minute and ten-minute intervals were computed.

Based on the historical measured data, the real-time forecasting is requested to generate the forecasts of the PV power produced during the following one minute, five minutes and ten minutes (i.e., this is one-step-ahead forecasting with one-, five- and ten-minute lead time, respectively). In the following subsections, the results of the application of the proposed Caputo-derivative method are reported together with a comparison with the other considered forecasting techniques to evaluate the accuracy of the results.

Forecasting output

With reference to the daily PV power profiles reported in Fig. 11, the results of the forecasted profiles carried out by applying the proposed Caputo-derivative method are reported in Figs. 12, 13 and 14 which refer to different lead times (which in the application correspond to the forecasting time horizons) and different numbers of past samples used for the forecast:

- one-minute lead time and 30 samples
- five-minute lead time and 12 samples
- ten-minute lead time and 12 samples.

In the three cases, a value of n_k equal to one has been assumed. Tab. 3 reports the performance indices evaluated on those single days.

The analysis of the results reported in Tab. 3 evidences that, with reference to the regular day (59th day, September 24), the forecasting indices have quite good values. They assume slightly worse values in the case of the irregular day (47th day, September 12), however, still being acceptable. The values of the indices in the case of one-minute lead time are generally better than those assumed in the case of five-minute and ten-minute lead times. This is an expected result since, by increasing the lead time, accuracy reduces. Particularly, it can be observed that the index R reaches a value very close to one in the case of one-minute lead time for both days. Its approximation to one still remains in the case of five-minute lead time and it assumes acceptable values in the case of ten-minute lead time.

TAB.3 PERFORMANCE INDICES EVALUATED ON THE TWO CONSIDERED DAYS

Lead time	Samples	RMSE [W]	MAE [W]	NMAPE [%]	rRMSE [%]	rMBE x1e-4 [%]	R
				59th day, September 24			
1 min	30 (30 min)	46.8903	21.5152	0.2152	0.026	-1.3899	0.9996
5 min	12 (60 min)	143.5294	71.5451	0.7155	0.0805	3.8048	0.9971
10 min	12 (120 min)	271.0762	140.0803	1.4008	0.1510	10.8921	0.9895
				47th day, September 12			
1 min	30 (30 min)	121.0304	57.6087	0.5761	0.0653	-2.3560	0.9976
5 min	12 (60 min)	221.9227	130.9621	1.3096	0.1185	9.9717	0.9921
10 min	12 (120 min)	317.0545	199.5311	1.9953	0.1681	36.1401	0.9839

Figs. 12-17 a) show the comparison of measured and forecasted power profiles for the two days and for the three considered lead times. Figs. 12-17 b) show the relative normalized errors, which is evaluated as:

$$err_k = \frac{\hat{y}_k - y_k}{y_k}. \tag{50}$$

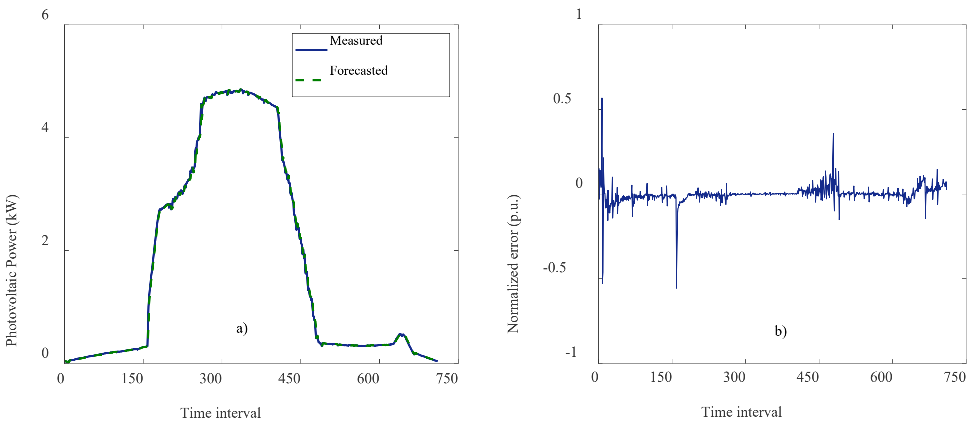

Fig. 12 -Forecast results for day #59 – 1 min lead time: photovoltaic power values (a) and normalized error (b)

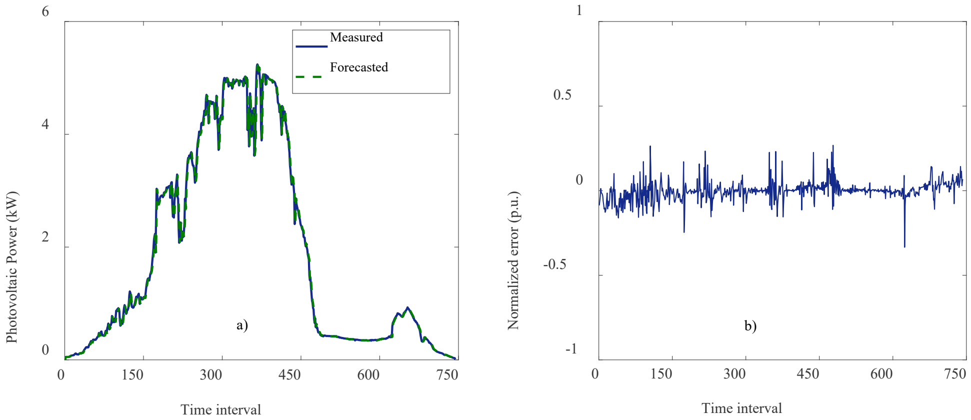

Fig. 13 -Forecast results for day #47 – 1 min lead time: photovoltaic power values (a) and normalized error (b)

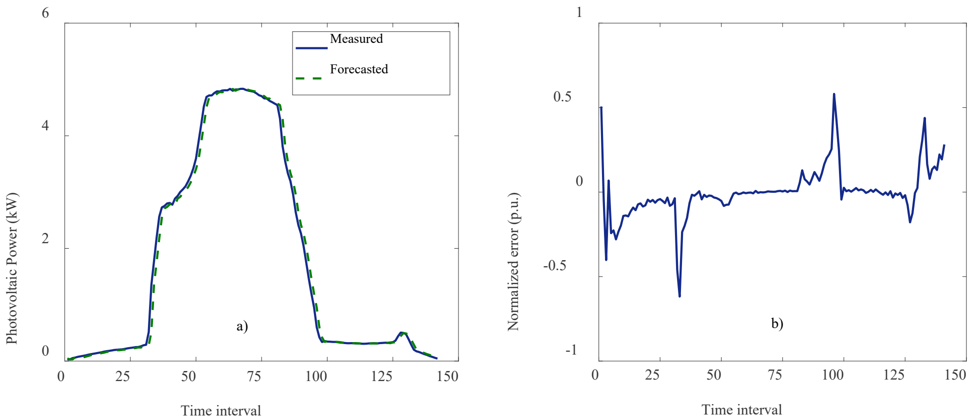

Fig. 14 -Forecast results for day #59 – 5 min lead time: photovoltaic power values (a) and normalized error (b)

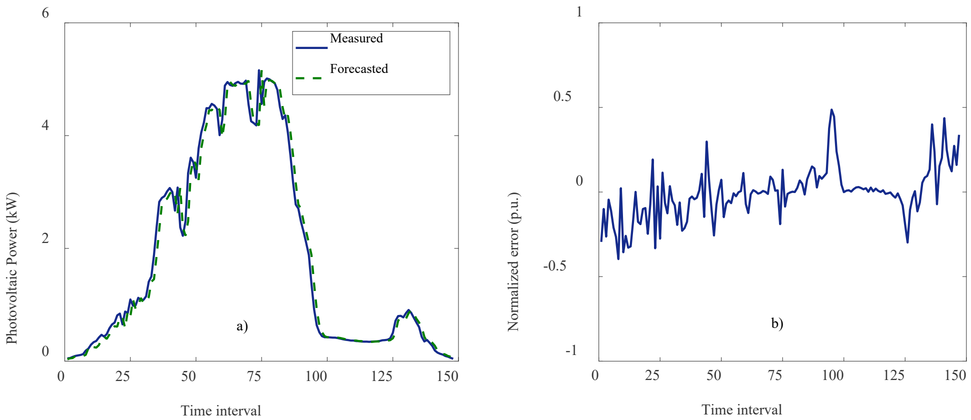

Fig. 15 -Forecast results for day #47 – 5 min lead time: photovoltaic power values (a) and normalized error (b)

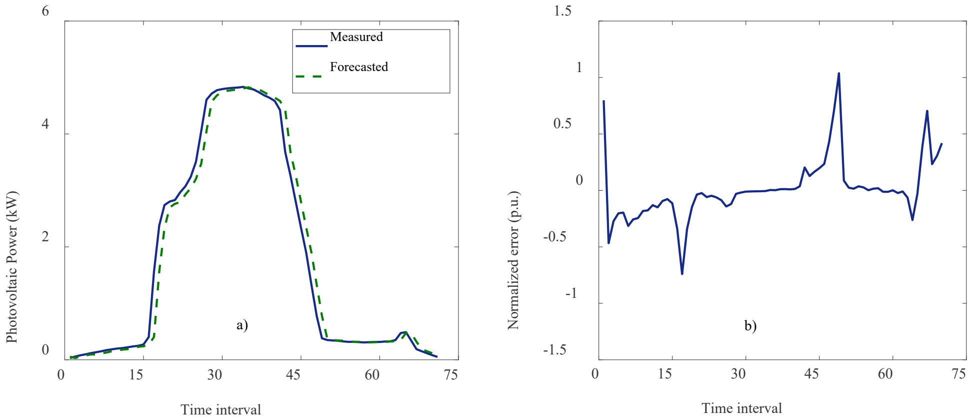

Fig. 16 -Forecast results for day #59 – 10 min lead time: photovoltaic power values (a) and normalized error (b)

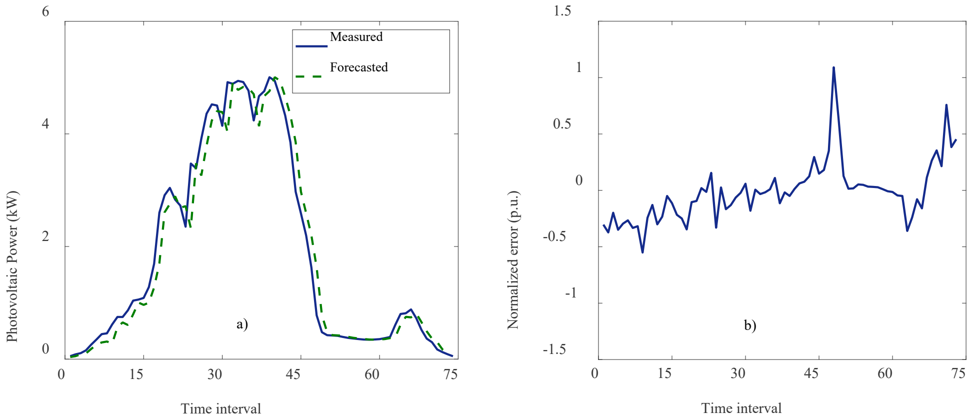

Fig. 17 -Forecast results for day #47 – 10 min lead time: photovoltaic power values (a) and normalized error (b)

The profiles reported in Fig. 12 confirm the results reported in Tab. 3. More specifically, the analysis of the figures evidences how measured and forecasted profiles almost overlap in the case of one-minute lead time for both the considered days with very low values of the normalized errors. The overlapping remains in the case of five-minute lead time with still contained values of the error and slightly reduces in the case of ten-minute lead time with higher values of the error. Regarding the error profile of the one-minute lead time forecasting, some spikes can be observed in correspondence of the irregular points of the power profile (Fig. 12.b). The same behavior can be observed in the case of five-minute and ten-minute lead times with slightly larger spikes.

A sensitivity analysis was performed to evaluate the effect of the choice of n_k on the forecasting performance. The results are reported in Fig. 18, with reference to the days #47 (Figs. 18.a, 18.b and 18.c) and #59 (Figs. 18.d, 18.e and 18.f), where the values of RMSE and NMAPE are reported versus n_k. In the figure, the results are reported referring to the three lead times, i.e., one minute (Figs. 18.a and 18.d), five minutes (Figs. 18.b and 18.e) and ten minutes (Figs. 18.c and 18.f).

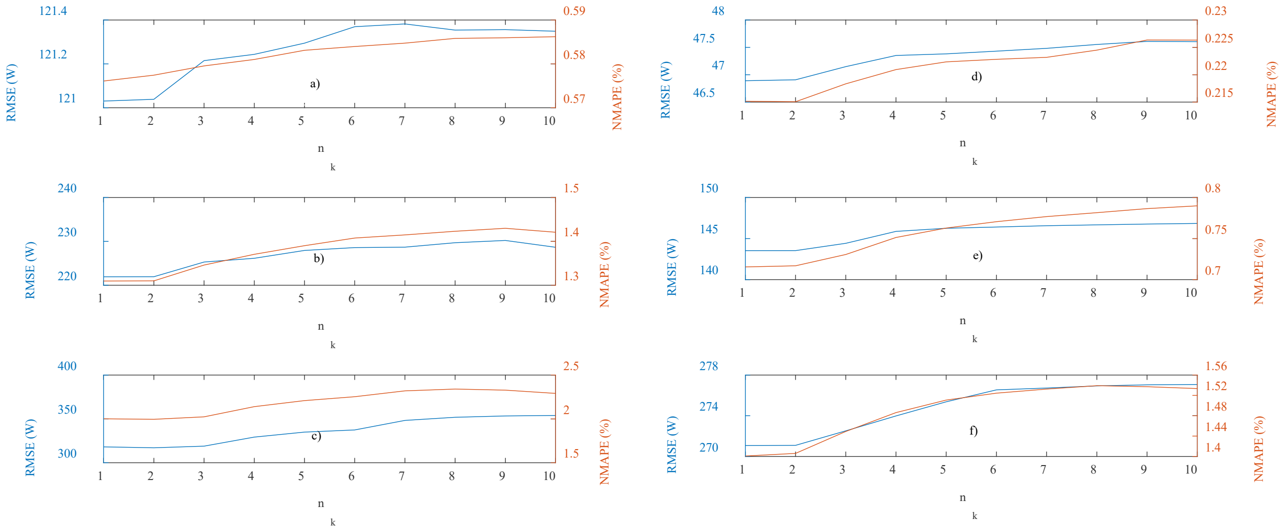

Fig. 18 -RMSE and NMAPE variations vs. n_k values for day #47 – 1 min lead time (a), – 5 min lead time (b) and – 10 min lead time (c) and for day #59 – 1 min lead time (d), – 5 min lead time € and – 10 min lead time (f)

Fig. 18 shows that better performance of the proposed method is obtained for low values of n_k. In particular, the minimum values of RMSE and NMAPE are reached always for $n_k = 1$, except for the NAMPE of Fig. 18.d where the minimum value is reached for $n_k = 2$. By increasing the value of n_k the values of the indices increase. The same considerations can be drawn for the other metrics whose values are not reported here for brevity.

Performance evaluation of the forecasting

In this Section, the performance of the procedure has been evaluated by comparing its accuracy with that obtained by means of the i) persistence, ii) derivative-persistence and iii) ARMA methods. The comparison includes also a sensitivity analysis with respect to the past samples used for the forecasting. More specifically, the persistence and derivative-persistence methods require a fixed number of past samples, that are one and three, respectively.

In what follows, the results of one-minute (Tab. 4), five-minute (Tab. 5) and ten-minute (Tab 6) lead time forecasting are reported. In the tables all the indices described above are reported except for the MAE since, in this application, it can be derived by multiplying the NMAPE by 100 being 10 kW the size of the plant.

Regarding the past samples, for the ARMA and Caputo-derivative methods, a number of past samples equal to seven (seven minutes), 15 (15 minutes) and 30 (30 minutes) have been assumed in the case of one-minute lead time. For the Caputo-derivative method also the case of three samples (three minutes) has been considered in order to allow comparison to the derivative-persistence method. In the case of five- and ten-minute lead times, still with reference to ARMA and Caputo-derivative methods, a larger lag time has been considered by using 12 (60 minutes) and 24 (120 minutes) samples in the case of five-minute lead time, and 12 (120 minutes) samples in the case of ten-minute lead time. The choice of the past samples used in the tables for comparing the various methods is due to the minimum number of samples required by each method for the forecasting. In particular, the persistence method operates by using only one previous sample, the derivative persistence needs exactly three samples, the Caputo-derivative needs three samples, at least. Caputo-derivative can also operate with different, greater numbers of past samples. ARMA also can operate with different number of samples, typically better operating with a higher number and, in the application proposed in this paper, seven has been found to be the minimum number of samples required. In the tables, to have a more complete comparison of the results obtained by using the Caputo derivative and ARMA, the results obtained by using three different values of numbers of samples for the forecasting are proposed.

The results reported in the tables show the efficacy of the proposed method for the real-time forecasting of the PV power. Generally, all of the considered methods show comparable performance with slightly different results. Particularly, in some circumstances the proposed method shows the best results depending on the number of samples considered in the forecast.

With reference to one-minute lead time, the results of Tab. 4 evidence that, the forecast carried out by using the Caputo-derivative method with three samples performs better than the persistence method in terms of RMSE. Regarding R it has the same value assumed in the case of persistence. Furthermore, the value of rMBE is better that the value it assumes with both the derivative-persistence and persistence approaches. Derivative-persistence method gives results better than those obtained by applying the persistence method regarding the NMAPE index. The Caputo-derivative also shows good performance when applied with 7, 15 and 30 samples compared to all of the other approaches. Particularly, the case of 30 samples gives the best results. This reveals the ability of the method to catch the history of the variable to be forecasted. It can be noted that, though appliable, the ARMA method doesn't give good results in the case of seven samples. By increasing the number of samples, better results are obtained even if they are still worse than those obtained by applying the Caputo-derivative. The results of ARMA also show that increasing the number of past samples, a better forecast is obtained, thus reflecting a better estimation of the lag coefficients.

TAB.4 PERFORMANCE INDICES EVALUATED FOR THE WHOLE FORECASTING PERIOD WITH LEAD TIME 1 MIN

Method	Samples	RMSE [W]	NMAPE [%]	rRMSE [%]	rMBE x1e-4 [%]	R
Persistence	1 (1 min)	208.7251	0.5652	0.1569	-0.2435	0.9902
Derivative-persistence	3 (3 min)	213.1019	0.5616	0.1602	-15.5737	0.9898
Caputo-derivative	3 (3 min)	208.7246	0.5650	0.1569	-0.0660	0.9902
ARMA	7 (7 min)	8885.6795	1.1072	6.6780	237.5481	0.1607
	15 (15 min)	249.3366	0.6933	0.1874	-2.5908	0.9860
	30 (30 min)	224.5512	0.6332	0.1688	-1.3241	0.9886
Caputo-derivative	7 (7 min)	208.7249	0.5651	0.1569	-17.9810	0.9902
	15 (15 min)	208.7248	0.5651	0.1569	-14.8004	0.9902
	30 (30 min)	208.7243	0.5651	0.1569	-0.0424	0.9902

With reference to the five-minute lead time (Tab. 5), by using three samples for the forecast, it still appears that the Caputo-derivative provides the best results in term of RMSE, and rRMSE, and the same value of the persistence in terms of R, while the derivative-persistence gives the best results in terms of NMAPE. By increasing the number of samples (7 and 12) the Caputo-derivative provides the best results for all of the indices except for the NMAPE for which the derivative-persistence still performs better. By further increasing the number of samples (24) the values of the indices slightly worsen.

TAB.5 PERFORMANCE INDICES EVALUATED FOR THE WHOLE FORECASTING PERIOD WITH LEAD TIME 5 MIN

Method	Samples	RMSE [W]	NMAPE [%]	rRMSE [%]	rMBE x1e-4 [%]	R
Persistence	1 (5 min)	247.1509	1.1333	0.1844	-1.7182	0.9860
Derivative-persistence	3 (15 min)	254.6339	1.0987	0.1899	-44.6768	0.9852
Caputo-derivative	3 (15 min)	247.1354	1.1324	0.1843	-0.6815	0.9860
ARMA	7 (35 min)	366.8468	1.5179	0.2736	172.1750	0.9702
	12 (60 min)	294.2581	1.3303	0.2195	92.5553	0.9808
	24 (120 min)	270.9479	1.2632	0.2021	165.900	0.9839
Caputo-derivative	7 (35 min)	247.1362	1.1328	0.1843	-0.7143	0.9860
	12 (60 min)	247.1303	1.1325	0.1843	0.5965	0.9860
	24 (120 min)	247.1524	1.1328	0.1844	3.6058	0.9860

TAB.6 PERFORMANCE INDICES EVALUATED FOR THE WHOLE FORECASTING PERIOD WITH LEAD TIME 10 MIN

Method	Samples	RMSE [W]	NMAPE [%]	rRMSE [%]	rMBE x1e-4 [%]	R
Persistence	1 (10 min)	284.0675	1.6205	0.2106	-5.0788	0.9814
Derivative-persistence	3 (30 min)	283.6419	1.5412	0.2103	-76.5393	0.9812

Caputo-derivative	3 (30 min)	283.9904	1.6183	0.2106	-2.3452	0.9814
ARMA	7 (70 min)	388.2195	2.0239	0.2878	316.5226	0.9683
	12 (120 min)	345.4801	1.8939	0.2562	319.1121	0.9752
Caputo-derivative	7 (70 min)	283.9578	1.6183	0.2105	-0.1360	0.9814
	12 (120 min)	283.9036	1.6177	0.2106	4.0855	0.9814

The results in Tab. 6 (ten-minute lead time) generally confirm the above considerations regarding the forecasts with three samples, except for RMSE and rRMSE which are better in the case of the derivative-persistence method. In both cases, however, they are better (RMSE) or equal (rRMSE) than the values they assume in the case of persistence. For other numbers of samples, the Caputo-derivative provides the best results in terms of rRMBE and the same value of the persistence for R while the derivative-persistence method proves to be always the best approach in terms of the other indices.

With reference to the different number of past samples used for the forecast, the Caputo-derivative shows always a robust behaviour. Compared to the ARMA method, in fact, it shows only slight performance variations with varying number of used past samples. Particularly, R is not affected at all by the variation of the number of past samples as well as it happens for NMAPE and rRMSE in the case of one-minute lead time. This means that, even not appropriate the choice of the number of past samples, the Caputo-derivative method gives always quite accurate results.

The proposed Caputo-derivative forecasting method was also applied to the dataset used in this document at the aim of forecasting the maximum PV power. The results obtained showed accuracy comparable as that discussed in the above sections. With respect to the dataset **SI1**, as an example, the results related to day #15 are reported in Fig. 19.a) A zoom referring to part of the day characterized by high irregularity is reported in Fig. 19.b). The accuracy of the proposed forecasting method and its feasibility clearly appear.

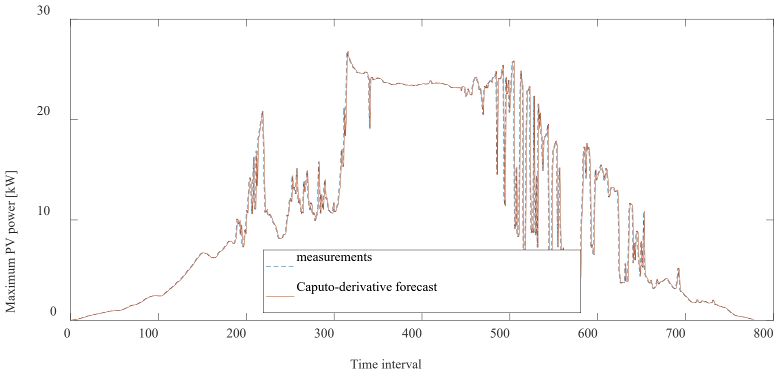

(a)

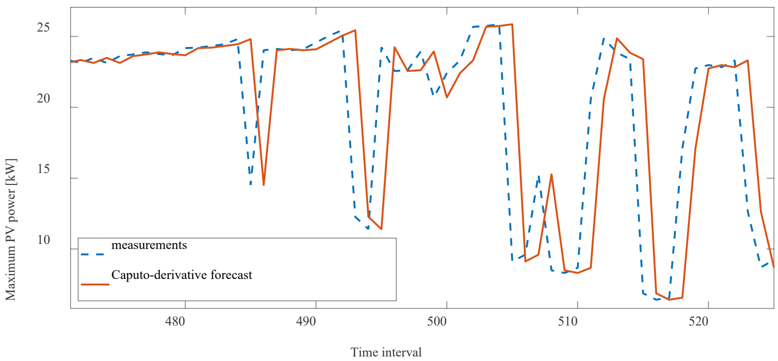

(b)

Fig. 19 - Comparison of Caputo-derivative method applied to the maximum PV power and actual measurements (a) and its zoom (b)

7.5.3 Application of the Bayesian Bootstrapping

Bayesian bootstrap in probabilistic PV power forecasting is applied to a data set of measured power produced by the PV system installed at the already mentioned reconfigurable low voltage distribution grid (ReIne laboratory [85]) located in Switzerland.

The NWPs used in the experiments are taken from the European Centre for Medium-range Weather Forecast (ECMWF) [89]. All the NWPs belong to the midnight run, i.e., they are issued at midnight and cover the 24 hours of the following day.

All the data are averaged to obtain an hourly time resolution. They are normalized to their respective minimum and maximum values to be processed by the forecasting models.

Data are stored from February 1, 2016 to November 30, 2018, for a total number of 24816 occurrences. In these experiments, the training set covers until January 31, 2018 and it is $\Omega^{\langle tr \rangle} = \{t: 1 \le t \le 17544\}$, whereas the test set covers the remaining months in 2018 and it is $\Omega^{\langle te\rangle} = \{t: 17545 \leq t \leq 24816\}$. The validation set $\Omega^{\langle va\rangle}$ used in the OQ-BB procedure to optimize the extraction of the final prediction from the sample Bayesian bootstrap distribution is applied on a rolling monthly window: for example, the validation set $\Omega^{\langle va\rangle} = \{t: 16801 \leq t \leq 17544\}$ that corresponds to data in January 2018 is used to optimize the extraction of the final prediction for February 2018, the validation set $\Omega^{\langle va\rangle} = \{t: 17545 \leq t \leq 18264\}$ that corresponds to data in February 2018 is used to optimize the extraction of the final prediction for March 2018, and so on.

The 1-hour-ahead probabilistic forecasts are generated by $Q = 19$ predictive quantiles at nominal coverages $\alpha_1, \dots, \alpha_{19} = 0.05, 0.10, \dots, 0.90, 0.95$. The sample size of the Bayesian bootstrap distribution is $R = 100$ and is kept at this value for all the experiments. All forecasts are generated using an i7-6700HQ CPU @2.60GHz equipped with 16 GB RAM in R, with the packages *bayesboot* [90], *quantreg* [91], *qrnn* [92] and *gbm* [93]. In any case, the time required to generate forecasts was in line with the requirements driven by the 1-hour lead time. Table 3 shows the PS, the AACE and the PINAW obtained using the Bayesian-bootstrap-based forecasting systems and the benchmarks, averaged across the test set. Bold values in Table 7 indicate the best performance for each model family.

TAB.7 PERFORMANCE OF THE PROBABILISTIC FORECASTS AVERAGED ACROSS THE TEST SET. BOLD VALUES INDICATE THE BEST PERFORMANCE FOR EACH MODEL FAMILY

Model family	Bootstrap	Forecasting system	Error score/index			
			PS [-]	AACE [%]	$PINAW_{10}$ [-]	$PINAW_{90}$ [-]
LQR	Bayesian	LQR-SM-BB	0.184	2.89	0.713	**11.637**
		LQR-OQ-BB	**0.183**	**1.42**	**0.632**	11.980
	Traditional	LQR-SM-TB	0.184	2.79	0.699	12.012
		LQR-OQ-TB	0.184	2.09	0.675	12.365
	None	LQR-NB	0.186	2.99	0.749	12.312
GBRT	Bayesian	GBRT-SM-BB	0.188	3.91	**0.560**	**7.938**
		GBRT-OQ-BB	**0.185**	**0.97**	0.675	11.481
	Traditional	GBRT-SM-TB	0.192	3.10	0.684	8.289
		GBRT-OQ-TB	0.190	1.23	0.731	11.705
	None	GBRT-NB	0.194	4.11	0.830	12.172
QRNN	Bayesian	QRNN-SM-BB	0.188	3.64	0.797	**7.135**
		QRNN-OQ-BB	**0.186**	**2.02**	**0.716**	10.200
	Traditional	QRNN-SM-TB	0.187	3.89	0.831	7.427
		QRNN-OQ-TB	**0.186**	2.08	0.782	8.985

	None	QRNN-NB	0.189	3.68	0.827	7.461
PM1			0.522	-	-	-
PM2			0.595	-	-	-

The reliability diagrams are shown for the LQR-OQ-BB, the GBRT-OQ-BB and the QRNN-OQ-BB in Figure 20(a), 20(b) and 20(c), respectively. The graphical inspection of the reliability diagrams denotes that forecasts are calibrated, as the estimated coverages tend to lie along the bisector curve. GBRT-OQ-BB forecasts only marginally deviate from the ideality, as confirmed by the smallest AACE index (0.97%) reported in Table 7.

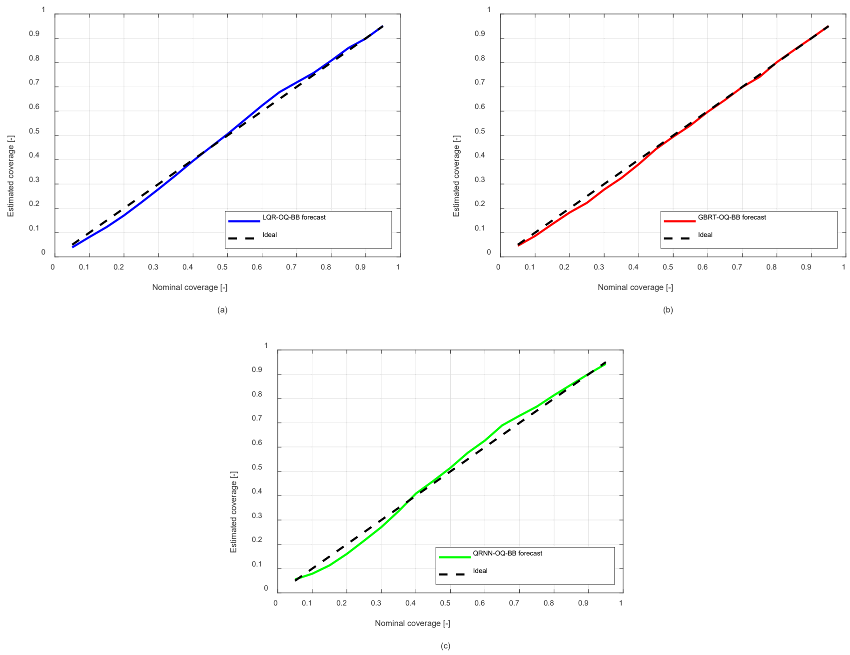

Fig. 20 - Reliability diagrams of the LQR-OQ-BB forecasts (a), GBRT-OQ-BB forecasts (b), and QRNN-OQ-BB forecasts (c).

LQR-OQ-BB forecasts, GBRT-OQ-BB forecasts and QRNN-OQ-BB forecasts during the first two weeks of the test period are plotted versus time and compared to the actual PV power in Figure 21(a), 21(b) and 21(c), respectively.

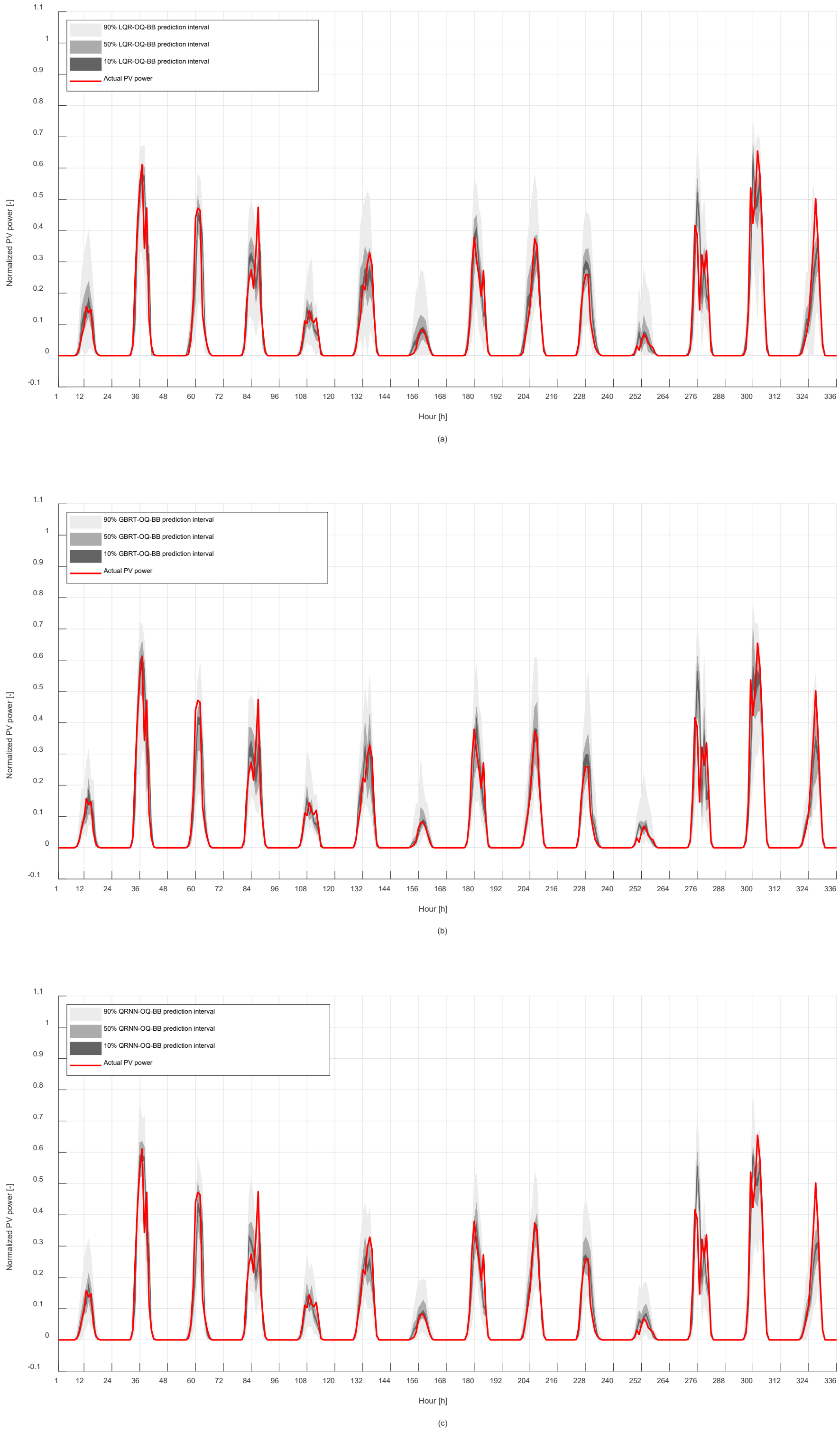

Fig. 21 - LQR-OQ-BB forecasts (a), GBRT-OQ-BB forecasts (b), and QRNN-OQ-BB forecasts (c) during the first two weeks of the test period.

- Results for Dataset_SI1

The results for **Dataset_SI1** are presented for a case study that was arranged to suit the real-world experimental framework of the optimization models. In particular, the LQR-SM-BB forecasting system was adapted to generate a point forecast of the maximum power producible by a controllable PV system. Since the proposal was developed within a probabilistic framework, only one nominal quantile coverage ($\alpha = 0.5$) is considered as the point output of the methodology. The forecasts are issued two-step-ahead, for all the 144 ten-minute sub-intervals of the day; NWPs were not included as candidate predictors. For **Dataset_SI1**, the selected underlying LQR model is:

$$\hat{P}_h^{\langle\alpha\rangle} = \hat{\beta}_0^{\langle\alpha\rangle} + \hat{\beta}_1^{\langle\alpha\rangle} \cdot P_{h-144}^{\langle\alpha\rangle} + \hat{\beta}_2^{\langle\alpha\rangle} \cdot P_{h-2}^{\langle\alpha\rangle} + \hat{\beta}_3^{\langle\alpha\rangle} \cdot P_{h-3}^{\langle\alpha\rangle} + \hat{\beta}_4^{\langle\alpha\rangle} \cdot P_{h-4}^{\langle\alpha\rangle} + \hat{\beta}_5^{\langle\alpha\rangle} \cdot P_{h-5}^{\langle\alpha\rangle} + \hat{\beta}_6^{\langle\alpha\rangle} \cdot P_{h-6}^{\langle\alpha\rangle} + \\ + \hat{\beta}_7^{\langle\alpha\rangle} \cdot P_{h-144}^{\langle\alpha\rangle} \cdot P_{h-2}^{\langle\alpha\rangle} + \hat{\beta}_8^{\langle\alpha\rangle} \cdot P_{h-144}^{\langle\alpha\rangle} \cdot P_{h-6}^{\langle\alpha\rangle}. \tag{50}$$

The number of predictors of the selected model is therefore $M_{tr} = 8$, and two of them are obtained as interacting predictors.

Table 8 shows the MAE and the RMSE calculated for the point forecasts of the maximum PV power, obtained through the LQR-SM-BB and the Persistence Model, during one day (144 forecast issues) of the test period characterized by adverse weather conditions. As seen, LQR-SM-BB returns a MAE (RMSE) that is about 8.8% (8.0%) smaller than the benchmark for this dataset, too. Fig. 22 shows the maximum PV power pattern and the forecasted values.

TAB.8 FORECAST RESULTS FOR ONE DAY (144 FORECAST ISSUES) OF THE TEST SET OF DATASET_SI1

Method	MAE [-]	RMSE [-]
LQR-SM-BB	5.53	12.58
PM	6.07	13.67

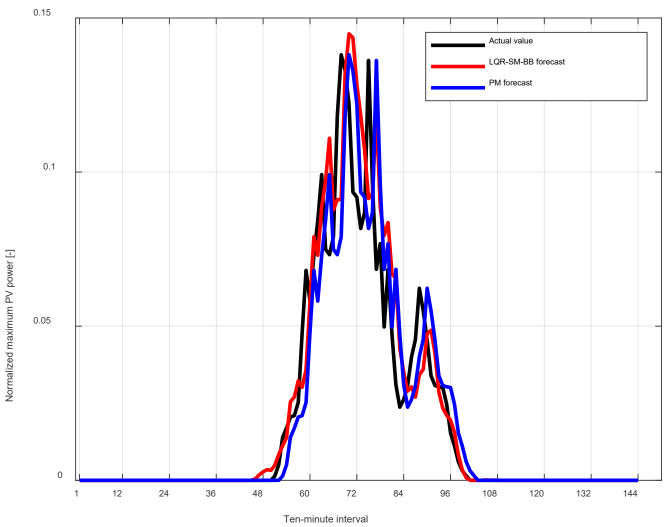

Fig. 22 - Fig. LQR-SM-BB predictions during one day, characterized by adverse weather conditions, of the test set of Dataset_SI1.

7.5.4 APPLICATION OF THE HIERARCHICAL PROBABILISTIC ELECTRIC VEHICLE LOAD FORECASTING

The data used for the experiments are discussed in Section 7.2 and span three years from July 1, 2015 to June 30, 2018. As discussed above, for the particular structure of the hierarchical forecasting system it is necessary to reserve a portion (individuated by the index set $\Omega_{tra}^{\langle B \rangle}$) of the available data to train the baseline models and another portion (individuated by the index set $\Omega_{tra}^{\langle H \rangle}$) to train the hierarchical PLQR model upon the predictions generated by the baseline models. To allow the out-of-sample assessment of the forecasting skill in the experimental framework, it is also mandatory to reserve some data (individuated by the index set Ω_{test}) only to test the performance of the forecasting system.

In the experiments presented here, $\Omega_{tra}^{\langle B \rangle}$ includes roughly 50% of the available data, $\Omega_{tra}^{\langle H \rangle}$ includes roughly 30% of the available data and Ω_{test} includes roughly 20% of the available data. The first one and half year (July 1, 2015 to December 31, 2016) is reserved for training the baseline models (i.e, making up the set $\Omega_{tra}^{\langle B \rangle}$ of 13200 points). Another year of data (the entire year 2017) is reserved to train the hierarchical model (i.e., making up the set $\Omega_{tra}^{\langle H \rangle}$ of 8760 points). The remaining half year (first six months of 2018) is reserved for testing the results (i.e., making up the set Ω_{test} of 4344 points).

In the framework considered in this research, baseline forecasts are issued for the training set $\Omega_{tra}^{\langle H \rangle}$ and the test set Ω_{test}, therefore the error indices and diagrams are calculated on the set $\Omega = \{\Omega_{tra}^{\langle H \rangle}, \Omega_{test}\}$. Hierarchical forecasts are issued for the test set Ω_{test} only, therefore the error indices and diagrams are calculated on the set $\Omega = \Omega_{test}$.

Probabilistic forecasts for low-level and high-level regions are provided by $Q = 9$ predictive quantiles at 0.1, 0.2, ..., 0.9 nominal coverages. Two different forecasting frameworks, i.e., hour-ahead forecasting (with lead time $k = 1$ hour) and day-ahead forecasting (with forecast origin at midnight of the day before the actual energy consumption, and lead times $k = 1,2,\dots,24$ hours), are considered in the experiments in order to evaluate the proposal in different practical implementations.

Assessment of hour-ahead baseline forecasts

Table 9 shows the PS and the AACE% of hour-ahead baseline probabilistic forecasts, averaged on the set $\Omega = \{\Omega_{tra}^{\langle H \rangle}, \Omega_{test}\}$. Bold values in Table 9 denote the smallest achieved indices for each region. The AACE% of BPersB is not presented, since this persistence-based benchmark generates the same predictive quantiles for each nominal coverage.

The baseline forecasts generated with the PCA pre-processing are more skilled than the corresponding "no PCA" forecasts in three upon four regions. The PS improvements are in the ranges 1% to 7.5% (Noordoost region), 1.5%

to 11% (Rijnmond region), and 2% to 9% (Zuidoost region). Utrecht region is the only exception to this behavior; it is worth noting however that the PS of GBRT forecasts is practically the same with (14.47 kWh) and without (14.46 kWh) PCA.

On average across the four regions, the GBRT baseline returns the most accurate forecasts, although GBRT, QRF and QRNN baseline forecasts give PS that are very close in all the four low-level regions. The improvement with respect to the seasonal BPersB ranges from 36% to 43%.

TAB.9 RESULTS OF HOUR-AHEAD BASELINE FORECASTS AT LOW-LEVEL REGIONS.

Model	Low-level region							
	Noordoost		Rijnmond		Utrecht		Zuidoost	
	PS [kWh]	AACE% [%]	PS [kWh]	AACE% [%]	PS [kWh]	AACE% [%]	PS [kWh]	AACE% [%]
GBRT baseline	**18.07**	1.55	**22.30**	1.67	14.47	2.94	17.51	1.40
QRF baseline	18.15	**1.40**	22.54	**0.20**	14.71	2.86	17.55	**0.68**
QRNN baseline	18.17	1.94	22.38	2.12	14.56	2.48	**17.48**	1.84
GBRT no PCA	18.23	2.06	22.64	3.18	**14.46**	2.37	17.90	1.35
QRF no PCA	18.55	3.11	23.33	3.44	14.73	**1.36**	18.40	2.05
QRNN no PCA	19.64	4.66	25.12	6.54	15.23	2.39	19.17	5.00
BPersB	28.34	-	38.84	-	22.85	-	30.75	-

*The most favorable value of the performance index in each column is highlighted in bold font

In order to evaluate the reliability of the hour-ahead baseline forecasts and as an example of the obtained results, Figure 23 shows the reliability diagrams of the GBRT, QRF and QRNN hour-ahead baseline forecasts for the EV load of Noordoost region, plotted against the ideal reliability bisector. The diagrams are very close to the ideal bisector, with the only exception of the extreme left and right coverages of the QRNN forecasts, which are respectively underestimated and overestimated.

Figure 24 shows the GBRT (Figure 24(a)), QRF (Figure 24(b)) and QRNN (Figure 24(c)) baseline forecasts against the actual EV load of Noordoost region during the second week of the test period.

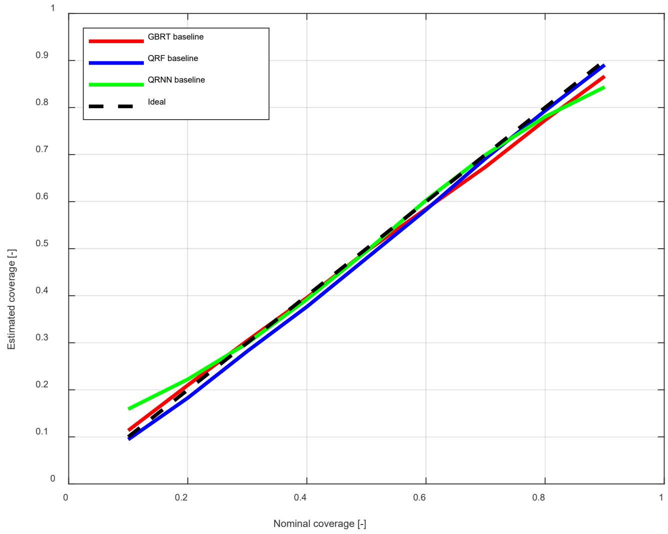

Fig. 23 - Reliability diagrams of the hour-ahead baseline forecasts for the EV load of Noordoost region.

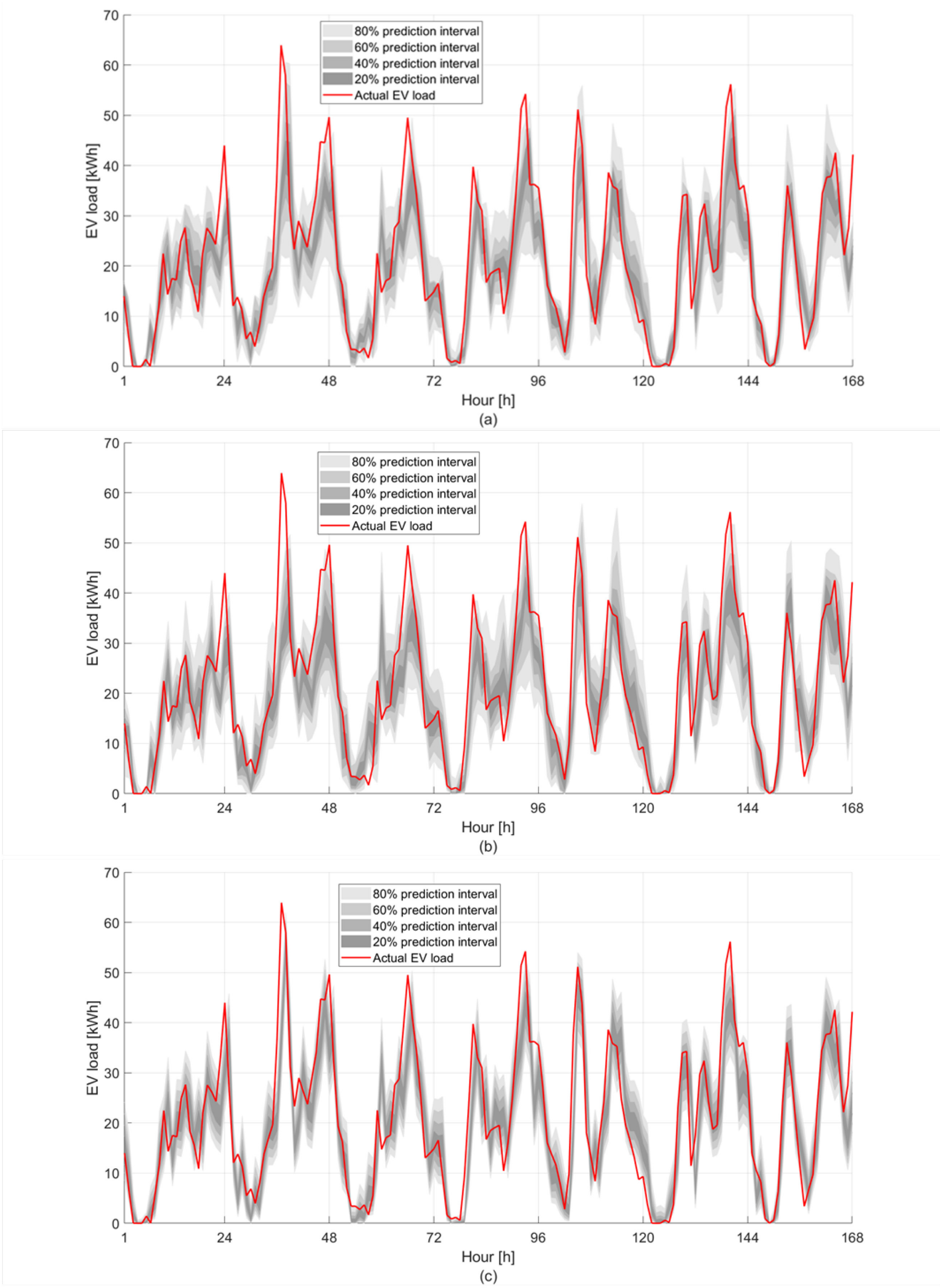

Fig. 24 - GBRT (a), QRF (b), and QRNN (c) hour-ahead baseline forecasts and actual EV load of Noordoost region during the 2nd week of the test period.

Assessment of hour-ahead hierarchical forecasts

Table 10 shows the PS and the AACE% of hour-ahead hierarchical probabilistic forecasts averaged on the set Ω_{test}. Bold values in Table 10 denote the smallest achieved indices for each low-level model. The AACE% of HPersB is not presented since this persistence-based benchmark generates the same predictive quantiles for each nominal coverage.

The PLQR proposal returns the smallest PS no matter which is the underlying probabilistic model used for generating the low-level EV load forecasts. It is also the most reliable model in two upon three cases.

The hierarchical approach returns more skilled forecasts than the "direct" approach by about 3.5% PS (QRF case) up to about 8% PS (GBRT case). As expected, the simple sum-and-sort (SaS) of homologous quantiles proves to be less skilled and very unreliable, as the AACE% is always beyond 7%. Results of the hierarchical approach without penalization (NPLQR) and without recent observations (PLQR no recency) are very close, but still are outperformed by the PLQR proposal. The improvement with respect to the persistence-based HpersB is about 54% in the three considered cases.

TAB.10 RESULTS OF HOUR-AHEAD HIERARCHICAL FORECASTS AT HIGH-LEVEL REGION. THE MOST FAVORABLE VALUE OF THE PERFORMANCE INDEX IN EACH COLUMN IS HIGHLIGHTED IN BOLD FONT

Model	GBRT		QRF		QRNN	
	PS [kWh]	AACE% [%]	PS [kWh]	AACE% [%]	PS [kWh]	AACE% [%]
PLQR proposal	**41.57**	**1.07**	**41.35**	**0.36**	**42.13**	1.75
Direct	45.29	1.63	42.91	1.42	43.59	1.95
SaS	46.62	7.29	48.92	9.50	44.92	8.17
NPLQR	43.38	1.45	44.18	0.88	42.68	**1.14**
PLQR no recency	43.28	1.74	44.09	0.83	42.63	1.49
HPersB	89.87	-	89.87	-	89.87	-

In order to evaluate the reliability of the hour-ahead hierarchical forecasts and as an example of the obtained results, Figure 25 shows the reliability diagrams of the PLQR proposal applied on GBRT, QRF and QRNN baseline forecasts, plotted against the ideal reliability bisector. In this case, the diagrams are all very close to the ideal bisector, no matter which is the underlying probabilistic model; the QRF-based hierarchical forecasts deviate less than the others from the ideal line.

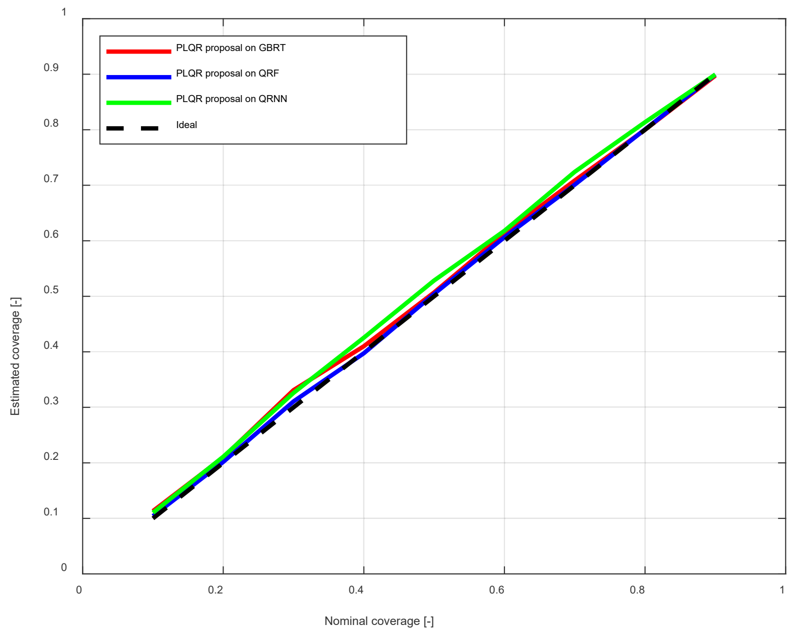

Fig. 25 - Reliability diagrams of the PLQR hour-ahead forecasts for the high-level EV load.

Figure 26 respectively shows the PLQR forecasts applied on GBRT (Figure 26(a)), QRF (Figure 26(b)) and QRNN (Figure 26(c)) baseline forecasts against the actual high-level EV load during the second week of the test period.

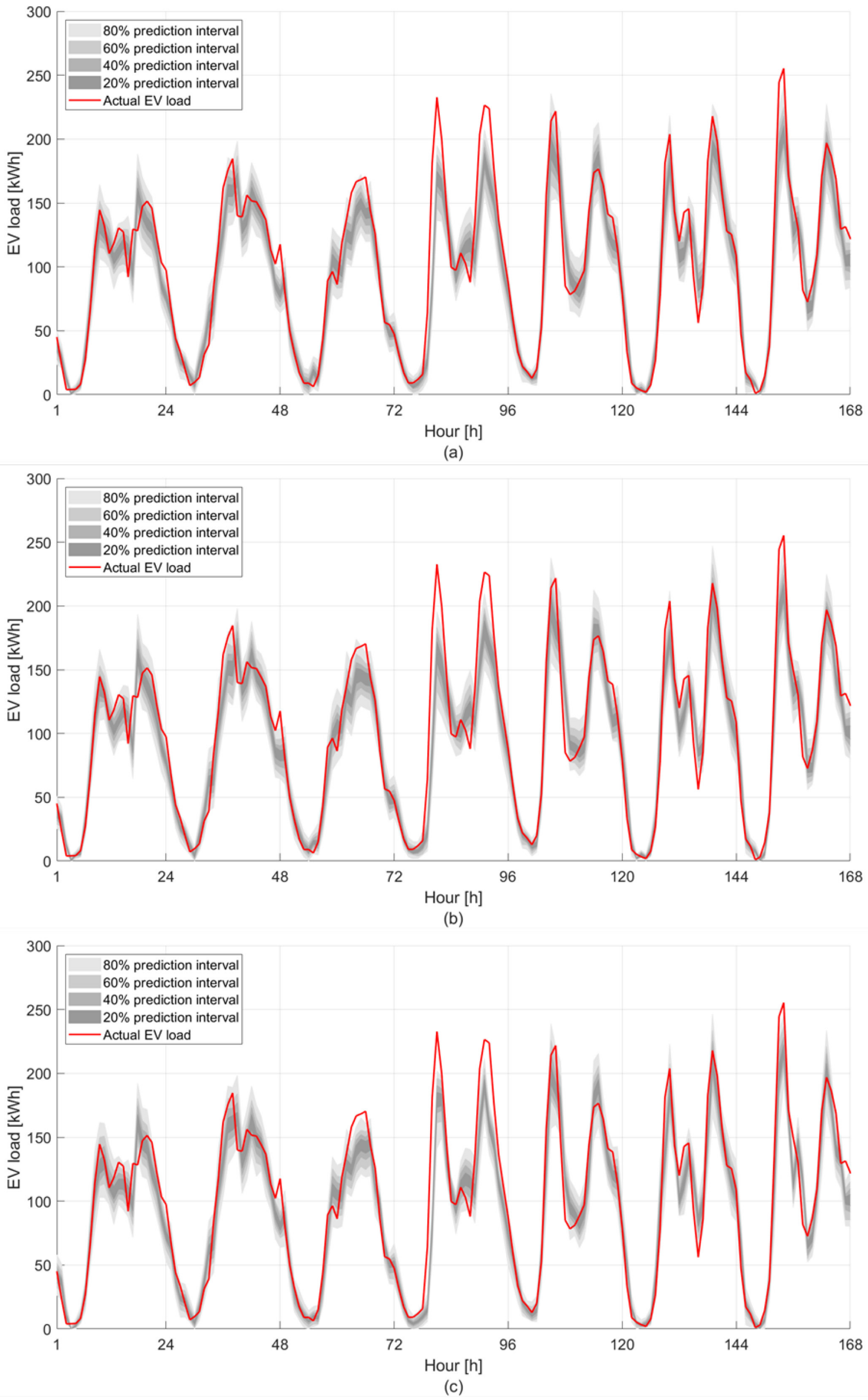

Fig. 26 - Hour-ahead PLQR on GBRT (a), QRF (b), and QRNN (c) baseline forecasts and actual high-level EV load during the 2nd week of the test period.

Assessment of day-ahead baseline and hierarchical forecasts

Day-ahead baseline and hierarchical forecasts are assessed in this sub-Section in a more compact form, as they are intended for comparative purposes. Table 11 shows the PS and the AACE% of day-ahead baseline probabilistic forecasts averaged on the set $\Omega = \{\Omega_{tra}^{\langle H \rangle}, \Omega_{test}\}$. Bold values in Table 11 denote the smallest achieved indices for each region. The AACE% of BPersB is not presented, since this persistence-based benchmark generates the same predictive quantiles for each nominal coverage.

The baseline forecasts generated with the PCA pre-processing are more skilled than the corresponding "no PCA" forecasts in all the four regions. The PS improvements are in the ranges 0% to 5% (Noordoost region), 0.5% to 9% (Rijnmond region), 0.5% to 5% (Utrecht region), and 1.5% to 9.5% (Zuidoost region). On average, the GBRT baseline returns the most skilled forecasts for the four regions, although GBRT, QRF and QRNN baseline forecasts give PS that are very close in all the four low-level regions. The improvement with respect to the BPersB ranges from 39% to 40%, which are values close to the hour-ahead case, indicating that the proposal is efficient in all the considered short-term forecasting horizons.

TAB.11 RESULTS OF DAY-AHEAD BASELINE FORECASTS AT LOW-LEVEL REGIONS. THE MOST FAVORABLE VALUE OF THE PERFORMANCE INDEX IN EACH COLUMN IS HIGHLIGHTED IN BOLD FONT

Model	Low-level region							
	Noordoost		Rijnmond		Utrecht		Zuidoost	
	PS [kWh]	AACE% [%]	PS [kWh]	AACE% [%]	PS [kWh]	AACE% [%]	PS [kWh]	AACE% [%]
GBRT baseline	**27.60**	3.51	**32.25**	2.92	20.65	4.53	25.56	1.89
QRF baseline	27.87	3.28	32.78	**2.63**	21.12	4.82	**25.54**	**1.19**
QRNN baseline	27.79	3.81	32.92	4.93	**20.61**	**4.06**	26.24	1.83
GBRT no PCA	**27.60**	**3.25**	32.35	3.03	20.74	4.85	25.94	1.99
QRF no PCA	28.15	3.98	33.34	2.91	21.17	4.07	26.19	1.79
QRNN no PCA	29.13	4.80	36.20	5.59	21.77	4.32	29.03	7.77
BPersB	45.18	-	52.73	-	33.86	-	42.53	-

Table 12 shows the PS and the AACE% of day-ahead hierarchical probabilistic forecasts averaged on the set Ω_{test}. Bold values in Table 12 denote the smallest achieved indices for each low-level model. The AACE% of HPersB is not presented, since this persistence-based benchmark generates the same predictive quantiles for each nominal coverage.

The PLQR proposal returns the smallest PS no matter which is the underlying probabilistic model used for generating the low-level EV load forecasts. It is also the most reliable model in two upon three cases. These outcomes match what was evidenced for the hour-ahead scenario.

The hierarchical approach returns more skilled forecasts than the “direct” approach by about 6.5% PS (GBRT case) up to about 9.5% PS (QRNN case). As expected, the simple sum-and-sort of homologous quantiles (SaS) proves to be less skilled and very unreliable, as the $AACE_{\%}$ is always beyond 8%. Results of the hierarchical approach without penalization (NPLQR) and without recent observations (PLQR no recency) are very close, but still are outperformed by the PLQR proposal. The improvement with respect to the persistence-based HPersB is about 39% in the three considered cases, which is a smaller improvement than the one obtained in the hour-ahead scenario, although still suggesting that the proposal enables skilled forecasts in the entire day-ahead scenario.

TAB.12 RESULTS OF DAY-AHEAD HIERARCHICAL FORECASTS AT HIGH-LEVEL REGION. THE MOST FAVORABLE VALUE OF THE PERFORMANCE INDEX IN EACH COLUMN IS HIGHLIGHTED IN BOLD FONT.

Model	GBRT		QRF		QRNN	
	PS [kWh]	$AACE_{\%}$ [%]	PS [kWh]	$AACE_{\%}$ [%]	PS [kWh]	$AACE_{\%}$ [%]
PLQR proposal	**69.64**	**1.32**	**69.88**	1.38	**70.47**	**1.54**
Direct	74.44	1.69	75.47	**1.14**	77.82	2.03
SaS	74.43	8.13	76.32	8.65	77.42	8.77
NPLQR	71.57	2.16	73.30	1.64	72.86	1.56
PLQR no recency	71.40	1.86	73.29	1.69	73.34	1.69
HPersB	114.85	-	114.85	-	114.85	-

Figure 27 shows the reliability diagrams of the PLQR proposal applied on GBRT, QRF and QRNN baseline forecasts, plotted against the ideal reliability bisector. All forecasts are very reliable, and they follow the same pattern across the nominal coverages.

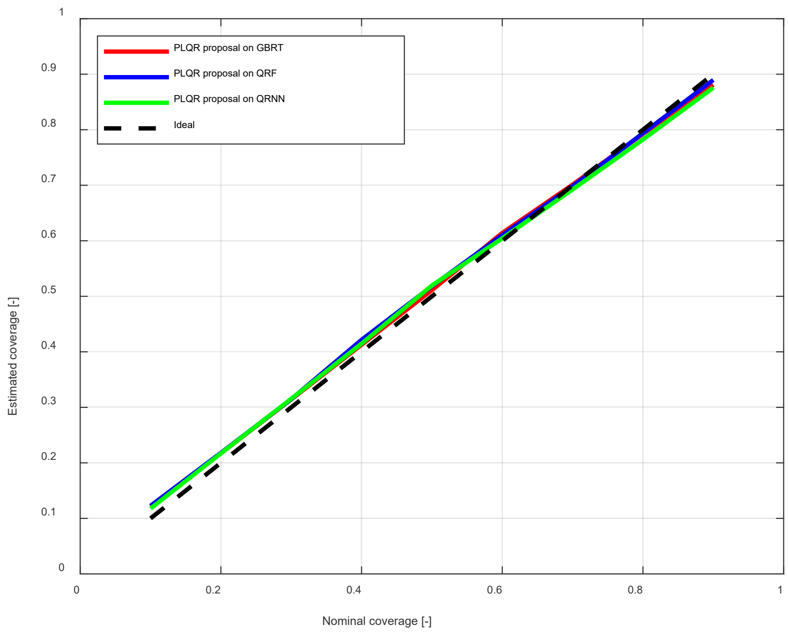

Fig. 27 - Reliability diagrams of the PLQR day-ahead forecasts for the high-level EV load.

8. COMPARISON WITH EXPECTED RESULTS

The activities related to Task 2.1 dealt with the design of databases of variables which allowed creating the dataset to be used to test the performance of the forecasting systems.

The activities related to Task 2.3 focused on the development of the real-time forecasting system. Several methods have been proposed and those based on data-driven ensemble approaches were exploited and validated to be used in the experimental stages of the project.

The activities related to the Task 2.4 allowed refining and revisiting the real-time forecasting systems with respect to the requirements of the optimization framework curried out in the other WPs.

Part of these activities were carried out in strict interaction with the partner University of Naples Parthenope for the data collection, data pre-processing and exploratory data analysis and for the theoretical development of the forecasting systems, and with the partner HEIG-VD for the acquisition of measurements available at the test distribution network at the ReIne laboratory.

The results obtained in this phase are coherent to the expected results.

9. HUMAN RESOURCES

The researchers of the University of Naples Federico II involved in the activities mentioned in this report are:

- Daniela Proto
- Fabio Mottola

10. PUBLICATIONS

The following publications have been produced:

- M. Bozorg, A. Bracale, M. Carpita, P. De Falco, F. Mottola, D. Proto, "Bayesian bootstrapping in real-time probabilistic photovoltaic power forecasting," Solar Energy, vol. 225, pp. 577-590, 2021.
- M. Bozorg, M. Carpita, P. De Falco, D. Lauria, F. Mottola, D. Proto, "A Derivative-Persistence Method for Real-time Photovoltaic Power Forecasting", accepted for publication in the proceedings of the International Conference on Smart Grids and Energy Systems SGES 2020, Perth, Australia, 23-26 November 2020.
- L. Buzna, P. De Falco, G. Ferruzzi, S. Khormali, D. Proto, N. Refa, M. Straka, G. van der Poel, "An ensemble methodology for hierarchical probabilistic electric vehicle load forecasting at regular charging stations," Applied Energy, Volume 283, 2021.
- D. Lauria, F. Mottola, D. Proto, "Caputo Derivative applied to Very Short Time Photovoltaic Power Forecasting", submitted to the Journal Applied Energy.
- "A multi-purpose Bayesian bootstrap approach for PV power and load forecasting at day-ahead and real-time horizons," to be submitted to an international conference.

APPENDIX

In this Section the baseline models used in the methods shown in the report are briefly recalled.

Linear Quantile Regression model

An LQR model allows estimating the cumulative distribution function of the PV power by means of a linear relationship between the power and informative predictors [19]. The linear relationship is established between the predictive α_q-quantile $\hat{P}_h^{\langle\alpha_q\rangle}$ of PV power and the predictors $\boldsymbol{z}_h = \{z_{h,1}, \dots, z_{h,N}\}$ through a set of model parameters $\boldsymbol{\beta}^{\langle\alpha_q\rangle} = \left\{\beta_0^{\langle\alpha_q\rangle}, \dots, \beta_N^{\langle\alpha_q\rangle}\right\}$ which have to be estimated. Both quantile and predictors refer to the time horizon h, and the forecast lead time k is assumed for predictors, i.e., their values are available at $h-k$, that is the forecast origin. For ease of notation, in what follows the forecast lead time k is not included in the symbols. The linear relationship imposed by a generic QR model is provided by:

$$P_h^{\langle\alpha_q\rangle}\left(\boldsymbol{z}_h \mid \boldsymbol{\beta}^{\langle\alpha_q\rangle}\right) = \beta_0^{\langle\alpha_q\rangle} + \sum_{n=1}^{N} \beta_n^{\langle\alpha_q\rangle} \cdot z_{h,n} \, , \tag{51}$$

where the vector $\boldsymbol{\beta}^{\langle\alpha_q\rangle} = \left\{\beta_0^{\langle\alpha_q\rangle}, \dots, \beta_N^{\langle\alpha_q\rangle}\right\}$ includes the $N+1$ parameters of the LQR model. The estimated values $\hat{\boldsymbol{\beta}}^{\langle\alpha_q\rangle}$ of $\boldsymbol{\beta}^{\langle\alpha_q\rangle}$ derive from the model training obtained by the minimization of a proper score evaluated respect to a known data set (i.e., the supervised training set that includes M_{tr} training PV power samples $\boldsymbol{P}^{\langle tr\rangle} = \{P_t, t \in \Omega^{\langle tr\rangle}\}$ and the corresponding predictors $\boldsymbol{Z}^{\langle tr\rangle} = \{\boldsymbol{z}_t, t \in \Omega^{\langle tr\rangle}\}$.

The PS is used for this purpose. PS is a score calculated on the training samples $\boldsymbol{P}^{\langle tr\rangle}$ and on the corresponding M_{tr} α_q-quantiles $\boldsymbol{P}^{\langle tr\rangle,\langle\alpha_q\rangle}\left(\boldsymbol{Z}^{\langle tr\rangle} \mid \boldsymbol{\beta}^{\langle\alpha_q\rangle}\right) = \left\{P_t^{\langle\alpha_q\rangle}\left(\boldsymbol{z}_t \mid \boldsymbol{\beta}^{\langle\alpha_q\rangle}\right), t \in \Omega^{\langle tr\rangle}\right\}$ given by the LQR model:

$$\begin{aligned} &PS\left[\boldsymbol{P}^{\langle tr\rangle}, \boldsymbol{P}^{\langle tr\rangle,\langle\alpha_q\rangle}\left(\boldsymbol{Z}^{\langle tr\rangle} \mid \boldsymbol{\beta}^{\langle\alpha_q\rangle}\right)\right] = \frac{1}{M_{tr}} \sum_{t\in\Omega^{\langle tr\rangle}} PS\left[P_t, P_t^{\langle\alpha_q\rangle}\left(\boldsymbol{z}_t \mid \boldsymbol{\beta}^{\langle\alpha_q\rangle}\right)\right] = \\ &\frac{1}{M_{tr}} \sum_{t\in\Omega^{\langle tr\rangle}} \left\{\alpha_q - \mathrm{I}\left[P_t \leq P_t^{\langle\alpha_q\rangle}\left(\boldsymbol{z}_t \mid \boldsymbol{\beta}^{\langle\alpha_q\rangle}\right)\right]\right\} \cdot \left[P_t - P_t^{\langle\alpha_q\rangle}\left(\boldsymbol{z}_t \mid \boldsymbol{\beta}^{\langle\alpha_q\rangle}\right)\right], \end{aligned} \tag{52}$$

where $\mathrm{I}\left[P_t \leq P_t^{\langle\alpha_q\rangle}\left(\boldsymbol{z}_t \mid \boldsymbol{\beta}^{\langle\alpha_q\rangle}\right)\right]$ is the indicator function that depends on condition in the brackets:

$$\mathrm{I}\left[P_t \leq P_t^{\langle\alpha_q\rangle}\left(\boldsymbol{z}_t \mid \boldsymbol{\beta}^{\langle\alpha_q\rangle}\right)\right] = \begin{cases} 1 & \text{if } P_t \leq P_t^{\langle\alpha_q\rangle}\left(\boldsymbol{z}_t \mid \boldsymbol{\beta}^{\langle\alpha_q\rangle}\right) \\ 0 & \text{if } P_t > P_t^{\langle\alpha_q\rangle}\left(\boldsymbol{z}_t \mid \boldsymbol{\beta}^{\langle\alpha_q\rangle}\right). \end{cases} \tag{53}$$

The estimated parameter vector $\widehat{\boldsymbol{\beta}}^{\langle\alpha_q\rangle}$ is eventually given by:

$$\widehat{\boldsymbol{\beta}}^{\langle\alpha_q\rangle} = \underset{\boldsymbol{\beta}^{\langle\alpha_q\rangle}}{\operatorname{argmin}} \; PS\left[\boldsymbol{P}^{\langle tr\rangle}, \boldsymbol{P}^{\langle tr\rangle,\langle\alpha_q\rangle}\left(\boldsymbol{Z}^{\langle tr\rangle} \mid \boldsymbol{\beta}^{\langle\alpha_q\rangle}\right)\right], \tag{54}$$

i.e., it is a function of $\boldsymbol{P}^{\langle tr\rangle}$ and $\boldsymbol{Z}^{\langle tr\rangle}$:

$$\widehat{\boldsymbol{\beta}}^{\langle\alpha_q\rangle} = \widehat{\boldsymbol{\beta}}^{\langle\alpha_q\rangle}\left(\boldsymbol{P}^{\langle tr\rangle}, \boldsymbol{Z}^{\langle tr\rangle}\right). \tag{55}$$

The LQR predictive α_q-quantile $\hat{P}_h^{\langle\alpha_q\rangle}$ of PV power for the time horizon h, returned by using the estimated parameters, consequently depends on $\boldsymbol{P}^{\langle tr\rangle}$ and $\boldsymbol{Z}^{\langle tr\rangle}$, too:

$$\hat{P}_h^{\langle\alpha_q\rangle}\left[\boldsymbol{z}_h \mid \widehat{\boldsymbol{\beta}}^{\langle\alpha_q\rangle}\left(\boldsymbol{P}^{\langle tr\rangle}, \boldsymbol{Z}^{\langle tr\rangle}\right)\right] = \hat{\beta}_0^{\langle\alpha_q\rangle} + \sum_{n=1}^{N} \hat{\beta}_n^{\langle\alpha_q\rangle} \cdot z_{h,n}. \tag{56}$$

Gradient Boosting Regression Trees

G GBRTs focus on the functional dependence $f^{\langle\alpha_q\rangle}(\cdot)$ between the response variable (the predictive α_q-quantile of PV power) $P_h^{\langle\alpha_q\rangle}$ and the corresponding predictors $\boldsymbol{z}_h$:

$$P_h^{\langle\alpha_q\rangle} = f^{\langle\alpha_q\rangle}(\boldsymbol{z}_h)\ . \tag{57}$$

Assuming $f^{\langle\alpha_q\rangle}$ to be unknown, the predictive α_q-quantile of PV power depends on the function $f^{\langle\alpha_q\rangle}$, i.e., $P_h^{\langle\alpha_q\rangle} = P_h^{\langle\alpha_q\rangle}(\boldsymbol{z}_h | f^{\langle\alpha_q\rangle})$. An estimation $\hat{f}^{\langle\alpha_q\rangle}$ of $f^{\langle\alpha_q\rangle}$ can be obtained by minimizing the PS over the training data [94]:

$$\hat{f}^{\langle\alpha_q\rangle} = \underset{f^{\langle\alpha_q\rangle}}{\operatorname{argmin}} \; PS\left[\boldsymbol{P}^{\langle tr\rangle}, \boldsymbol{P}^{\langle tr\rangle,\langle\alpha_q\rangle}\left(\boldsymbol{Z}^{\langle tr\rangle} \mid f^{\langle\alpha_q\rangle}\right)\right]. \tag{58}$$

The iterative procedure for solving (48) starts at iteration $j = 0$ by initializing $\hat{f}_{\langle 0\rangle}$ at the constant value:

$$\hat{f}_{\langle 0\rangle}^{\langle\alpha_q\rangle} = \hat{\rho}_{\langle 0\rangle}^{\langle\alpha_q\rangle} = \underset{\rho}{\operatorname{argmin}} \sum_{t\in\Omega^{\langle tr\rangle}} PS[P_t, \rho]. \tag{59}$$

UNIONE EUROPEA

Ministero dell'Istruzione, dell'Università e della Ricerca

The GBRT iterative procedure at the iteration $j > 0$ uses gradient descent to create new learners and the new estimation is made through the negative gradient, that is the negative partial derivative of the PS loss function evaluated for the m^{th} historical observation P_t:

$$g_t^{\langle\alpha_q\rangle}(\boldsymbol{z}_t) = -\left\{ \frac{\partial PS\left[P_t, f_{\langle j-1\rangle}^{\langle\alpha_q\rangle}(\boldsymbol{z}_t)\right]}{\partial f_{\langle j-1\rangle}^{\langle\alpha_q\rangle}(\boldsymbol{z}_t)} \Bigg|_{f_{\langle j-1\rangle}^{\langle\alpha_q\rangle}(\boldsymbol{z}_t) = \hat{f}_{\langle j-1\rangle}^{\langle\alpha_q\rangle}(\boldsymbol{z}_t)} \right\}. \tag{60}$$

The weak learner to make predictions is a regression tree fitted on a random subsample extracted from the original data, using the negative gradients as response variables and the predictors as input variables. More specifically, the predicted value $\hat{g}_t^{\langle\alpha_q\rangle}$ for the t^{th} negative gradient, given the predictors $\boldsymbol{z}_t$, can be written as:

$$\hat{g}_t^{\langle\alpha_q\rangle}(\boldsymbol{z}_t) = \sum_{s=1}^{S} \bar{g}^{\langle\alpha_q\rangle,\langle s\rangle} \cdot \mathrm{I}\left[\boldsymbol{z}_t \in \mathcal{R}_{\ell^{\langle s\rangle}}\right], \tag{61}$$

where $\bar{g}^{\langle\alpha_q\rangle,\langle s\rangle}$ is the average of the negative gradient values contained in the s^{th} leaf of the fitted tree, S is the total number of leaves, $\mathcal{R}_{\ell^{\langle s\rangle}}$ is the rectangular subspace domain corresponding to the s^{th} terminal leaf $\ell^{\langle s\rangle}$, and the indicator function assumes value 1 if predictors $\boldsymbol{z}_t$ belong to the subspace $\mathcal{R}_{\ell^{\langle s\rangle}}$ (or, equivalently, if predictors $\boldsymbol{z}_t$ individuate the s^{th} leaf on the fitted tree), and 0 otherwise. At the j^{th} iteration the updated weak learner is given by:

$$\hat{f}_{\langle j\rangle}^{\langle\alpha_q\rangle} = \hat{f}_{\langle j-1\rangle}^{\langle\alpha_q\rangle} + \hat{\rho}_{\langle j\rangle}^{\langle\alpha_q\rangle}, \tag{62}$$

where $\hat{\rho}_{\langle j\rangle}^{\langle\alpha_q\rangle}$ is the gradient descent step size to update the estimate of $f^{\langle\alpha_q\rangle}$ at the j^{th} iteration. The gradient descent is obtained by adding the outcome of the regression tree, $\rho \cdot \hat{g}_t^{\langle\alpha_q\rangle}(\boldsymbol{z}_t)$, to the previous estimate $\hat{f}_{\langle j-1\rangle}^{\langle\alpha_q\rangle}$, in order to get an improved estimate, i.e.:

$$\hat{\rho}_{\langle j\rangle}^{\langle\alpha_q\rangle} = \underset{\rho}{\operatorname{argmin}} \sum_{t\in\Omega^{\langle tr\rangle}} PS\left[P_t, \hat{f}_{\langle j-1\rangle}^{\langle\alpha_q\rangle}(\boldsymbol{z}_t) + \rho \cdot \hat{g}_t^{\langle\alpha_q\rangle}(\boldsymbol{z}_t)\right]. \tag{63}$$

Since the value $\hat{g}_t^{\langle\alpha_q\rangle}(\boldsymbol{z}_t)$ is constant in the terminal leaf individuated by $\boldsymbol{z}_t$ (i.e. it is the average of the negative gradient values contained in the unique $\tilde{s}^{\text{th}}$ leaf, $\ell^{\langle\tilde{s}(\boldsymbol{z}_t)\rangle}$, individuated by $\boldsymbol{z}_t$), the problem in (27) can be solved separately for each s^{th} leaf subspace [95], yielding the simplified expression [96]:

$$\hat{\rho}_{\langle j\rangle}^{\langle\alpha_q\rangle,\langle s\rangle} = \underset{\rho}{\operatorname{argmin}} \sum_{t\in\Omega^{\langle tr\rangle}} \left\{PS\left[P_t, \hat{f}_{\langle j-1\rangle}^{\langle\alpha_q\rangle}(\boldsymbol{z}_t)+\rho\right]\cdot \mathrm{I}\left[\boldsymbol{z}_t \in \mathcal{R}_{\ell^{\langle s\rangle}}\right]\right\}. \tag{64}$$

Hence, at the j^{th} iteration, the updated weak learner can be expressed as:

$$\hat{f}_{\langle j\rangle}^{\langle\alpha_q\rangle} = \hat{f}_{\langle j-1\rangle}^{\langle\alpha_q\rangle} + \upsilon \cdot \sum_{s=1}^{S} \hat{\rho}_{\langle j\rangle}^{\langle\alpha_q\rangle,\langle s\rangle} \cdot \mathrm{I}\left[\boldsymbol{z}_t \in \mathcal{R}_{\ell^{\langle s\rangle}}\right], \tag{65}$$

where υ is the weight of each learner (called *shrinkage* or *leaning rate*), whose value is strictly related to the optimal number of iterations [97] since smaller values involve more iterations and usually more skilled forecasts [98].

An ending condition for the iterative procedure is reaching values of $\hat{\rho}_{\langle j\rangle}^{\langle\alpha_q\rangle,\langle s\rangle}$ smaller than a given threshold. Assuming that this is obtained at the iteration $\bar{J}$, the prediction is:

$$\hat{P}_h^{\langle\alpha_q\rangle}(\boldsymbol{z}_h|\hat{f}_{\langle\bar{J}\rangle}^{\langle\alpha_q\rangle}) = \hat{f}_{\langle\bar{J}\rangle}^{\langle\alpha_q\rangle}(\boldsymbol{z}_h)\ , \tag{66}$$

and, since it is easy to verify that that $\hat{f}_{\langle\bar{J}\rangle}^{\langle\alpha_q\rangle}$ is estimated upon training data $\boldsymbol{P}^{\langle tr\rangle}, \boldsymbol{Z}^{\langle tr\rangle}$, the GBRT predictive α_q-quantile $\hat{P}_h^{\langle\alpha_q\rangle}$ of PV power for the time horizon h, consequently depends on $\boldsymbol{P}^{\langle tr\rangle}$ and $\boldsymbol{Z}^{\langle tr\rangle}$, too:

$$\hat{P}_h^{\langle\alpha_q\rangle}\left[\boldsymbol{z}_h \mid \hat{f}_{\langle\bar{J}\rangle}^{\langle\alpha_q\rangle}(\boldsymbol{P}^{\langle tr\rangle}, \boldsymbol{Z}^{\langle tr\rangle})\right] = \hat{f}_{\langle\bar{J}\rangle}^{\langle\alpha_q\rangle}(\boldsymbol{z}_h). \tag{67}$$

Quantile Regression Neural Network

QRNN exploits a neural network to generate predictive quantiles of PV power. It estimates conditional quantiles for specified values of quantile probability using regression equations and reproducing the behaviour of human brain to discern among the informative inputs and to produce an output. An efficient approach is the Monotone Composite Quantile Regression Neural Network (MCQRNN) proposed in [81] which is based on the

Multi-Layer Perceptron (MLP) neural network with partial monotonicity. It assumes the predictive α_q-quantile $\hat{P}_h^{\langle\alpha_q\rangle}$ of PV power coming from a weighted combination of L hidden layer outputs:

$$P_h^{\langle\alpha_q\rangle}(\boldsymbol{z}_h|\boldsymbol{\vartheta}^{\langle\alpha_q\rangle}) = \sum_{l=1}^{L}\left[\Phi\left(\sum_{c\in\Xi_1} z_{h,c}\cdot e^{\gamma_{c,l}^{\langle\alpha_q\rangle}} + \sum_{c\in\Xi_2} z_{h,c}\cdot\gamma_{c,l}^{\langle\alpha_q\rangle} + \tau_l^{\langle\alpha_q\rangle}\right)\cdot e^{\mu_l^{\langle\alpha_q\rangle}}\right] + \varepsilon^{\langle\alpha_q\rangle}, \tag{68}$$

where $\Phi(\cdot)$ is the function applied by each of the L neurons in the network hidden layer (in this paper, the hyperbolic tangent function), Ξ_1 is the set of indices for predictors monotonically increasing with the predictors, Ξ_2 is the corresponding set of indices for predictors without monotonicity constraints (note that $\boldsymbol{z}_h = \{z_{h,c}, c \in \Xi_1\} \cup \{z_{h,c}, c \in \Xi_2\}$), and $\boldsymbol{\gamma}_1^{\langle\alpha_q\rangle}, \dots, \boldsymbol{\gamma}_L^{\langle\alpha_q\rangle}$, $\boldsymbol{\mu}^{\langle\alpha_q\rangle} = \{\mu_1^{\langle\alpha_q\rangle}, \dots, \mu_L^{\langle\alpha_q\rangle}\}$, $\boldsymbol{\tau}^{\langle\alpha_q\rangle} = \{\tau_1^{\langle\alpha_q\rangle}, \dots, \tau_L^{\langle\alpha_q\rangle}\}$, and $\varepsilon^{\langle\alpha_q\rangle}$ are the parameters (all included in the vector $\boldsymbol{\vartheta}^{\langle\alpha_q\rangle}$, for clarity of representation) of the QRNN.

These parameters are once again estimated set by minimizing the PS over a training dataset [81], i.e., by solving the following constrained optimization problem:

$$\begin{aligned}
&\widehat{\boldsymbol{\vartheta}}^{\langle\alpha_q\rangle} = \underset{\boldsymbol{\vartheta}^{\langle\alpha_q\rangle}}{\operatorname{argmin}} \sum_{t\in\Omega^{\langle tr\rangle}} PS\left[P_t, P_t^{\langle\alpha_q\rangle}\right],\\
&\text{s.t.}\\
&\frac{\partial P_t^{\langle\alpha_q\rangle}}{\partial z_{t,c}} \geq 0, \quad \forall c \in \Xi_1.
\end{aligned} \tag{69}$$

It is easy to verify that that parameters $\widehat{\boldsymbol{\vartheta}}^{\langle\alpha_q\rangle}$ are estimated upon training data $\boldsymbol{P}^{\langle tr\rangle}, \boldsymbol{Z}^{\langle tr\rangle}$. The QRNN predictive α_q-quantile $\hat{P}_h^{\langle\alpha_q\rangle}$ of PV power for the time horizon h consequently depends on $\boldsymbol{P}^{\langle tr\rangle}$ and $\boldsymbol{Z}^{\langle tr\rangle}$, too:

$$\hat{P}_h^{\langle\alpha_q\rangle}\left[\boldsymbol{z}_h \mid \widehat{\boldsymbol{\vartheta}}^{\langle\alpha_q\rangle}\left(\boldsymbol{P}^{\langle tr\rangle}, \boldsymbol{Z}^{\langle tr\rangle}\right)\right] = \sum_{l=1}^{L}\left[\Phi\left(\sum_{c\in\Xi_1} z_{h,c}\cdot e^{\hat{\gamma}_{c,l}^{\langle\alpha_q\rangle}} + \sum_{c\in\Xi_2} z_{h,c}\cdot\hat{\gamma}_{c,l}^{\langle\alpha_q\rangle} + \hat{\tau}_l^{\langle\alpha_q\rangle}\right)\cdot e^{\hat{\mu}_l^{\langle\alpha_q\rangle}}\right] + \hat{\varepsilon}^{\langle\alpha_q\rangle}. \tag{70}$$

Quantile Regression Forests

QRF allows estimating the conditional quantiles of the response variable P_i (in this paper, the EV load at the i^{th} region) given the predictors $\boldsymbol{x}_{i,h}$ [81]. In this case, conditional quantiles are not obtained by minimizing a loss function but rather they are given by building several trees in a random forest. QRFs approximate the value of the predictive conditional cumulative distribution $\hat{F}(P_{i,h} \leq P^*|\boldsymbol{x}_{i,h})$ in the point P^* as a weighted mean of the training observations that are smaller than P^*:

UNIONE EUROPEA

Ministero dell'Istruzione, dell'Università e della Ricerca

$$\hat{F}(P_{i,h} \leq P^*|\boldsymbol{x}_{i,h}) = \sum_{n\in\Omega_{tra}^{\langle B\rangle}}\left[\omega_n(\boldsymbol{x}_{i,h}) \cdot \mathrm{I}\{P_{i,n} \leq P^*\}\right], \tag{71}$$

where $\mathrm{I}\{P_{i,n} \leq P^*\}$ is a function which assumes value 1 if $P_{i,n} \leq P^*$, and 0 otherwise. In (71) the weights $\omega_n(\boldsymbol{x}_{i,h})$ are given, assuming that there are T trees in the forest, by:

$$\omega_n(\boldsymbol{x}_{i,h}) = \frac{1}{T} \cdot \sum_{t=1}^{T} \frac{\mathrm{I}\left\{x_{i,n} \in \mathcal{R}_{\ell^{\langle \tilde{s}_t(x_{i,h})\rangle}}\right\}}{\sum_{n\in\Omega_{tra}^{\langle B\rangle}} \mathrm{I}\left\{x_{i,n} \in \mathcal{R}_{\ell^{\langle \tilde{s}_t(x_{i,h})\rangle}}\right\}} \tag{72}$$

where $\mathcal{R}_{\ell^{\langle \tilde{s}_t(x_{i,h})\rangle}} \subseteq \mathbb{R}^A$ (A being the cardinality of predictors) is the rectangular subspace domain corresponding to the terminal leaf $\ell^{\langle \tilde{s}_t(x_{i,h})\rangle}$ individuated by dropping $\boldsymbol{x}_{i,h}$ down the t^{th} tree.

The predictive α_q-quantile $\hat{P}_{i,h}^{\langle\alpha_q\rangle}$ is the α_q-quantile of the continuous predictive cumulative distribution $\hat{F}(P_{i,h} \leq P^*|\boldsymbol{x}_{i,h})$, defined in terms of probability (equal to α_q) of $P_{i,h}$ being smaller than $\hat{P}_{i,h}^{\langle\alpha_q\rangle}$ for given predictors $\boldsymbol{x}_{i,h}$:

$$\hat{P}_{i,h}^{\langle\alpha_q\rangle} = \inf\left\{P^* : \hat{F}(P_{i,h} \leq P^*|\boldsymbol{x}_{i,h}) \geq \alpha_q\right\}. \tag{73}$$

The quantile extraction is iterated Q times for different quantile coverages, allowing for generating probabilistic forecasts of the EV load at the i^{th} region as a set of Q predictive quantiles $\hat{P}_{i,h}^{\langle\alpha_1\rangle}, \dots, \hat{P}_{i,h}^{\langle\alpha_Q\rangle}$.

REFERENCES

[1] C. Wan, J. Zhao, Y. Song, Z. Xu, J. Lin, Z. Hu, "Photovoltaic and solar power forecasting for smart grid energy management," CSEE Journal of Power and Energy Systems, vol. 1, no. 4, 2015, pp. 38-46

[2] C. Skittides, W.G. Früh, "Wind forecasting using Principal Component Analysis," Renewable Energy, vol. 69, 2014, pp. 365-374

[3] R. Langella, D. Proto, A. Testa, "Solar Radiation Forecasting, Accounting for Daily Variability," Energies, 9, 200, 2016

[4] A. Kumler, Y. Xie, Y. Zhang, "A New Approach for Short-Term Solar Radiation Forecasting Using the Estimation of Cloud Fraction and Cloud Albedo," Golden, CO: National Renewable Energy Laboratory. NREL/TP-5D00-72290. [Online] Available: https://www.nrel.gov/docs/fy19osti/72290.pdf.

[5] R. Ahmed, V. Sreeram, Y. Mishra, M.D. Arif, "A review and evaluation of the state-of-the-art in PV solar power forecasting: Techniques and optimization," Renewable and Sustainable Energy Reviews, vol. 124, 2020

[6] Y. Chu, B. Urquhart, S.M.I. Gohari, H.T.C. Pedro, J. Kleissl, C.F.M. Coimbra, "Short-term reforecasting of power output from a 48 MWe solar PV plant," Solar Energy, vol. 112, 2015, pp. 68-77.

[7] A. Bracale, G. Carpinelli, and P. De Falco, "Developing and comparing different strategies for combining probabilistic photovoltaic power forecasts in an ensemble method," Energies, vol. 12, no. 6, 1011, 2019.

[8] S. Dutta, Y. Li, A. Venkataraman, L. M. Costa, T. Jiang, R. Plana, P. Tordjman, F. H.g Choo, C. .k Foo, H.s B. Puttgen, "Load and Renewable Energy Forecasting for a Microgrid using Persistence Technique," Energy Procedia, vol. 143, 2017, pp. 617-622

[9] R. Huang, T. Huang, R. Gadh, N. Li, "Solar generation prediction using the ARMA model in a laboratory-level micro-grid," 2012 IEEE Third International Conference on Smart Grid Communications (SmartGridComm), Tainan, 2012, pp. 528-533

[10] J. Antonanzas, N. Osorio, R. Escobar, R. Urraca, F.J. Martinez-de-Pison, F. Antonanzas-Torres, "Review of photovoltaic power forecasting," Solar Energy, vol. 136, 2016, pp. 78-111

[11] C.F.M. Coimbra, H.T.C. Pedro, Stochastic-Learning Methods. In Solar Energy Forecasting and Resource Assessment. Academic Press, 2013, pp. 383-406

[12] H.T.C. Pedro, C.F.M. Coimbra, "Assessment of forecasting techniques for solar power production with no exogenous inputs," Solar Energy, vol. 86, no. 7, 2012, pp. 2017-2028

[13] J. Zhang, A. Florita, B.-M. Hodge, S. Lu, H.F. Hamann, V. Banunarayanan, A.M. Brockway, "A suite of metrics for assessing the performance of solar power forecasting," Solar Energy, vol. 111, 2015, pp. 157-175

[14] M. Lipperheide, J.L. Bosch, J. Kleissl, "Embedded nowcasting method using cloud speed persistence for a photovoltaic power plant," Solar Energy, vol. 112, 2015, pp. 232-238

[15] J.H. Tato, M.C. Brito, "Using Smart Persistence and Random Forests to Predict Photovoltaic Energy Production," Energies, 12, 100, 2019.

[16] A. Kumler, Y. Xie, Y. Zhang, "A Physics-based Smart Persistence model for Intra-hour forecasting of solar radiation (PSPI) using GHI measurements and a cloud retrieval technique," Sol Energy, vol. 177, 2019, pp. 494-500

[17] J. Ma, Y. V. Makarov, C. Loutan, Z. Xie, "Impact of wind and solar generation on the California ISO's intra-hour balancing needs," 2011 IEEE Power and Energy Society General Meeting, Detroit, MI, USA, 2011, pp. 1-6.

[18] Juban, R., Ohlsson, H., Maasoumy, M., Poirier, L., & Zico Kolter, J. (2016). A multiple quantile regression approach to the wind, solar, and price tracks of GEFCom2014. International Journal of Forecasting, 32(3), 1094-1102.

[19] Lauret, P., David, M., & Pedro, H. (2017). Probabilistic solar forecasting using quantile regression models. Energies, 10(10), 1591.

[20] Pedro, H.T.C., Coimbra, C.F.M., David, M., & Lauret, P. (2018). Assessment of machine learning techniques for deterministic and probabilistic intra-hour solar forecasts. Renewable Energy, 123, 191-203.

[21] Almeida, M.P., Perpiñán, O., & Narvarte, L. (2015). PV power forecast using a nonparametric PV model. Solar Energy, 115, 354-368.

[22] Ren, Y., Suganthan, P.N., & Srikanth N. (2015). Ensemble methods for wind and solar power forecasting—A state-of-the-art review. Renewable and Sustainable Energy Reviews, 50, 82-91.

[23] S. Vergura and F. Vacca, "Bootstrap technique for analyzing energy data from PV plant," 2009 International Conference on Clean Electrical Power, Capri, 2009, pp. 268-275.

[24] Y. Wen et al., "Performance Evaluation of Probabilistic Methods Based on Bootstrap and Quantile Regression to Quantify PV Power Point Forecast Uncertainty," in IEEE Transactions on Neural Networks and Learning Systems, vol. 31, no. 4, pp. 1134-1144, April 2020

[25] K. Doubleday, S. Jascourt, W. Kleiber and B. Hodge, "Probabilistic Solar Power Forecasting Using Bayesian Model Averaging," IEEE Trans. on Sustainable Energy (in press), doi: 10.1109/TSTE.2020.2993524

[26] H. Lee and B. Lee, "Confidence-aware deep learning forecasting system for daily solar irradiance," in IET Renewable Power Generation, vol. 13, no. 10, pp. 1681-1689, 29 7 2019

[27] J. Roos, S. Bonnevay and G. Gavin, "Short-Term Urban Rail Passenger Flow Forecasting: A Dynamic Bayesian Network Approach," 2016 15th IEEE International Conference on Machine Learning and Applications (ICMLA), Anaheim, CA, 2016, pp. 1034-1039

[28] E. Valsera-Naranjo, A. Sumper, R. Villafafila-Robles, D. Martínez-Vicente, "Probabilistic method to assess the impact of charging of electric vehicles on distribution grids," Energies, vol. 5, pp. 1503-1531, 2012.

[29] J. Saarenpaa, M. Kolehmainen, H. Niska, "Geodemographic analysis and estimation of early plug-in hybrid electric vehicle adoption," Applied Energy, vol. 107, pp. 456-464, 2013.

[30] Y. Mu, J. Wu, N. Jenkins, H. Jia, and C. Wang, "A spatial–temporal model for grid impact analysis of plug-in electric vehicles," Applied Energy, vol. 114, pp. 456-465, 2014.

[31] A. Lojowska, D. Kurowicka, G. Papaefthymiou, and L. van der Sluis, "From transportation patterns to power demand: Stochastic modeling of uncontrolled domestic charging of electric vehicles," in Proc. of 2011 IEEE Power and Energy Society General Meeting, Detroit, MI, USA, 2011, pp. 1-7, 2011.

[32] Z. Luo, Y. Song, Z. Hu, Z. Xu, X. Yang, and K. Zhan, "Forecasting charging load of plug-in electric vehicles in China," in Proc. of 2011 IEEE Power and Energy Society General Meeting, Detroit, MI, USA, 2011, pp. 1-8, 2011.

[33] R.C. Leou, C.L. Su, and C.N. Lu, "Stochastic analyses of electric vehicle charging impacts on distribution networks," IEEE Transactions on Power Systems, vol. 29, no. 3, pp. 1055-1063, 2014.

[34] E.S. Xydas, C.E. Marmaras, L.M. Cipcigan, A.S. Hassan, and N. Jenkins, "Forecasting electric vehicle charging demand using support vector machines," in Proc. of 2013 48th International Universities' Power Engineering Conference (UPEC), Dublin, Ireland, 2013, pp. 1-6, 2013.

[35] M.H. Amini, A. Kargarian, and O. Karabasoglu, "ARIMA-based decoupled time series forecasting of electric vehicle charging demand for stochastic power system operation," Electric Power Systems Research, vol. 140, pp. 378-390, 2016.

[36] H.M. Louie, "Time-series modeling of aggregated electric vehicle charging station load," Electric Power Components and Systems, vol. 45, no. 14, pp. 1498-1511, 2017.

[37] M. Straka, and L. Buzna, "Use cases and introductory analysis of the dataset collected within the large network of public charging stations," in Proc. of 18th Multi-conference on Reliability and Statistics in Transportation and Communication, Riga, Latvia, 2018.

[38] L. Buzna, P. De Falco, S. Khormali, D. Proto, M. Straka, "Electric vehicle load forecasting: a comparison between time series and machine learning approaches," in Proc. of 1st International Conference on Energy Transition in the Mediterranean Area (SyNERGY MED 2019), Cagliari, Italy, 2019.

[39] S. Xydas, C. E. Marmaras, L. M. Cipcigan, A. S. Hassan, and N. Jenkins, "Electric vehicle load forecasting using data mining methods," in Proc. of 2013 IET Hybrid and Electric Vehicles Conference (HEVC 2013), London, UK, 2013.

[40] A. Lucas, R. Barranco, and N. Refa, "EV idle time estimation on charging infrastructure, comparing supervised machine learning regressions," Energies, vol. 12, no. 2, pp. 269, 2019.

[41] M. Majidpour, et al., "Forecasting the EV charging load based on customer profile or station measurement?," Applied Energy, vol. 163, pp. 134-141, 2016.

[42] J. Huber, D. Dann, and C. Weinhardt, "Probabilistic forecasts of time and energy flexibility in battery electric vehicle charging," Applied Energy, vol. 262, 114525, 2020.

[43] J. Zhu, et al., "Electric vehicle charging load forecasting: A comparative study of deep learning approaches," Energies, vol. 12, no. 14, 2692, 2019.

[44] M. Neaimeh, et al., "A probabilistic approach to combining smart meter and electric vehicle charging data to investigate distribution network impacts," Applied Energy, vol. 157, pp. 688-698, 2015.

[45] A. Ul-Haq, et al., "Probabilistic modeling of electric vehicle charging pattern associated with residential load for voltage unbalance assessment," Energies, vol. 10, no. 9, 1351, 2017.

[46] Q. Gong, S. Midlam-Mohler, V. Marano, and G. Rizzoni, "Study of PEV charging on residential distribution transformer life," IEEE Transactions on Smart Grid, vol. 3, no. 1, pp. 404-412, 2012.

[47] G. Li, and X. Zhang, "Modeling of plug-in hybrid electric vehicle charging demand in probabilistic power flow calculations," IEEE Transactions on Smart Grid, vol. 3, no. 1, pp. 492-499, 2012.

[48] P. Olivella-Rosell, R. Villafafila-Robles, A. Sumper, and J. Bergas-Jane, "Probabilistic agent-based model of electric vehicle charging demand to analyse the impact on distribution networks," Energies, vol. 8, pp. 4160-4187, 2015.

[49] T. Hong, J. Xie, and J. Black, "Global energy forecasting competition 2017: Hierarchical probabilistic load forecasting," International Journal of Forecasting, vol. 35, no. 4, pp. 1389-1399, 2019.

[50] T. Ren, P.N. Suganthan, and N. Srikanth, "Ensemble methods for wind and solar power forecasting—A state-of-the-art review," Renewable and Sustainable Energy Reviews, vol. 50, pp. 82-91, 2015.

[51] T. Zhao, J. Wang, and Y. Zhang, "Day-ahead hierarchical probabilistic load forecasting with linear quantile regression and empirical copulas," IEEE Access, vol. 7, pp. 80969-80979, 2019.

[52] Y. Wang, at al., "Combining probabilistic load forecasts," IEEE Transactions on Smart Grid, vol. 10, no. 4, pp. 3664-3674, 2019.

[53] ElaadNL website. Available online: https://www.elaad.nl (Accessed on June 25 2020).

[54] European Centre for Medium-Range Weather Forecasts website. Available online: https://www.ecmwf.int/ (Accessed on June 25 2020).

[55] M. Straka, et al., "Predicting popularity of electric vehicle charging infrastructure in urban context," IEEE Access, vol. 8, pp. 11315-11327, 2020.

[56] More than half of the public charging stations of pioneer EVnetNL will be transferred to municipalities. Available online: https://www.evnet.nl/nieuws/meer-dan-de-helft-van-publieke-laadpalen-van-pionier-evnetnl-gaat-over-naar-gemeenten/ (Accessed on June 25 2020).

[57] C. Bikcora, N. Refa, L. Verheijen, and S. Weiland, "Prediction of availability and charging rate at charging stations for electric vehicles," in Proc. of 2016 International Conference on Probabilistic Methods Applied to Power Systems (PMAPS 2016), pp. 1-6, 2016.

[58] COROP regions. Available online: https://www.regioatlas.nl/indelingen/indelingen_indeling/t/corop_regio_s (Accessed on June 25 2020).

[59] D.C. Montgomery, C.L. Jennings, and M. Kulahci. Introduction to Time Series Analysis and Forecasting. 2nd edition. Wiley Series in Probability and Statistics, 2015.

[60] M. Straka, and L. Buzna, "Use cases and introductory analysis of the dataset collected within the large network of public charging stations," in Reliability and Statistics in Transportation and Communication (RelStat 2018).

Lecture Notes in Networks and Systems, vol 68, I. Kabashkin, I. Yatskiv (Jackiva), O. Prentkovskis (eds.). Springer, Cham, 2019.

[61] L. Alfieri, and P. De Falco, “Wavelet-based decompositions in probabilistic load forecasting,” IEEE Transactions on Smart Grid, vol. 11, no. 2, pp. 1367-1376, 2020.

[62] G. James, D. Witten, T. Hastie, and R. Tibshirani. An Introduction to Statistical Learning: With Applications in R. Springer, vol. 112, 2013.

[63] T. Hong, P. Pinson, S. Fan, H. Zareipour, A. Troccoli, and R. J. Hyndman, “Probabilistic energy forecasting: Global Energy Forecasting Competition 2014 and beyond,” International Journal of Forecasting, vol. 32, no. 3, pp. 896–913, 2016

[64] IEEE open data sets, available http://site.ieee.org/pes-iss/data-sets

[65] Y.Dimitrov, “Approximations for the Caputo Derivative,” Journal of Fractional Calculus and Applications, Vol. 9(1), Jan. 2018, Pages 35-63

[66] Y.Dimitrov, “Approximations for the Caputo Derivative,” Journal of Fractional Calculus and Applications, Vol. 9(1), Jan. 2018, Pages 35-63

[67] T. Hastie, R. Tibshirani, and J. Friedman. The elements of statistical learning: Data mining, inference, and prediction, 2nd edition. Springer Series in Statistics, 2009.

[68] M.A. Clyde, and H.K.H. Lee. Bagging and the Bayesian bootstrap. Artificial Intelligence and Statistics, eds. Richardson, T. & Jaakkola, T. New York: Elsevier, pp. 169-174, 2001.

[69] D.B. Rubin, “The Bayesian bootstrap,” The Annals of Statistics, vol. 9, no. 1, pp. 130-134, 1981.

[70] J.H. Friedman, “Stochastic gradient boosting,” Computational Statistics & Data Analysis, vol. 38, no. 4, pp. 367-378, 2002.

[71] P. Lauret, M. David, and P. Pinson. "Verification of solar irradiance probabilistic forecasts." Solar Energy 194 (2019): 254-271.

[72] Bracale, A., Carpinelli, G., & De Falco, P. (2016). A probabilistic competitive ensemble method for short-term photovoltaic power forecasting. IEEE Transactions on Sustainable Energy, 8(2), 551-560

[73] Gneiting, T., & Raftery A.E. Strictly proper scoring rules, prediction, and estimation. Journal of the American Statistical Association, 102(477), 359-378.

[74] Alfieri, L., & De Falco, P. (2020). Wavelet-based decompositions in probabilistic load forecasting. IEEE Transactions on Smart Grid, 11(2), 1367-1376

[75] T. Hong, and S. Fan. “Probabilistic electric load forecasting: A tutorial review,” International Journal of Forecasting, vol. 32, no. 3, pp. 914-938, 2016.

[76] T. Hong, et al., “Probabilistic energy forecasting: Global energy forecasting competition 2014 and beyond,” International Journal of Forecasting, vol. 32, no. 3, pp. 896-913, 2016.

[77] D.W. Van der Meer, J. Widén, and J. Munkhammar, “Review on probabilistic forecasting of photovoltaic power production and electricity consumption,” Renewable and Sustainable Energy Reviews, vol. 81, pp. 1484-1512, 2018.

[78] R. Koenker, and G. Basset, “Regression quantiles,” Econometrica, vol. 46, pp. 33-50, 1978.

[79] J.H. Friedman, “Stochastic gradient boosting,” Computational Statistics & Data Analysis, vol. 38, no. 4, pp. 367-378, 2002.

[80] N. Meinshausen, “Quantile Regression Forests,” Journal of Machine Learning Research, vol. 7, pp. 983-999, 2006.

[81] A.J. Cannon, “Non-crossing nonlinear regression quantiles by monotone composite quantile regression neural network, with application to rainfall extremes,” Stochastic Environmental Research and Risk Assessment, vol. 32, no. 11, pp. 3207-3225, 2018.

[82] T. Gneiting, and A.E. Raftery, “Strictly proper scoring rules, prediction, and estimation,” Journal of the American statistical Association, vol. 102, no. 477, pp. 359-378, 2007.

[83] F. Golestaneh, P. Pinson, and H.B. Gooi, “Very short-term nonparametric probabilistic forecastng of renewable energy generation—With application to solar energy,” IEEE Transactions on Power Systems, vol. 31, no. 5, pp. 3850-3863, 2016.

[84] J.W. Messner, P. Pinson, J. Browell, M.B. Bjerregard, and I. Schicker, “Evaluation of wind power forecasts-An up-to-date view,” Wind Energy, vol. 23, no. 6, pp. 1-21, 2020.

[85] M. Carpita, J. Affolter, M. Bozorg, D. Houmard and S. Wasterlain, “ReIne, a flexible laboratory for emulating and testing the Distribution grid,” 2019 21st European Conference on Power Electronics and Applications (EPE '19 ECCE Europe), Genova, Italy, 2019, pp. 1-6

[86] G.E.P. Box, G.M. Jenkins, G.C. Reinsel, Time Series Analysis, Forecasting and Control. Wiley, 2011.

[87] A. Bracale, G. Carpinelli, P. De Falco, R. Rizzo, A. Russo, “New advanced method and cost-based indices applied to probabilistic forecasting of photovoltaic generation,” Journal of Renewable and Sustainable Energy, vol. 8, no. 2, 023505, 2016.

[88] IEEE open data sets, available http://site.ieee.org/pes-iss/data-sets.

[89] European Centre for Medium-range Weather Forecasts (ECMWF) website. Available online: https://www.ecmwf.int/ (Accessed on October 1 2020).).

[90] R *bayesboot* package: An implementation of Rubin’s (1981) Bayesian bootstrap. Available online: https://CRAN.R-project.org/package=bayesboot (Accessed on October 1 2020).

[91] R *quantreg* package: Quantile regression. Available online: https://CRAN.R-project.org/package=quantreg (Accessed on October 1 2020).

[92] R *qrnn* package: Quantile regression neural network. Available online: https://CRAN.R-project.org/package=qrnn (Accessed on October 1 2020).

[93] R *gbm* package: Generalized boosted regression models. Available online: https://CRAN.R-project.org/package=gbm (Accessed on October 1 2020).

[94] N. Alexey, K. Alois, “Gradient boosting machines, a tutorial”, Frontiers in Neurorobotics, 7, 2013.

[95] J.H. Friedman, “Stochastic gradient boosting,” Computational Statistics & Data Analysis, vol. 38, no. 4, pp. 367-378, 2002.

[96] L. Buzna, P. De Falco, G. Ferruzzi, S. Khormali, D. Proto, N. Refa, M. Straka, G. van der Poel, “Hierarchical Probabilistic Electric Vehicle Load Forecasting,” Applied Energy (submitted)

[97] R gbm package: generalized boosted regression models. Available online: https://CRAN.R-project.org/package=gbm (Accessed on June 25 2020).

[98] C. Persson, P. Bacher, T. Shiga, and H. Madsen, “Multi-site solar power forecasting using gradient boosted regression trees”, Solar Energy, vol. 150, pp. 423-436, 2015.